Asous, Waleed Asad

LIGHT SCATTERING IN SPHERICAL ATMOSPHERES

The University of Arizona PH.D. 1982

LIGHT SCATTERING IN SPHERICAL ATMOSPHERES

by

Waleed Asad Asous

A Dissertation Submitted to the Faculty of the

DEPARTMENT OF ELECTRICAL ENGINEERING

In Partial Fulfillment of the Requirements
For the Degree of

DOCTOR OF PHILOSOPHY

In the Graduate College

THE UNIVERSITY OF ARIZONA

1 9 8 2

THE UNIVERSITY OF ARIZONA
GRADUATE COLLEGE

As members of the Final Examination Committee, we certify that we have read the dissertation prepared by Waleed A. Asous

entitled Light Scattering in Spherical Atmospheres

and recommend that it be accepted as fulfilling the dissertation requirement for the Degree of Doctor of Philosophy.

Roland N. Stack	4/14/82
	Date
John A. Reagan	4/14/82
	Date
Allen Q. Howard Jr.	14 April 1982
	Date
	Date
	Date

Final approval and acceptance of this dissertation is contingent upon the candidate's submission of the final copy of the dissertation to the Graduate College.

I hereby certify that I have read this dissertation prepared under my direction and recommend that it be accepted as fulfilling the dissertation requirement.

Benjamin M. Herman	4/14/82
Dissertation Director	Date

STATEMENT BY AUTHOR

This dissertation has been submitted in partial fulfillment of requirements for an advanced degree at The University of Arizona and is deposited in the University Library to be made available to borrowers under rules of the Library.

Brief quotations from this dissertation are allowable without special permission, provided that accurate acknowledgment of source is made. Requests for permission for extended quotation from or reproduction of this manuscript in whole or in part may be granted by the head of the major department or the Dean of the Graduate College when in his judgment the proposed use of the material is in the interests of scholarship. In all other instances, however, permission must be obtained from the author.

SIGNED: Waleed Aswas

ACKNOWLEDGMENTS

I wish to express my deepest appreciation to Dr. Benjamin M. Herman for his guidance and encouragement throughout the course of this work. Also, I wish to acknowledge the valuable discussions with Gen. S. R. Browning.

This dissertation would never have been attempted but for the efforts and encouragement of my parents, Mr. and Mrs. Asad Asous, and my family who deserve to be recognized here, particularly, my brother, Wadea. The cheerful support and understanding of my wife, Rebecca, is deeply appreciated.

This research was supported by a grant from the Office of Naval Research, under contract N00014-81-K-0442.

TABLE OF CONTENTS

LIST OF ILLUSTRATIONS

LIST OF ILLUSTRATIONS--Continued

LIST OF ILLUSTRATIONS--Continued

LIST OF ILLUSTRATIONS--Continued

LIST OF TABLES

ABSTRACT

The scattered radiation fields in spherical planetary atmospheres have been considered by a new method which is called the Quasi-Spherical method. This method is applicable to planets with radii which are much larger than the height of their atmospheres.

The scattering of 0.5 μm radiation in a conservative and vertically inhomogeneous atmosphere has been discussed. Results comparing the emerging radiation from plane-parallel and spherical models for the earth's atmosphere have been presented for four different aerosol distributions in addition to the normal molecular composition. These results indicate measurable differences on the order of 10 to 300% as the angle of observation and/or the angle of incident sun falls within 10° from the horizon. Also, the obtained results in the spherical atmosphere show that additional layers of aerosols in either the stratosphere or the troposphere can be detected by satellite or aircraft radiometric measurements, while the plane-parallel atmosphere does not permit such a detection.

The accuracy of the obtained results by the present method can be increased by increasing the number of spherical shells in the spherical atmosphere. The emerging radiation in homogeneous and inhomogeneous Rayleigh atmospheres as computed by the Quasi-Spherical and the Monte Carlo methods compare quite well.

By applying the divergence theorem it was shown by the present method that the total flux in the spherical atmosphere is conserved within 1.351%.

CHAPTER I

INTRODUCTION

Electromagnetic wave propagation and scattering phenomena in the atmosphere has been of great interest for a long time. The geometry and composition of the atmosphere affect the resulting scattered and absorbed radiant energy from the sun. Usually the atmosphere is assumed to consist of spherical particles of different size distributions where the density of these particles varies with height in addition to the normal molecular composition. Because of the complexity of this problem most of the analyses of the radiation field use a plane-parallel geometry. In the past three decades several methods have been developed to solve the radiative transfer equation in a plane-parallel atmosphere. A review of these methods can be found in Van de Hulst's (1980) recent book. So far, the Monte Carlo (or random walk) method is the only technique that has been used in obtaining solutions in spherical and plane-parallel atmospheres. The basic partial differential equation of radiative transfer in a spherical geometry was derived by Lenoble and Sekera (1961). Since the resulting equation has no known analytic solution for the intensity distribution, several investigators such as Sobolev (1975) and Wilson and Sen (1980 a and b) have obtained approximate solutions in terms of the moments of intensity. Also, the much easier problem of isotropic scattering in thermally emitting spherical atmospheres has been based on the moments of

intensity. These types of solutions do not give the angular distribution of the intensity which is desirable in many applications.

Herein, we introduce a new numerical method which is called the Quasi-Spherical method to solve the radiative transfer equation in spherical planetary atmospheres. This method will be applied to a spherical atmosphere which includes, for example, aerosols and molecules with various vertical distributions. The results indicate that the plane-parallel geometry is not adequate when the angle of the sun and/or the angle of observation is within 10° from the horizon. Furthermore, these results reveal that in satellite and aircraft radiometric measurements of the intensity distribution, vertical inhomogeneities, such as stratospheric and tropospheric layers can be detected in a spherical atmosphere, while the same is not true for a plane-parallel atmosphere.

The Quasi-Spherical method is used in computing the scattered radiation fields in a spherical atmosphere which is divided into several spherical shells of homogeneous volume extinction coefficient. This method is quite fast and can easily include vertical inhomogeneities. Because of the approximate nature of the new method, the accuracy of the numerical solutions can be increased by increasing the number of spherical shells. For each thin spherical shell the solution of the radiative transfer equation in a plane-parallel atmosphere is employed, but the actual spherical geometry is used to determine the various angles and optical depths appearing in the solution. This approach is valid as long as the height of the atmosphere is much

smaller than the radius of the planet. As the case in a plane-parallel atmosphere a Gauss-Seidel iterative technique (see Herman and Browning, 1965) that uses a linear fit for the intensity distribution as a function of optical depth (see Herman et al, 1980) is used in determining multiple scattering, but in the present case, corrections for the sphericity are included.

Chapter II presents the radiative transfer equation and its formal solution. It gives a brief discussion of the radiation fields in a plane-parallel and horizontally homogeneous atmosphere illuminated by plane-parallel solar radiation. Also, it discusses the solution to the radiative transfer equation in a spherical atmosphere.

The formulation of the Quasi-Spherical method is given in Chapter III. In addition, the obtained results in spherical molecular atmospheres, both vertically homogeneous and inhomogeneous are compared to the Monte Carlo method. As a limiting case, the radius of the earth is increased by one hundred times and the resulting intensities are compared to those in a plane-parallel conservative atmosphere.

The Quasi-Spherical method is applied to conservative spherical atmospheres in Chapter IV. The difference between the results in plane-parallel and spherical atmospheres are discussed. By applying the divergence theorem the conservation of total flux in a spherical atmosphere is examined.

Summary and conclusions are given in Chapter V. Finally, Appendix A presents the method used in obtaining the optical depth as a function of height.

CHAPTER II

FORMULATION OF THE PROBLEM

The analysis of the radiation field in a planetary atmosphere which emits, scatters and absorbs radiant energy has been of great interest for a long time. The fundamental equation that governs the behavior of the radiation field is the Radiative Transfer Equation. The solution of this equation is described by an integro-differential equation which is very difficult to solve, but has a relatively simple mathematical form. The advent of digital computers has helped in obtaining solutions to the problem.

Two assumptions are usually made in the study of radiative transfer in planetary atmospheres: (1) that the atmosphere consists of plane-parallel layers, and (2) that these layers are illuminated by plane-parallel solar radiation over their entire extent. These assumptions are actually valid as long as the solar radiation and/or the angles of observations are sufficiently high above the horizon. This fact will be examined at a greater depth in the next two chapters. On the other hand, if the angles of observations and/or the solar radiation are near or below the horizon, the spherical nature of the atmosphere must be taken into consideration.

In this chapter we begin by presenting the radiative transfer equation and its formal solution. Next, we will discuss the radiation field in a plane-parallel and horizontally homogeneous atmosphere illuminated

by plane-parallel solar radiation. Finally, the solution of the radiative transfer equation in spherical geometry will be discussed.

Radiative Transfer Theory

The transfer of energy through a medium is described by the Radiative Transfer Equation, also called the Transport Equation. The equation is based on the principle of energy conservation and the condition of thermodynamical equilibrium. For a complete discussion and derivation of the Radiative Transfer Equation the reader is referred to the textbooks by Chandrasekhar, 1960; Sobolev, 1963; Ishimaru, 1978; and others. The basic differential equation is given by

$$\frac{1}{K_{T\lambda}} \frac{dI_\lambda(s)}{ds} = -I_\lambda(s)+J_\lambda(s) \tag{2.1}$$

where ds is an infinitesimal length along the direction of radiant energy. The monochromatic specific intensity, I_λ, is the radiant power which is associated with single wavelength, λ, per unit area normal to the direction of the radiant power, per unit element of solid angle containing the radiant power. The total volume extinction coefficient, $K_{T\lambda}$, at a given wavelength, is the extinction cross-section per unit volume of the medium. The source function, J_λ, at a given wavelength, usually includes all sources that contribute to the intensity I_λ in any given direction. Since throughout this dissertation we will be concerned in finding the intensity at one wavelength, the subscript λ will be dropped.

The formal solution to Eq (2.1) can be readily obtained, and it has the following form

$$I(s) = I(0)e^{-\tau(s,0)} + \int_0^s J(s')e^{-\tau(s,s')}K_T ds' \tag{2.2}$$

where $\tau(s,s')$ is the optical thickness of the material along a particular direction between the points s and s' as illustrated in Fig. 2-1, defined as

$$\tau(s,s') = \int_{s'}^{s} K_T(s)ds \tag{2.3}$$

Physically, the integral term in Eq (2.2) expresses the contribution to the intensity at any given point in a given direction resulting from the emission of all points, s', along the line of sight attenuated by the factor $\exp[-\tau(s,s')]$ to allow for absorption and/or scattering by the intervening medium. The first term in Eq (2.2) represents the contribution to the intensity resulting from the incident radiation at the boundary (i.e., s=0) attenuated by the factor $\exp[-\tau(s,0)]$. Since the source function in a scattering atmosphere depends on the intensity distribution, the integral in Eq (2.2), in general, cannot be evaluated analytically. However, for isotropic scattering the source function is independent of direction and the integral can be easily evaluated. Accordingly, the intensity depends on the geometry, the sources and the composition of the medium in question.

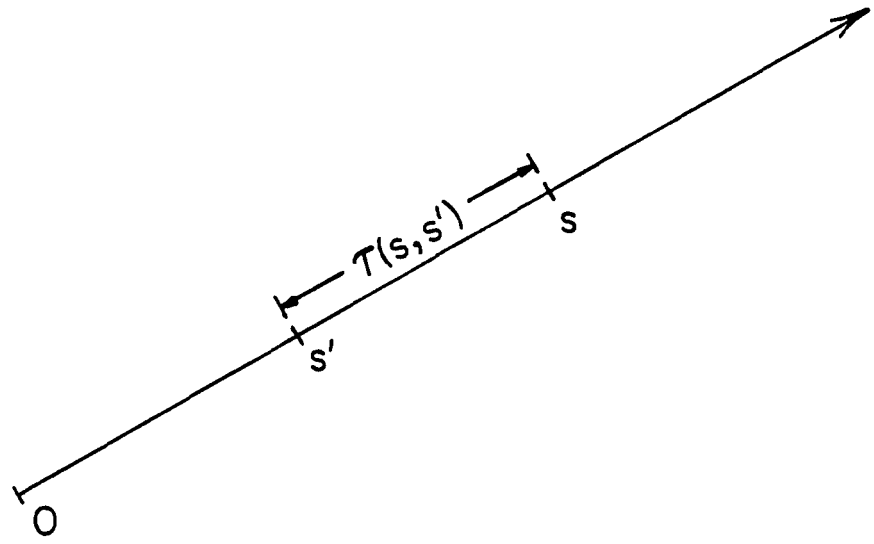

Fig. 2-1. Optical depth between points s´ and s.

Radiative Transfer in a Plane-Parallel Atmosphere

For a plane-parallel and horizontally homogeneous scattering atmosphere the radiative transfer equation (2.1) becomes

$$\frac{-\cos\theta}{K_T}\frac{dI(z,\theta,\phi)}{dz} = I(z,\theta,\phi)-J(z,\theta,\phi) \tag{2.4}$$

where θ denotes the zenith angle measured from the local upward-pointing normal to the planet's surface (i.e., z-axis), and ϕ is the azimuthal angle measured from a suitably chosen x-axis.

To simplify the previous equation we introduce the normal optical thickness defined by

$$\tau = \int_z^\infty K_T(z')dz' \tag{2.5}$$

where τ is usually zero at the top of the atmosphere and increases downward reaching a total optical thickness of τ_T at the planetary surface. Substituting Eq (2.5) into Eq (2.4) yields

$$-\mu\frac{dI(\tau,\mu,\phi)}{d\tau} = I(\tau,\mu,\phi)-J(\tau,\mu,\phi) \tag{2.6}$$

where $\mu=\cos\theta$, assuming the atmosphere is illuminated by a plane-parallel source, such as the sun. By solving Eq (2.6) for the downward traveling intensities at the optical depth τ we obtain

$$I(\tau,-\mu,\phi) = I(0,-\mu,\phi)e^{-\tau/\mu} + \int_0^{\tau} F_o(0,-\mu_o,\phi_o)P(\tau',\mu,-\mu_o,\phi-\phi_o)$$

$$e^{-\tau'/\mu_o} e^{-(\tau-\tau')/\mu} \frac{d\tau'}{\mu} + \int_0^{\tau}\int_0^{2\pi}\int_{-1}^{1} I(\tau',\mu',\phi')$$

$$P(\tau',\mu,\mu',\phi-\phi')e^{-(\tau-\tau')/\mu}\frac{d\tau'd\mu'd\phi'}{\mu}, \quad 0<\mu\leq 1 \qquad (2.7)$$

In the above equation, μ_o and ϕ_o correspond to the direction of the incident solar flux, F_o, and $P(\tau,\mu,\mu',\phi-\phi')$ is the scattering phase function at the optical thickness τ which expresses the fraction of the intensity scattered from the incident direction μ', ϕ' to the scattered direction μ, ϕ. The first integral in Eq (2.7) represents single scattering, while the second integral represents multiple scattering. Thus, the downward traveling intensities at the optical thickness τ in a given direction consist of three terms: incident, single scattering and multiple scattering.

Similarly, the upward traveling intensities are given by

$$I(\tau,\mu,\phi) = I(\tau_T,\mu,\phi)e^{-(\tau_T-\tau)/\mu}$$

$$+ \int_{\tau}^{\tau_T} F_o(0,-\mu_o,\phi_o)P(\tau',\mu,-\mu_o,\phi-\phi_o)e^{-\tau'/\mu_o}e^{-(\tau'-\tau)/\mu}\frac{d\tau'}{\mu}$$

$$+ \int_{\tau}^{\tau_T}\int_0^{2\pi}\int_{-1}^{1} I(\tau',\mu',\phi')P(\tau',\mu,\mu',\phi-\phi')e^{-(\tau'-\tau)/\mu}\frac{d\tau'd\mu'd\phi'}{\mu}$$

$$0<\mu\leq 1 \quad . \qquad (2.8)$$

The expression for the upward traveling intensities include; incident, single scattering and multiple scattering terms, as the case of the downward traveling intensities. Using Eqs (2.7-8) and suitable boundary conditions enables one to determine the intensities in a plane-parallel atmosphere.

Radiative Transfer in a Spherical Atmosphere

Determining the diffused or the scattered intensity in a spherical atmosphere requires obtaining a solution to the radiative transfer equation in spherical geometry. The geometry of such a problem is illustrated in Fig. 2-2. F_o is the incident plane-parallel solar radiation from the sun on a planet of radius R. The position of a point in the atmosphere is specified by a radial distance r and an angle α (the angle between the radius vector and the direction toward the sun). The direction of radiation is characterized by the local zenith angle θ and the local azimuthal angle ϕ. Consequently, the intensity is a function of four independent variables, namely; r, α, θ and ϕ. The desired differential equation which was given by Lenoble and Sekera (1961) and Sobolev (1975) has the following form:

$$\cos\theta\frac{\partial I}{\partial r} + \frac{\sin\theta\sin\phi}{r}\frac{\partial I}{\partial \alpha} - \frac{\sin\theta}{r}\frac{\partial I}{\partial \theta} - \frac{\cot\alpha\sin\theta\sin\phi}{r}\frac{\partial I}{\partial \phi} = -K_T(I-J) \qquad (2.9)$$

In the absence of the source function, J, the above equation reduces to a homogeneous partial differential equation which has no known analytic or closed form solution. Therefore, the more complicated problem of analytically solving Eq (2.9) in the presence of the

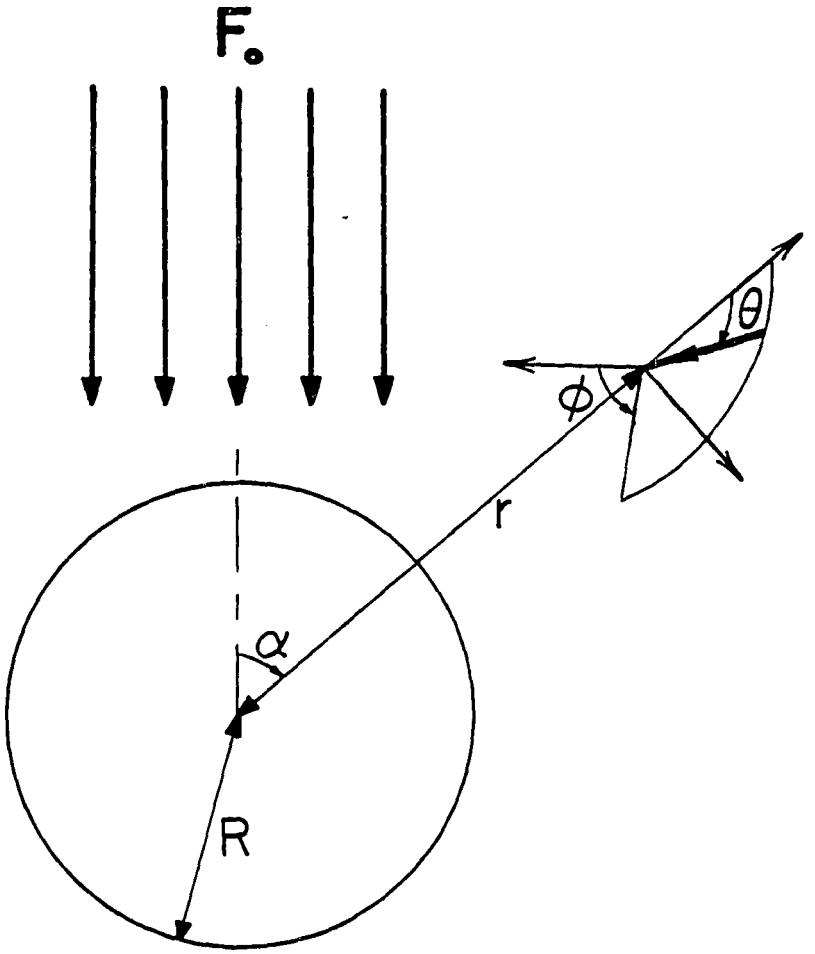

Fig. 2-2. Illustration of the geometry in a spherical atmosphere.

source function is virtually impossible. Although, in principle, an approximate solution can be obtained by finite difference procedures, it is deemed impractical due to the required computer storage and computing time.

Because of the complexity of Eq (2.9) only few approximate solutions have been attempted. The resulting solutions are given in terms of the mean, the flux and the higher order moments of intensity. The introduction of the moments of the intensity reduces Eq. (2.9) to a simpler differential equation which depends only on the variables r and α. Sobolev (1975) discussed the problem of anisotropic scattering in a spherical atmosphere which is illuminated by a plane-parallel source. He obtained an approximate solution in terms of the moments of intensity in an atmosphere in which the volume extinction coefficient is exponentially varying or constant with altitude. Wilson and Sen (1980a,b) used a three stream method based on the moments of intensity to compute brightness in an inhomogeneous, optically thin and spherically symmetric atmosphere in which the extinction coefficient decreases exponentially with altitude.

If the medium of the atmosphere has a spherical symmetry (i.e., $\frac{\partial I}{\partial \alpha} = \frac{\partial I}{\partial \phi} = 0$), then Eq (2.9) becomes

$$\cos\theta \frac{\partial I}{\partial r} - \frac{\sin\theta}{r} \frac{\partial I}{\partial \theta} = -K_T(I-J) \qquad (2.10)$$

Several investigators have obtained analytical and numerical

approximate solutions to Eq (2.10). Most of these solutions are concerned with isotropic scattering in thermally emitting atmospheres. Chandrasekhar (1960) discussed briefly the solution to Eq (2.10) and pointed out the similarities between the plane-parallel and the spherically symmetrical cases. Chapman (1966) considered the formal solution for a gray atmosphere for the special case where $K_T=r^{-3}$. Hummer and Rybicki (1971) developed a computational method that involves iteration on the "Eddington Factor," and presented results for $K_T=r^{-n}$, n=3/2, 2 and 3. Leong and Sen (1972) discussed a probabilistic model for time-dependent transfer problems in an inhomogeneous, isotropically scattering, spherical shell medium. Schmid-Burgk (1975) applied an integral equation that utilizes the moments of intensity through extended atmospheres and shells of spherical symmetry assuming that the volume extinction coefficient is a known function of radius. Later, Simonneau (1976) presented an approximate method without restricting K_T to radial variations, and solved for the intensity in the inward and the outward radial directions for conservative and non-conservative atmospheres. Unno and Kondo (1976) used a modified Eddington approximation to formulate a two stream model of the intensity in a medium that has K_T varying radially. The problem of isotropic scattering in an atmosphere with spherical symmetry, which is illuminated by a plane-parallel source, was considered by Minn and Sobolev (1963).

To summarize, there is no exact or analytic solution to the radiative transfer equation in a spherical atmosphere. Furthermore, the much easier problem with spherical symmetry cannot be solved in closed

form. So far, only approximate solutions have been obtained in anisotropic and isotropic spherical atmospheres. Most of these solutions are given in terms of the moments of intensity which do not give the angular distribution of the intensity.

CHAPTER III

QUASI-SPHERICAL METHOD

Plane-parallel geometry has been used in the study of light scattering in a planetary atmosphere because of its relative simplicity. However, such geometry is inaccurate in certain applications.

In this chapter, a new method; the Quasi-Spherical method, will be introduced to study scattering of light in spherical atmospheres. This method will be limited to a planet with a radius much larger than the height of its atmosphere.

First, the formulation of the Quasi-Spherical method will be discussed in detail. Next, the obtained results in a homogeneous molecular (Rayleigh) spherical atmosphere will be compared to the Monte Carlo method. Finally, as a limiting case, the radius of the earth will be increased one hundred times and the results compared to the resulting intensities in a plane-parallel atmosphere.

Mathematical Formulation

The Quasi-Spherical method will be used in obtaining an approximate solution to the integro-differential equation of radiative transfer in a scattering spherical atmosphere when the radius of the planet is much larger than the height of its atmosphere. Basically, this method assumes that a small portion of the atmosphere is locally

plane-parallel, and uses the exact spherical geometry to obtain the appropriate optical thicknesses as well as other geometrical factors.

We shall assume that a planet of radius, R, is illuminated by parallel solar irradiance, F_o, and the height of its atmosphere is h_T, and has a total normal optical thickness of τ_T. The atmosphere is divided into N, spherical shells, each having a homogeneous volume extinction coefficient, K_T.

The geometry of the problem in the case of downward traveling intensities in the plane of incident solar radiation is depicted in Fig. 3-1. The i^{th} layer is the spherical shell bounded by the optical thicknesses τ_{i+1} and τ_i, or equivalently, between the heights z_i and z_{i+1}. For convenience, the azimuthal angle, ϕ, is measured from the plane that coincides with that of the incident sun, while the zenith angle, θ, is measured from the normal to the surface of the earth at the observer location, P. The local zenith angle along the line of sight, θ_ℓ, is the angle between the line of sight XP and the local normal. For example, θ_ℓ^i and θ_ℓ^{i+1} are the local zenith angles at the top and bottom of the i^{th} layer, respectively. Likewise, the local zenith angle along the solar beam, θ_s, is the angle between the local normal and a beam from the incident solar radiation. Along the line of signt XP there are (i+1) local solar zenith angles down to the i^{th} layer. For example, θ_s^{i+1} is the local solar zenith angle at the bottom of the i^{th} layer, while θ_s^i is that angle at the top of the i^{th} layer (or the bottom of the $(i-1)^{th}$ layer), and so on. Because of spherical symmetry, the angle θ_ℓ^i is independent of the azimuthal angle ϕ, but θ_s^i

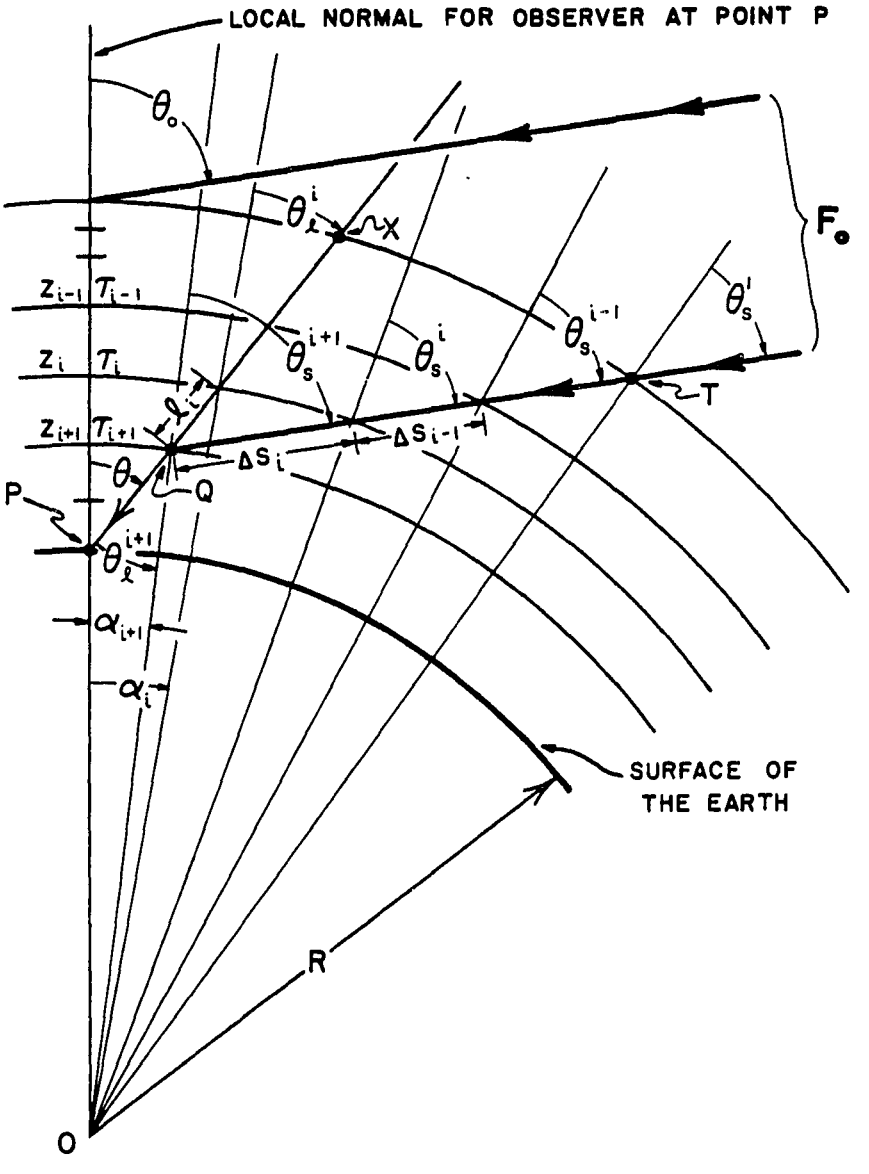

Fig. 3-1. Geometry of a spherical atmosphere in the plane of incident radiation for downward traveling intensities.

depends on ϕ. The geometrical lengths along the line of sight, XP, and the solar beam, QT, within the i^{th} layer are ℓ_i and Δs_i, respectively. Furthermore, the sum of the solar beam penetration within each layer along the solar beam, QT, is s_i, or mathematically,

$$s_i = \sum_{j=1}^{i} \Delta s_j, \quad i=1,2,\ldots N \tag{3.1}$$

Applying the law of sines to triangle OPQ in Fig. 3-1 yields,

$$\theta_{\ell}^{i+1} = \sin^{-1}\left(\frac{R \sin\theta}{R+z_{i+1}}\right) \tag{3.2}$$

and

$$\alpha_{i+1} = \theta - \theta_{\ell}^{i+1} \tag{3.3}$$

Hence, by using Eqs. (3.2-3), while varying the height z_{i+1} one can determine all angles θ_{ℓ}^{i+1} along the line of signt XP. By using Eq (3.3), the angle θ_s^{i+1} can be found from

$$\cos\theta_s^{i+1} = \cos\theta_o \cos\alpha_{i+1} + \sin\theta_o \sin\alpha_{i+1} \cos\phi \tag{3.4}$$

After determining the angle θ_s^{i+1} one can calculate the remaining local zenith angles along the solar beam QT (see Fig. 3-1), for example,

$$\theta_s^i = \sin^{-1}\left[\left(\frac{R + z_i}{R + z_{i+1}}\right) \sin\theta_s^{i+1}\right] . \tag{3.5}$$

Proceeding to calculate the length ℓ_i we get

$$\ell_i = \frac{\left(R + z_{i+1}\right) \sin\Delta\theta_\ell}{\sin\theta_\ell^i} \tag{3.6}$$

where $\Delta\theta_\ell = \theta_\ell^{i+1} - \theta_\ell^i$.

Similarly, Δs_i is determined by

$$\Delta s_i = \frac{\left(R + z_{i+1}\right) \sin\Delta\theta_s}{\sin\theta_s^i} \tag{3.7}$$

where $\Delta\theta_s = \theta_s^{i+1} - \theta_s^i$.

For an observer positioned anywhere along the normal to the earth's surface, the singly scattered intensity, I_{ss}, in the direction (θ, ϕ) is the total contribution of scattering from incident solar radiation into that direction, attenuated until reaching the observer. Since the incident intensities in the downward direction at the top of the atmosphere are zero, the singly scattered intensity at the earth's surface is given by

$$I_{ss}(z=0,\theta,\phi) = \int_0^L F_o P(\ell, \theta, \theta_o, \phi) e^{-\tau_s(\ell)} e^{-(\tau_L - \tau_\ell)} K_T(\ell) d\ell,$$

$$0 \leqslant \theta \leqslant \pi/2 \tag{3.8}$$

where $d\ell$ is an infinitesimal length along the line of sight, L is the total geometrical length of the line of sight measured from the top of

the atmosphere to the observer's position, while $K_T(\ell)$ is the total extinction coefficient along ℓ. The optical thicknesses τ_s and τ_ℓ are measured along the solar beam and line of sight, respectively. The scattering phase function from the solar beam into the direction (θ, ϕ) is represented by $P(\ell, \theta, \theta_o, \phi)$. Likewise, the upward traveling singly scattered intensities at the top of the atmosphere in the direction (θ, ϕ) that intersects the earth's surface are given by

$$I_{ss}\left(z=h_T, \theta, \phi\right) = I(z=0, \theta, \phi)e^{-\tau_L} + \int_0^L F_o P(\ell, \theta, \theta_o, \phi) e^{-\tau_s(\ell)} e^{-\tau_\ell} K_T(\ell) d\ell, \quad \pi/2 \leqslant \theta \leqslant \pi \tag{3.9}$$

where the first term on the righthand side is the contribution from ground reflection. Without loss of generality, we assume the scattering phase function $P(\ell, \theta, \theta_o, \phi)$ does not vary along the line of sight. The resulting simplified integrals in Eqs (3.8-9) cannot be evaluated analytically, contrary to the situation in a plane-parallel atmosphere. Usually, numerical integration schemes are employed to evaluate these integrals, but such approaches are very sensitive to geometrical or optical length of the line of sight. Consequently, the computing time will vary considerably depending on the length of the integration path. Instead, by assuming a segment of the atmosphere is locally flat or plane-parallel, one utilizes the analytically integrable results in evaluating the layer contribution to the singly scattered intensity. In fact, such an assumption is acceptable as long as the height of the atmosphere is much smaller than the radius of the planet

in question. Accordingly, the i^{th} layer singly scattered intensity in the downward direction (see Fig. 3-1) is

$$I_{ss}(\tau_{\ell}^{i+1},\ \theta,\ \phi) = F_o P(\theta,\ \theta_o,\ \phi)\frac{\mu_{oe}^{i} e^{-\tau_s^{i-1}}}{\mu_{oe}^{i}-\mu_e^{i}}\left(e^{-\Delta\tau_s^{i}}-e^{-\Delta\tau_{\ell}^{i}}\right),$$

$$0\leqslant\theta\leqslant\pi/2,\ \tau_i\leqslant\tau\leqslant\tau_{i+1} \tag{3.10}$$

where the optical thickness from the top of the atmosphere to the top of the i^{th} layer along the solar beam QT is expressed as

$$\tau_s^{i-1} = \sum_{j=1}^{i-1}\bar{K}_{Tj}\Delta s_j \quad . \tag{3.11a}$$

Here, $\bar{K}_{Tj}$ is the homogeneous volume extinction coefficient within the j^{th} spherical shell. Also, the solar optical thickness within the i^{th} layer is given by

$$\Delta\tau_s^{i} = \bar{K}_{Ti}\Delta s_i \quad . \tag{3.11b}$$

Similarly, optical thickness along the line of sight within the i^{th} layer is given by

$$\Delta\tau_{\ell}^{i} = \bar{K}_{Ti}\ell_i \quad . \tag{3.11c}$$

The "effective" cosine, μ_{oe}^{i}, of the solar elevation angle is defined by

$$\mu_{oe}^{i} = \frac{\Delta z_i}{\Delta s_i} \tag{3.12a}$$

where $\Delta z_i = z_i - z_{i+1}$.

Also, the "effective" cosine of the elevation angle of the line of sight is given by

$$\mu_e^i = \frac{\Delta z_i}{\ell_i} \quad . \tag{3.12b}$$

Therefore, the singly scattered intensity, I_{ss}, at point P is the sum of all the layer contributions along XP attenuated to the observer, that is,

$$I_{ss}\left(\tau_L,\ \theta,\ \phi\right) = \sum_{i=1}^{N} I_{ss}\left(\tau_\ell^{i+1},\ \theta,\ \phi\right) e^{-\left(\tau_L - \tau_\ell^{i+1}\right)},\quad 0 \leqslant \theta \leqslant \pi/2 \tag{3.13}$$

Similarly, the expression for upward traveling singly scattered intensities at point P, as illustrated in Fig. 3-2a for a line of sight, AP, that intersects the planet's surface can be obtained as follows

$$I_{ss}(0,\ \theta,\ \phi) = \sum_{i=1}^{N} I_{ss}\left(\tau_\ell^i,\ \theta,\ \phi\right) e^{-\tau_\ell^i},\quad \pi/2 \leqslant \theta \leqslant \pi \tag{3.14}$$

where

$$I_{ss}\left(\tau_\ell^i,\ \theta,\ \phi\right) = F_o P\left(\theta,\ \theta_o,\ \phi\right) \frac{\mu_{oe}^i\, e^{-\tau_s^i}}{\mu_{oe}^i + \mu_e^i} \left(e^{\Delta\tau_s^i} - e^{-\Delta\tau_\ell^i}\right),$$

$$\tau_i \leqslant \tau \leqslant \tau_{i+1} \tag{3.15}$$

In general, the solar optical thickness τ_s does not vary linearly along any line of sight. However, the above mentioned approach implies uniform solar penetration along the segment QA of the line of sight from the top of the i^{th} spherical shell between the points A and B

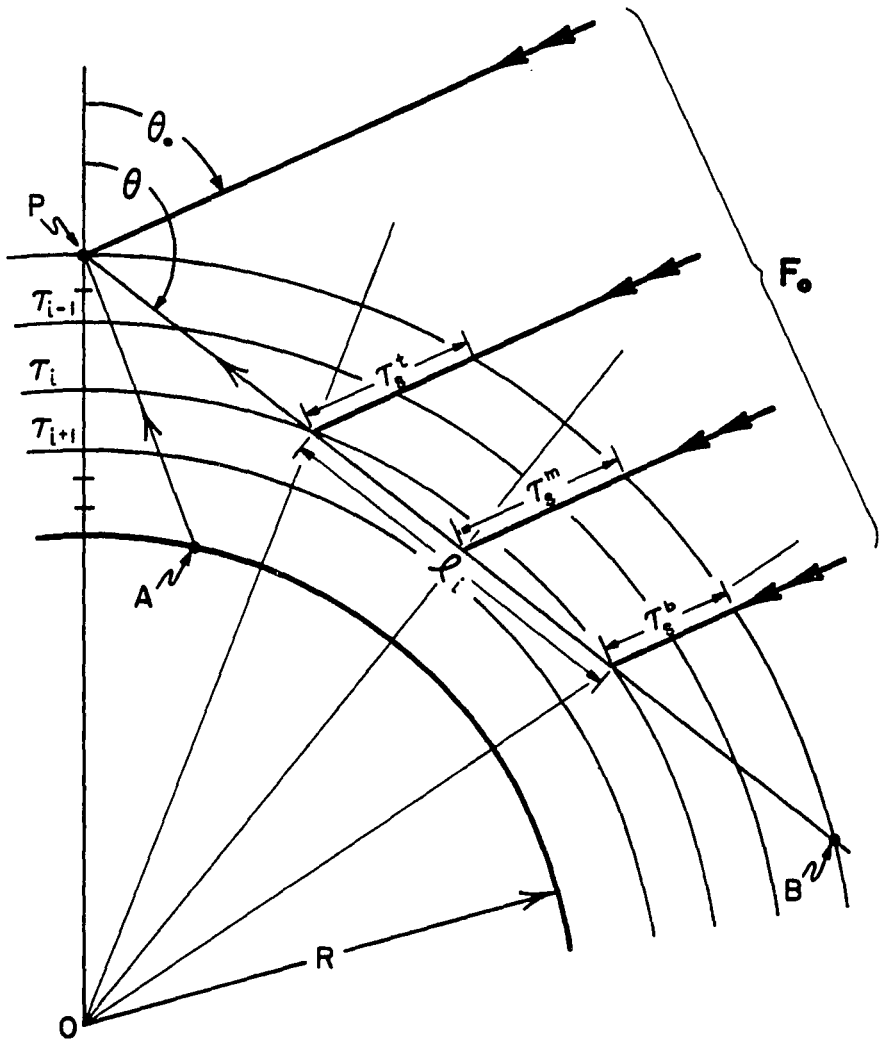

Fig. 3-2a. Geometry of a spherical atmosphere in the plane of incident solar radiation for upward traveling intensities.

to the top of the atmosphere, as shown in Fig. 3-2b (i.e., AC and BT and all between distances are equal). Of course, this introduces an error in the layer contribution to singly scattered intensities. Although the error increases as the angles of observation and incident sun approach the horizon, it can be reduced by increasing the number of spherical shells in the atmosphere. It is interesting to note that if τ_s varies linearly along the line of sight, the resulting layer contribution has the same form as Eqs (3.10 and 3.15).

So far we have considered the cases in which the line of sight for upward traveling beams intersects the planet's surface and in the process penetrates each spherical shell once. However, due to the sphericity of the atmosphere, all the lines of sight above the tangent to the planet's surface will go through the whole atmosphere penetrating each spherical shell twice with the exception of one. For example, the line BP in Fig. 3-2a illustrates this situation in the plane $\phi=0$. The layer singly scattered intensity is found by applying Eq (3.15) to every segment of line of sight within each layer except the deepest penetrated layer. Here, rather than assuming uniform solar penetration to the top of the i^{th} layer, a weighted distribution will be assumed. The solar optical thicknesses at the two edges of the i^{th} layer are multiplied by a factor of $\frac{1}{4}$, while the one at the midpoint is multiplied by $\frac{1}{2}$; i.e., $\tau_s^i = \left(\tau_s^t+\tau_s^b\right)/4 + \tau_s^m/2$. In addition, the "effective" cosine expressions are modified as follows

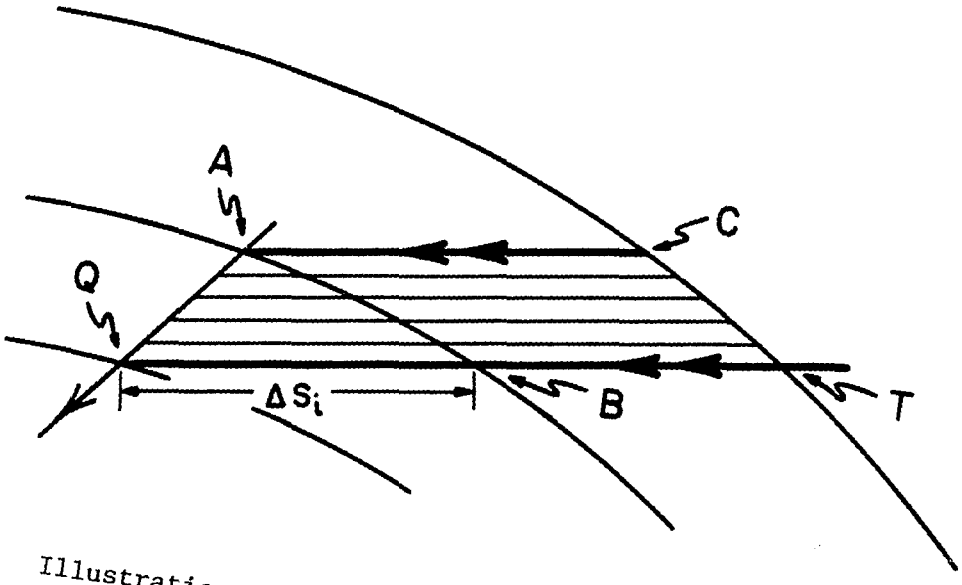

Fig. 3-2b. Illustration of solar penetration from the top of the atmosphere to a spherical shell along a portion QA of the line of sight XP in Fig. (3-1).

$$\mu_{oe}^{m} = \frac{\Delta z'}{\Delta s^{m}} \tag{3.16a}$$

$$\mu_{e}^{m} = \frac{\Delta z'}{\ell_{i/2}} \tag{3.16b}$$

where $\Delta z' = \left(R+z_i\right) + \left(R+h_T\right)\cos\theta$

and Δs^{m} is the solar beam within the i^{th} layer evaluated at the mid-point.

In the past two decades several methods have been developed to solve the problem of radiative transfer in plane-parallel atmospheres. Basically, these methods vary in calculating multiple scattering, because single scattering is analytically determined. A review of the various methods can be found in Van de Hulst's (1980) recent book. So far, as noted by Lenoble (1977), the Monte-Carlo method is the only technique that has been used in both spherical and plane-parallel atmospheres.

Herman (1963 and 1965) introduced a Gauss-Seidel iterative technique over optical depth to solve the problem of radiative transfer in a plane-parallel atmosphere. Since then several refinements were introduced, such as the Fourier expansion in azimuthal angle (see Dave & Gazdag, 1970; Herman and Browning, 1975), more recently, the semi-analytical technique to integrate the radiative transfer equation over optical depth (see Herman et al, 1980). Herein, we will use a linear fit to the intensity distribution as a function of optical depth in conjunction with the Gauss-Seidel iterative technique and apply the semi-analytic technique referred to above.

The scattering in a spherical atmosphere is a split boundary problem, as is the case in plane-parallel atmospheres, whereby the incident downward traveling intensities at the top of the atmosphere are zero and the upward traveling intensities at the bottom are usually obtained from the ground reflectivity or albedo. The problem is set up by dividing the atmosphere into several spherical shells. Each shell is assumed to have a uniform volume extinction coefficient. Singly scattered intensities are computed by the method outlined earlier. Rather than computing these intensities in all directions of interest at each level, we will compute them at the top and bottom of the atmosphere, namely, at points X and Y (see Fig. 3-3). Then the intensities for a particular level as measured along the line of sight from either the top or the bottom of the atmosphere are shifted to the normal line XY. Fig. 3-3 illustrates this situation in the planes $\phi = 0^\circ$ and 180° for the n^{th} level at the observer's location P. For example, the downward traveling intensity b along the line of sight that reaches X is assumed to equal the intensity b′ at point P, and similarly the intensity c′ is set equal to c. Likewise, the upward traveling intensity a along the line of sight that reaches Y is assumed to equal a′ at P. These assumptions will be used in determining multiple scattering. Even though the shifting of intensities is an approximation, it seems to be valid as long as the radius R is much larger than h_T which makes the levels in the atmosphere nearly flat over the region from which most of the multiply scattered light comes from, and the maximum angle of shifting, as measured at the center of the planet, very small (i.e.,

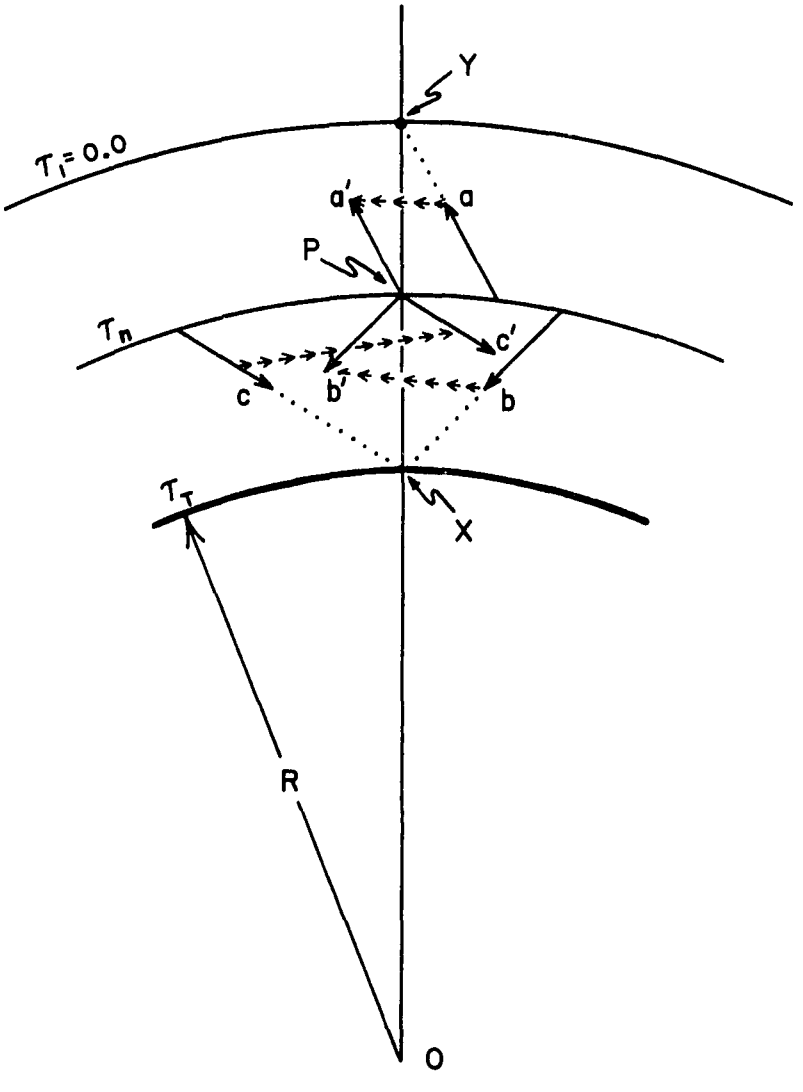

Fig. 3-3. Shifting of intensities in the azimuthal plane (0°, 180°) for multiple scattering.

for R = 6370 km, h_T = 50 km and $\theta = 85^\circ$; $\alpha_{max} < 4^\circ$). Furthermore, for an atmosphere with relatively small τ_T, the contribution of single scattering dominates that of multiple scattering and consequently the error due to shifting of intensities for computing multiple scattering introduces a much smaller error in the total intensity. However, for an optically thick atmosphere the shifting of intensities may not be valid since the total intensity is dominated by multiple scattering. In fact, the intensities in such a situation can be calculated at each level along the normal line without shifting by the method outlined earlier in this section. The disadvantage in this procedure lies in the large increase of computing time in comparison with the procedure that uses shifting, and in the complexity of properly establishing a finite grid system.

In the Gauss-Seidel iteration scheme the singly scattered intensities are used as an initial guess. Then, starting from the top of the atmosphere, the downward traveling intensities at the second level are computed by assuming a linear fit for the intensity distribution over the layer and at the same time updating the previous guess. This procedure continues until the ground is reached; meanwhile all the intensities in the downward direction have been updated. Accordingly, the intensity at the second level due to multiple scattering in the direction (θ, ϕ) is

$$I_{ms}\left(\tau_\ell^2, \theta, \phi\right) = \int_0^{\tau_\ell^2} e^{-\left(\tau_\ell^2 - \tau_\ell\right)} d\tau_\ell \int_0^{2\pi}\int_0^{\pi} P\left(\theta, \theta', \phi-\phi'\right) I\left(\tau_\ell, \theta', \phi'\right) \sin\theta' d\theta' d\phi', \quad 0 \leqslant \theta \leqslant \pi/2 \tag{3.17}$$

The evaluation of the second and third integrals will be done numerically; that is, replacing those integrals by summation over θ' and ϕ' and at the same time taking an average value within each summation interval for the scattering phase function $P(\theta, \theta', \phi-\phi)$. In addition, we will assume a linear distribution for the intensity as a function of optical thickness, that is

$$I\left(\tau_\ell, \theta, \phi\right) = a_n \cdot \left(\tau_\ell - \tau_\ell^n\right) + I\left(\tau_\ell^n, \theta, \phi\right), \quad \tau_\ell^n \leq \tau_\ell \leq \tau_\ell^{n+1} \tag{3.18}$$

where a_n is a constant that depends on optical thickness as well as the intensities at the top and bottom of the layer in question [i.e., $a_n = \frac{I\left(\tau_\ell^{n+1}\right) - I\left(\tau_\ell^n\right)}{\tau_\ell^{n+1} - \tau_\ell^n}$; $n = 1, 2, 3...$]. In order to generalize the application of Eq (3.17) we replace superscripts 2 by (n+1) and 1 by n. Now, substituting Eq (3.18) into Eq (3.17) and analytically integrating over τ_ℓ yields

$$I_{ms}\left(\tau_\ell^{n+1}, \theta, \phi\right) = \sum_{\Delta\theta_j'} \sum_{\Delta\phi_k'} \left\{ \left[\beta_n I\left(\tau_\ell^n, \bar{\theta}_j', \phi_k'\right) + \beta_{n+1} I\left(\tau_\ell^{n+1}, \bar{\theta}_j', \phi_k'\right) \right] \cdot P\left(\theta, \bar{\theta}_j', \phi-\phi_k'\right) \left(\cos\bar{\theta}_j' - \cos\bar{\theta}_{j+1}'\right) \Delta\phi_k' \right\} \tag{3.19}$$

where $\Delta\theta_j' = \left(\theta_{j+1}' - \theta_j'\right)$, $\bar{\theta}_j' = \left(\theta_{j+1}' + \theta_j'\right)/2$, $\Delta\phi_k' = \left(\phi_{k+1}' - \phi_k'\right)$ for $\binom{j}{k} = 1, 2, \ldots\ldots$

$$\beta_n = \frac{1}{\Delta\tau_\ell^n} \left(1 - e^{-\Delta\tau_\ell^n}\right) - e^{-\Delta\tau_\ell^n} \tag{3.20a}$$

$$\beta_{n+1} = 1 - \frac{1}{\Delta\tau_\ell^n} \left(1 - e^{-\Delta\tau_\ell^n}\right) \tag{3.20b}$$

where $\Delta\tau_{\ell}^{n} = \tau_{\ell}^{n+1} - \tau_{\ell}^{n}$.

Consequently, the diffused or scattered intensity in the downward direction at the $(n+1)^{th}$ level during the downward pass in the iteration procedure becomes

$$I\left(\tau_{\ell}^{n+1},\theta,\phi\right) = I\left(\tau_{\ell}^{n},\theta,\phi\right)e^{-\Delta\tau_{\ell}^{n}} + I_{ss}\left(\tau_{\ell}^{n+1},\theta,\phi\right) + I_{ms}\left(\tau_{\ell}^{n+1},\theta,\phi\right),$$

$$0\leqslant\theta\leqslant\pi/2 \qquad (3.21)$$

To begin the upward pass in the iteration scheme the upward traveling intensities at the ground level are determined by knowing ground reflectivity or albedo, A, and the total downward flux, F_D, which is the sum of the diffused downward flux, F_d and the unscattered flux F_{us}. Assuming the ground is a Lambertian reflector, the resulting upward traveling intensity is

$$I(z=0,\theta,\phi) = \frac{A}{\pi}\left(F_d + F_{us}\right), \quad \pi/2\leqslant\theta\leqslant\pi \qquad (3.22)$$

where the diffused downward flux is defined as

$$F_d = \int_0^{2\pi}\int_0^{\pi/2} I\left(\tau_L,\theta,\phi\right)\cos\theta\sin\theta d\theta d\phi \qquad (3.23)$$

and the unscattered flux F_{us} into a particular direction as seen by an observer along the normal line at the top of the atmosphere is a function of the angles θ and ϕ, and is defined by

$$F_{us}(\theta,\phi) = \mu_{os}F_o\, e^{-\tau_s(\theta,\phi)} \qquad (3.24)$$

where μ_{os} is the cosine of the local zenith angle at the planet's surface, and τ_s is the solar optical thickness from the top of the atmosphere to the planet's surface.

The iteration procedure in the upward direction begins by invoking the boundary condition at the ground [i.e., Eq (3.22)] and assuming a linear distribution for the intensity as function of optical depth as well as using the latest updated downward traveling intensities. Again during the upward pass we will update only the upward traveling intensities. The resulting upward traveling intensities at the n^{th} level during the upward pass can be written as

$$I\left(\tau_\ell^n,\theta,\phi\right) = I\left(\tau_\ell^{n+1},\theta,\phi\right)e^{-\Delta\tau_\ell^n} + I_{ss}\left(\tau_\ell^n,\theta,\phi\right) + I_{ms}\left(\tau_\ell^n,\theta,\phi\right)$$

$$\pi/2 \leqslant \theta \leqslant \pi \qquad (3.25)$$

where multiple scattering I_{ms} at the n^{th} level is defined by

$$I_{ms}\left(\tau_\ell^n,\theta,\phi\right) = \sum_{\Delta\bar{\theta}_j'} \sum_{\Delta\phi_k'} \left[\beta_n I\left(\tau_\ell^{n+1},\bar{\theta}_j',\phi_k'\right) + \beta_{n+1} I\left(\tau_\ell^n,\bar{\theta}_j',\phi_k'\right)\right]$$

$$\cdot P\left(\theta,\bar{\theta}_j',\phi-\phi_k'\right)\left(\cos\bar{\theta}_{j+1}'-\cos\bar{\theta}_j'\right)\Delta\phi_k' \quad . \qquad (3.26)$$

In the above expression the intensities at levels n+1 and n are multiplied by the coefficients β_n and β_{n+1}, respectively. Thereby, the coefficients role in Eq (3.26) is the opposite of that in Eq (3.19). The Gauss Seidel iteration in the upward pass continues until the top of the atmosphere is reached. This iteration procedure is repeated up

and down the atmosphere until the intensities converge to within a prescribed value.

Checking Results and Procedure

In a complex mathematical formulation of physical phenomenon such as that of scattering of light in a spherical atmosphere, usually the non-analytical solutions are obtained by numerical methods. The validity of the assumptions that were made during the formulation as well as the accuracy of the numerical solution can be checked either experimentally or by other methods. So far, the numerical results for this problem have been obtained only by Monte Carlo Methods. Collins et al (1972) used backward Monte Carlo calculations to characterize the emerging polarized radiation from spherical atmospheres, while Blattner and Wells (1973) used the same method to study the effect of neglecting polarization in molecular and turbid atmospheres. In addition, they discussed briefly the resulting error in using plane-parallel atmospheres in place of a spherical atmosphere and investigated the influence of dust layers at various altitudes on the color ratio during twilight. Also, Blattner et al (1974) used the backward Monte Carlo method to present results of sky radiation during twilight in a molecular plus ozone atmosphere. Whitney et al (1973) introduced a new method which leads to discretization of the integro-differential equation of radiative transfer. This method was applied to plane-parallel and spherical atmospheres. The resulting intensities in the plane-parallel atmospheres showed an error on the order of 5 to 10% when compared with Coulson's (1960). In addition, the resulting intensities in a spherical

atmosphere were compared with those obtained by the backward Monte Carlo method, but the comparison was inconclusive since the results appeared on semi-log paper where errors up to 100% are barely noticable. Furthermore, Whitney's calculations were limited to a very small range of observation angles. Unfortunately, this leads us to believe that Whitney's et al (1973) results cannot be used in checking results, particularly in a spherical atmosphere. Recently, Marchuk et al (1980) discussed the application of the Monte Carlo methods for obtaining numerical solutions in direct and inverse problems of radiative transfer in a spherical atmosphere.

In this dissertation we will neglect polarization since the introduced error in the scattered intensities due to neglect of polarization is relatively small (see Blattner et al, 1973).

Consider a homogeneous molecular or Rayleigh spherical atmosphere with $\tau_T = .25$. This unrealistic atmosphere is chosen to check the emerging total scattered intensities obtained by the present Quasi-Spherical method against those intensities obtained by the backward Monte Carlo method. In addition, such an atmosphere simplifies evaluating the singly scattered intensities by numerical integration methods, in order that these intensities may be compared with those obtained by the Quasi-Spherical method. Incidentally, it is very important to use the exact input parameters in the problem of scattering in a spherical atmosphere because the solution is nonlinear. The following input parameters are chosen: $R = 6378.4$ (km), $h_T = 50$ (km), $F_o = \pi$ and $\theta_o = 84.26^\circ$.

The scattering phase function in a Rayleigh atmosphere is given as

$$P_R(\Theta) = \frac{3}{16\pi}(1.0 + \cos^2\Theta) \tag{3.27}$$

where the scattering angle Θ is obtained from

$$\cos\Theta = \cos\theta\cos\theta' + \sin\theta\sin\theta'\cos\phi \quad . \tag{3.28}$$

We begin by calculating the emerging singly scattered intensities from the top and the bottom of the atmosphere. Originally, the atmosphere was divided into ten spherical shells of equal optical thicknesses and the height distribution for these shells was based on a vertically nonhomogeneous distribution of density in a Rayleigh atmosphere. The resulting geometrical thickness of the top spherical shell was approximately 34 (km). In order to obtain a finer resolution in the intensity profile we divide the top shell into ten sub-shells of equal heights above the tangent height for the zenith angle $\theta = 95^\circ$; e.g., $h_{tan} = R\left(\frac{1}{\sin\theta} - 1.0\right)$ or $h_{tan} = 24.364$ km. Nonetheless, when considering the homogeneous Rayleigh atmosphere we retained the height distribution from the non-homogeneous case. This assumption was not necessary but it simplified inputing the height distribution as a function of optical depth to our model. The zenith angle for the transmitted intensities varies between 0° and 90°, while for the reflected intensities it varies between 90° and 180°. In our calculations we considered the zenith angles 5°, 15°, 25°, 35°, 45°, 55°, 65°, 75°, 76°, 77°, 78°, 79°, 80°, 81°, ... 89.0° for the transmitted intensities and 91°, 91.5°, 92°, ... 96.5°, 97°, 97.14°, 105°, 115°, 125°, ... 175° for the reflected

intensities. Furthermore, we computed the intensities for the azimuthal angles 0°, 30°, 60°, 90°, 120°, 150° and 180°. Notice, the azimuthal plane 0° and 180° is a plane of symmetry in our problem, due to the spherical geometry and the nature of the solar radiation. Accordingly, the intensities for the azimuthal angles between 180° and 360° will not be computed. Eqs (3.13 and 14) were used in calculating the singly scattered intensities by the Quasi-Spherical method, while Eqs (3.8 and 9) were used for the same intensities by numerical integration. In the numerical integration scheme, each line of sight is divided into several segments. Also, the solar radiation at the midpoint of each segment is determined. Then, by replacing the integration in Eqs (3.8) and (3.9) with a summation we obtained the singly scattered intensities. Furthermore, the number of segments is increased until convergence is ensured. Now, the two different methods of calculation are used in the homogeneous Rayleigh atmosphere. Transmitted and reflected singly scattered intensities as a function of zenith angle in the plane of incident solar radiation are shown in Figs. 3-4 and 5, respectively. These figures indicate almost identical results as obtained by the two methods. In fact, the results obtained by the Quasi-Spherical method have higher values than those obtained by the numerical integration method at one end of the abscissa, while the opposite behavior occurs at the other end. For example, for $\theta = 5^\circ$ and 89° in Fig. 3-4 the differences are on the order of +1.5% and -1.4%, respectively. However, by increasing the number of the spherical shells from 20 to 30 the corresponding differences decrease to $\pm 1.0\%$. Such behavior is expected and, in fact, is consistent

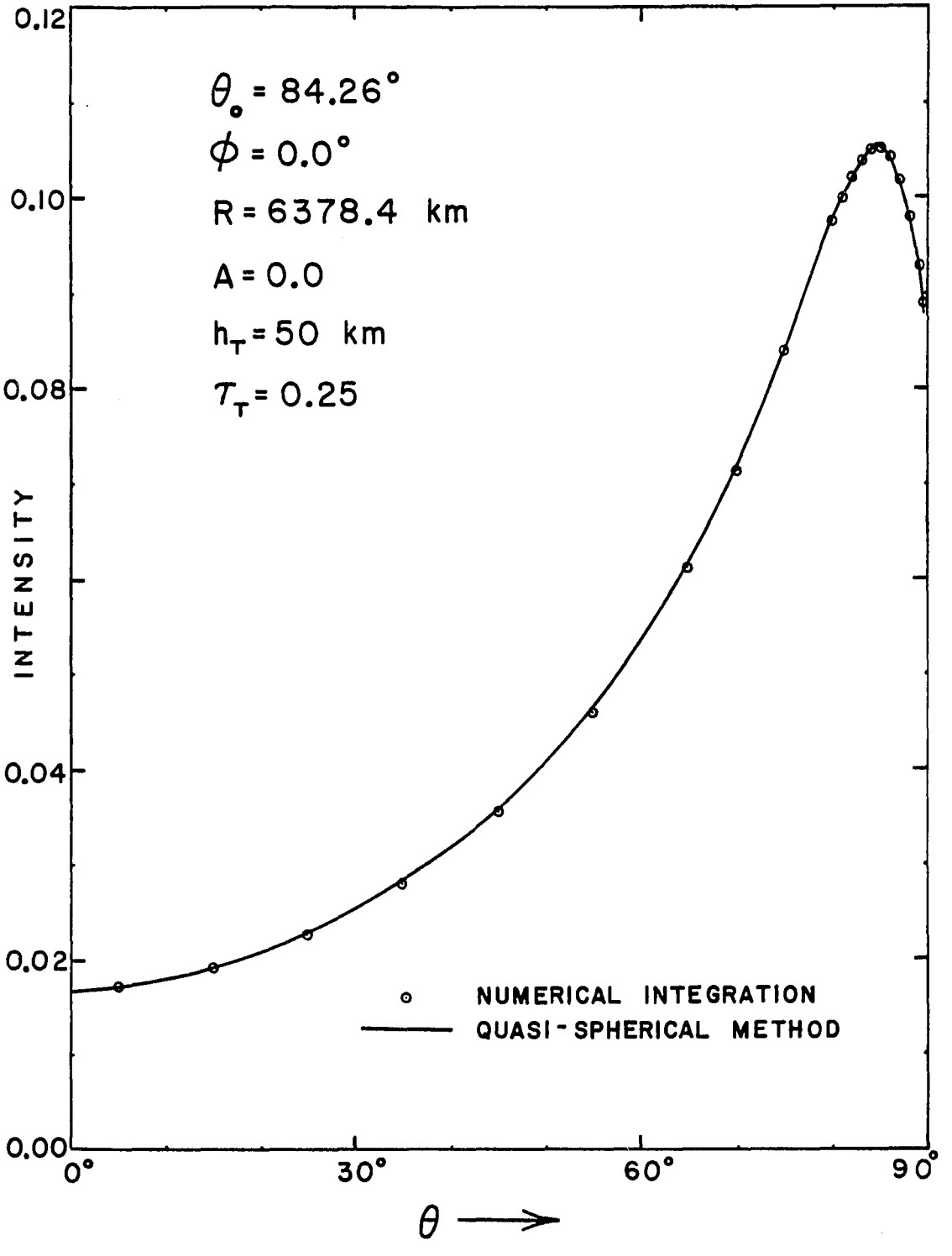

Fig. 3-4. Transmitted singly scattered intensities in a homogeneous Rayleigh atmosphere.

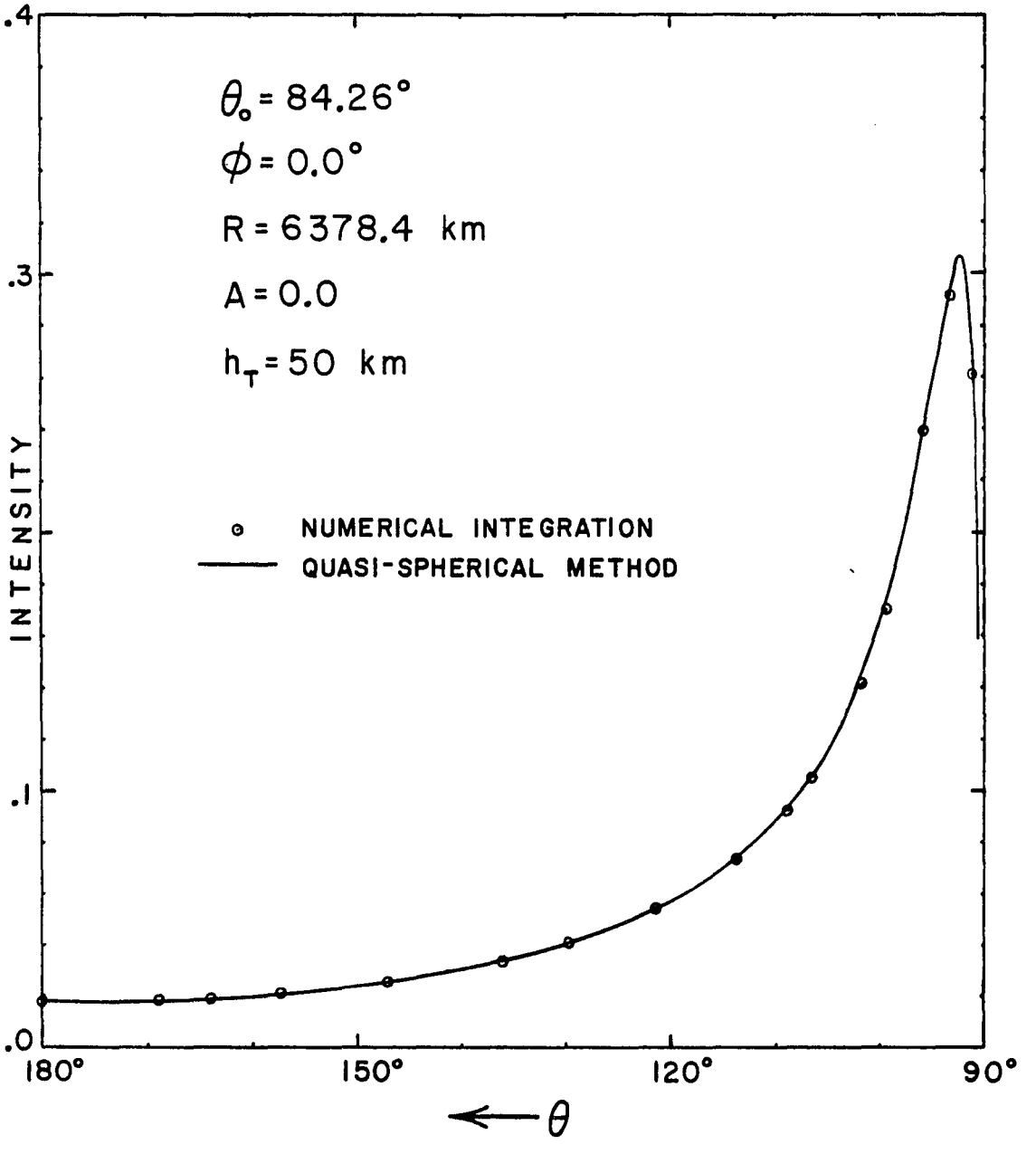

Fig. 3-5. Reflected singly scattered intensities in a homogeneous Rayleigh atmosphere.

with the observation that was made in the previous section. Therefore, the Quasi-Spherical method gives relatively accurate values for single scattering and moreover, the accuracy increases by increasing the number of spherical shells.

After computing single scattering we proceed to calculate the total emerging radiation at the top and the bottom of the homogeneous Rayleigh atmosphere by the iteration method that was outlined earlier. Also, the emerging total radiation in the same atmosphere, but a plane-parallel or flat atmosphere is computed. The resulting intensities in both spherical and flat plus the ones obtained in a polarized spherical atmosphere by the backward Monte Carlo method (see Collins et al, 1972 and Blattner, 1981) are shown in Fig. 3-6 through Fig. 3-14. Figs. 3-6 and 7 show the transmitted intensities as a function of zenith angle when A = 0.0 for the azimuthal planes (0°, 180°) and (30°, 150°), respectively. Similarly, Figs 3-8 and 9 show the transmitted intensities when A = 0.8. It is noticed that the transmitted intensities in the spherical atmosphere are always higher than those in the flat one. This is primarily due to the smaller attenuation in the spherical case. As expected, when $\theta_o \simeq 90^\circ$ in a Rayleigh flat atmosphere the transmitted intensity profile is almost symmetrical about $\theta = 0.0^\circ$ for each azimuthal plane. Such behavior is evident for both ground reflectivities A = 0.0 and 0.8 as depicted in Figs. 3-6 through 3-9. On the other hand the transmitted intensity profile in the spherical atmosphere is not symmetrical and, in fact, has higher values for the zenith angles in $\phi = 0^\circ$ and 30° than those in $\phi = 150^\circ$ and 180°. For example, in

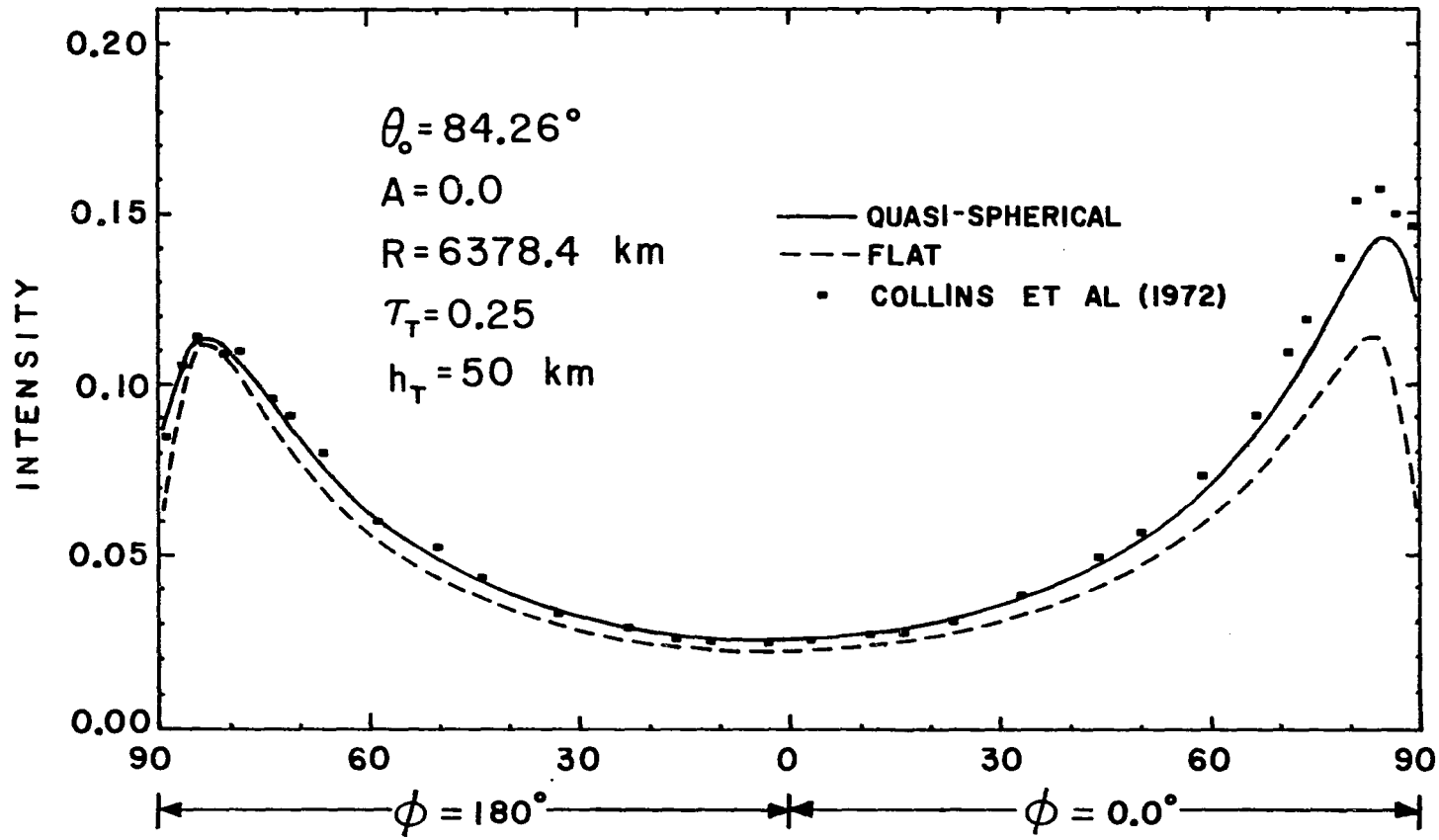

Fig. 3-6. Transmitted intensity as a function of zenith angle for the azimuthal plane (0°, 180°) in a homogeneous Rayleigh atmosphere, w/A = 0.0.

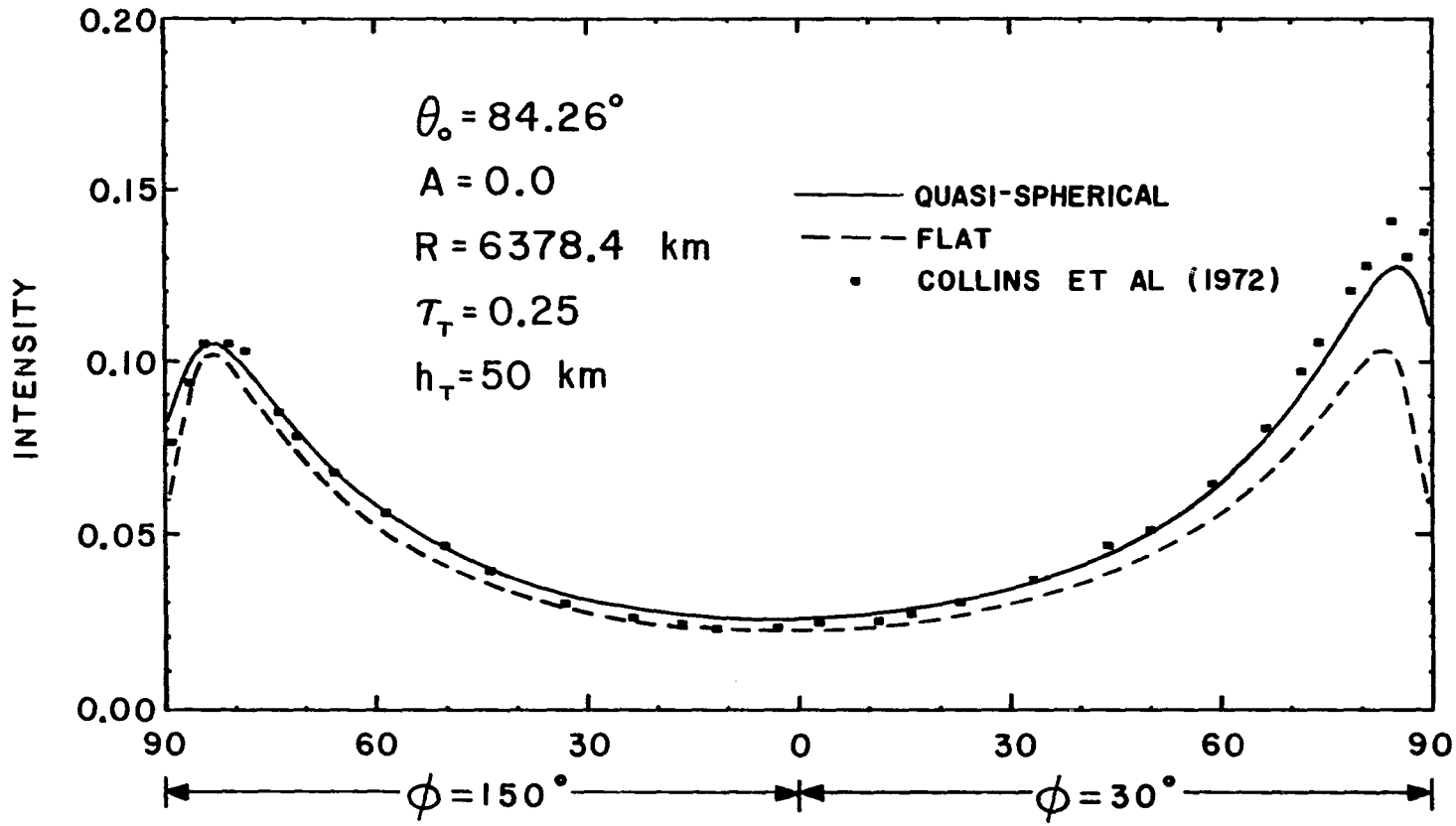

Fig. 3-7. Transmitted intensity as a function of zenith angles for the azimuthal plane (30°, 150°) in a homogeneous Rayleigh atmosphere, w/A = 0.0.

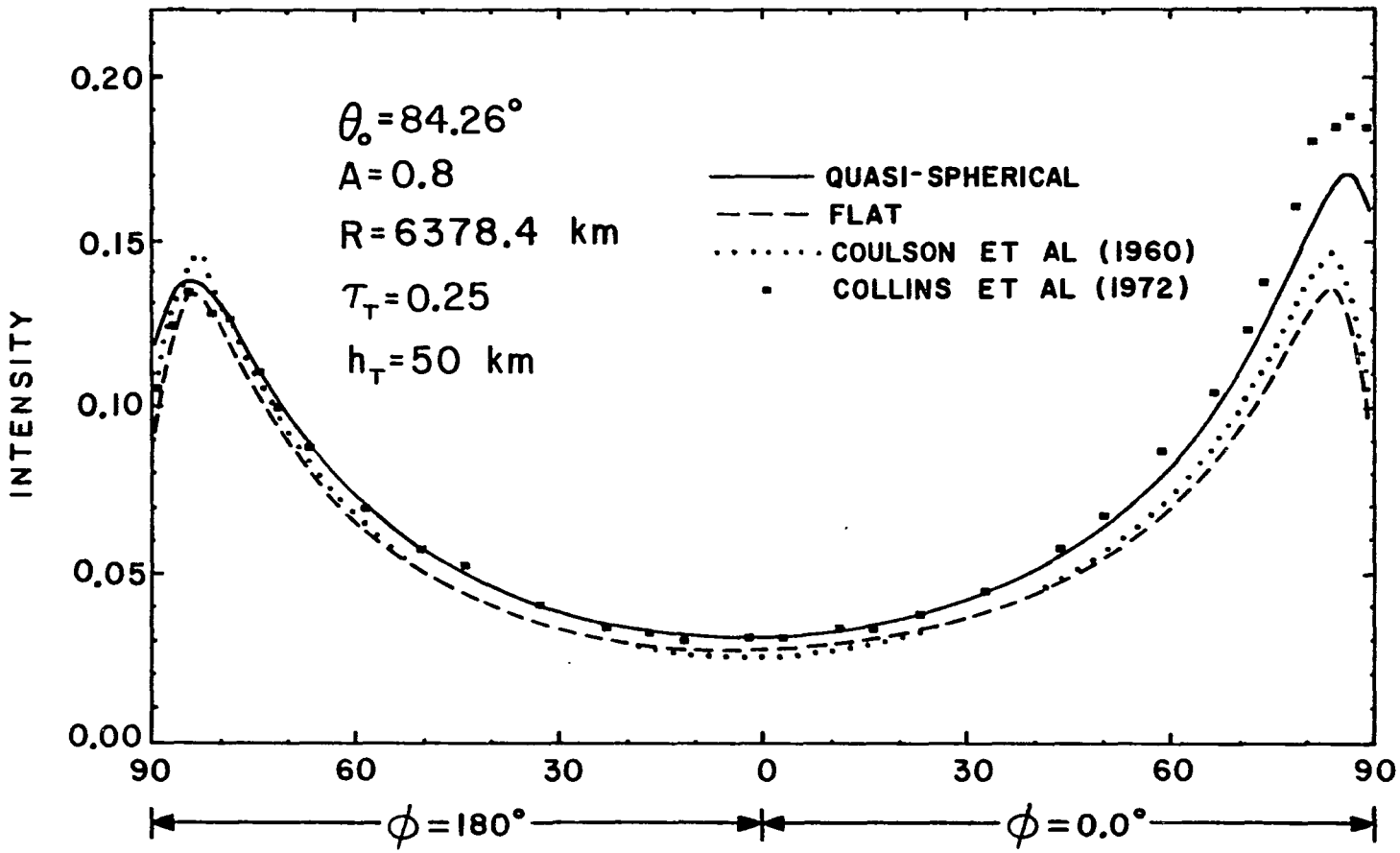

Fig. 3-8. Transmitted intensity as a function of zenith angle for the azimuthal plane (0°, 180°) in a homogeneous Rayleigh atmosphere, w/A = 0.8.

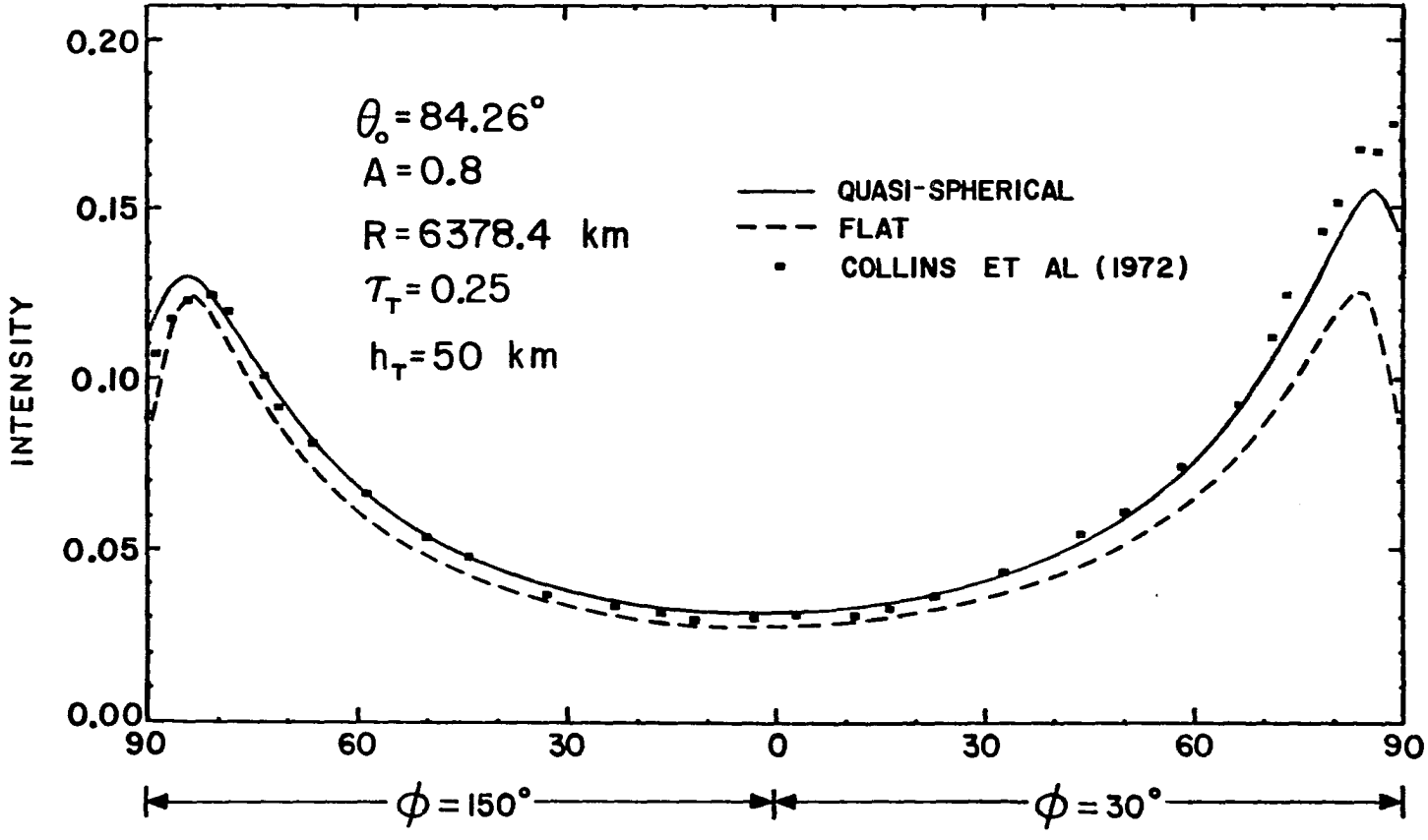

Fig. 3-9. Transmitted intensity as a function of zenith angle for the azimuthal plane (30°, 150°) in a homogeneous Rayleigh atmosphere, w/A = 0.8.

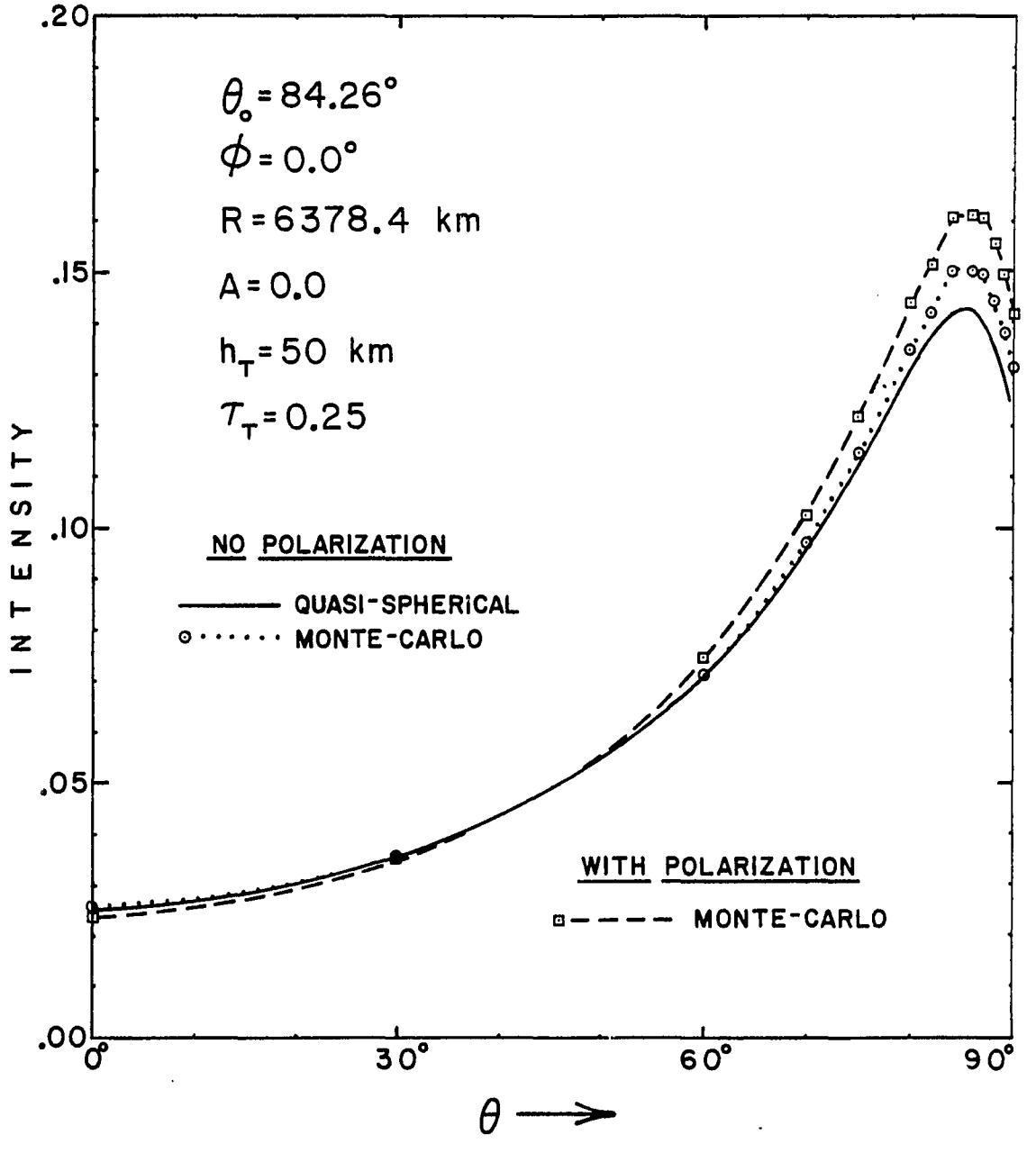

Fig. 3-10. Transmitted intensity for $\phi = 0°$ in a homogeneous Rayleigh atmosphere.

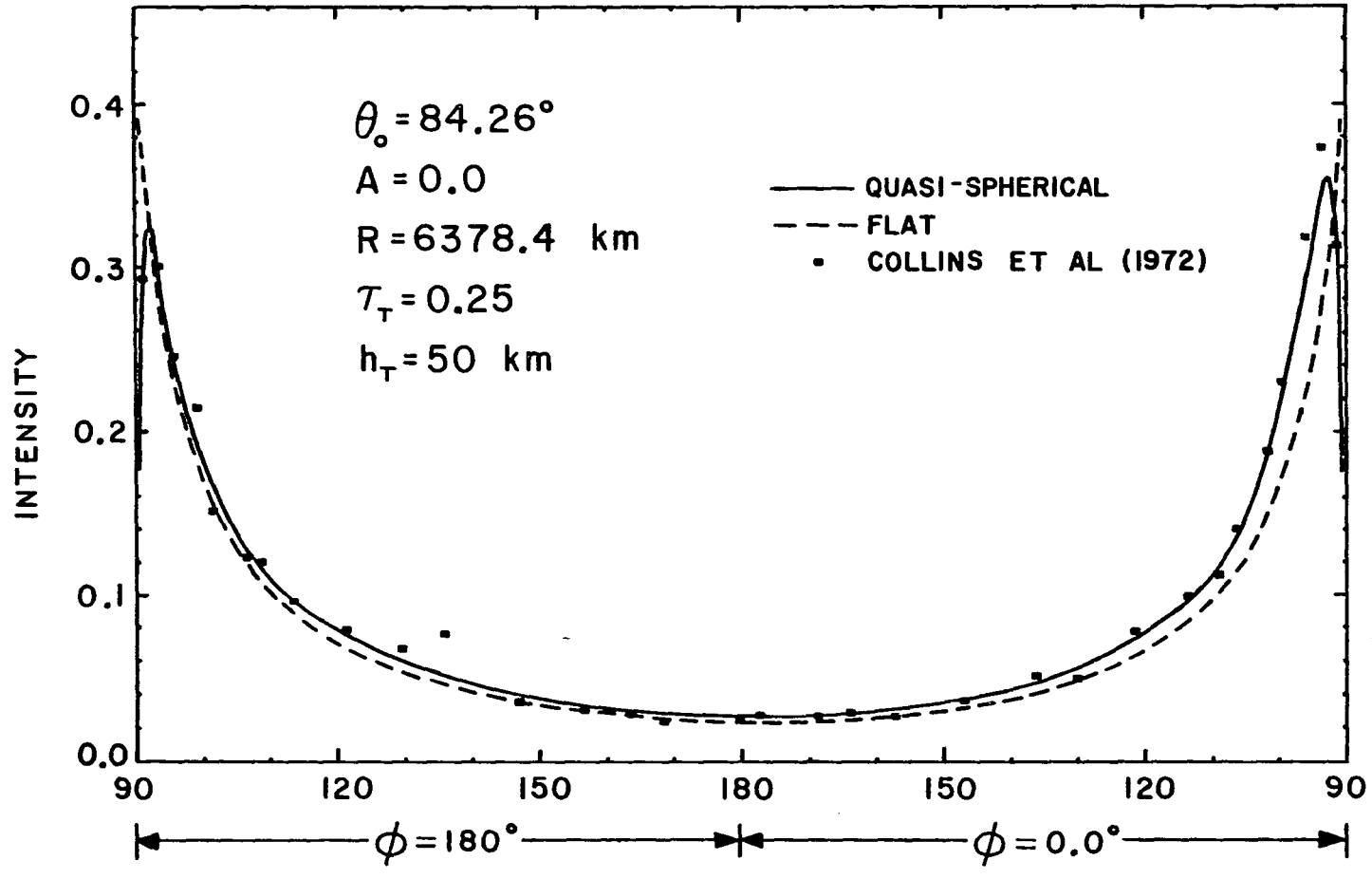

Fig. 3-11. Reflected intensity as a function of zenith angle for the azimuthal plane (0°, 180°) in a homogeneous Rayleigh atmosphere, w/A = 0.0.

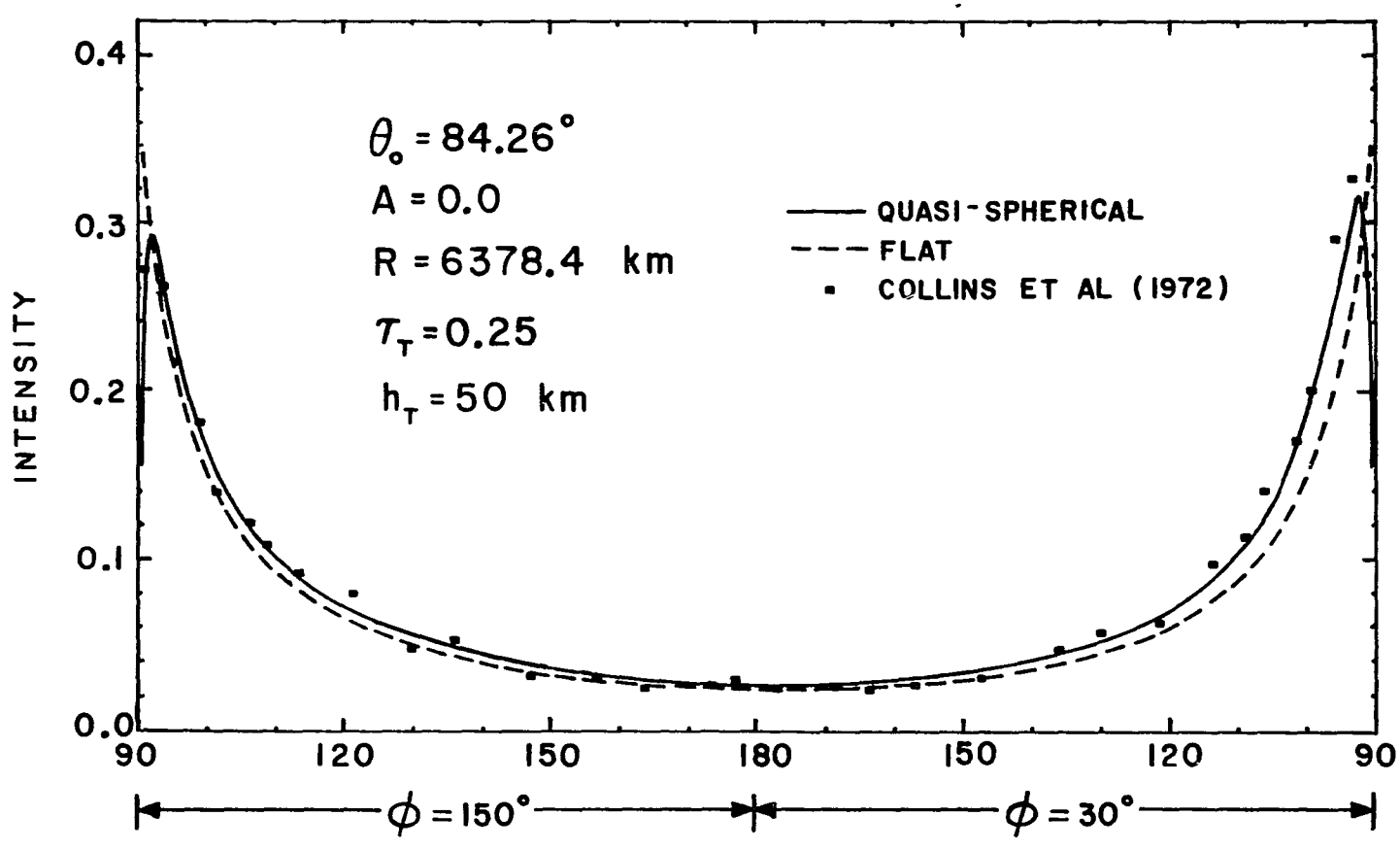

Fig. 3-12. Reflected intensity as a function of zenith angle for the azimuthal plane (30°, 150°) in a homogeneous Rayleigh atmosphere, w/A = 0.0.

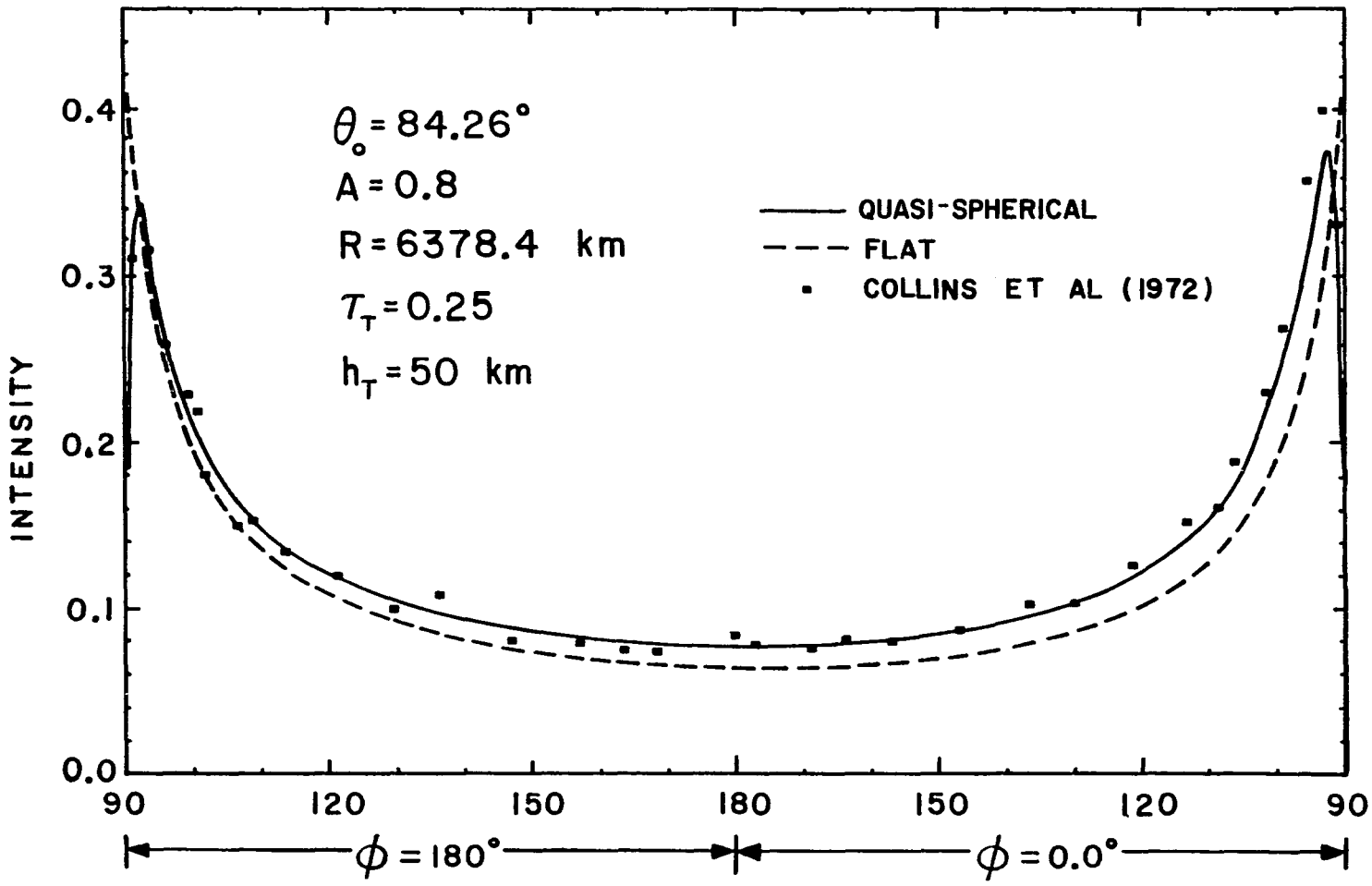

Fig. 3-13. Reflected intensity as a function of zenith angle for the azimuthal plane (0°, 180°) in a homogeneous Rayleigh atmosphere, w/A = 0.8.

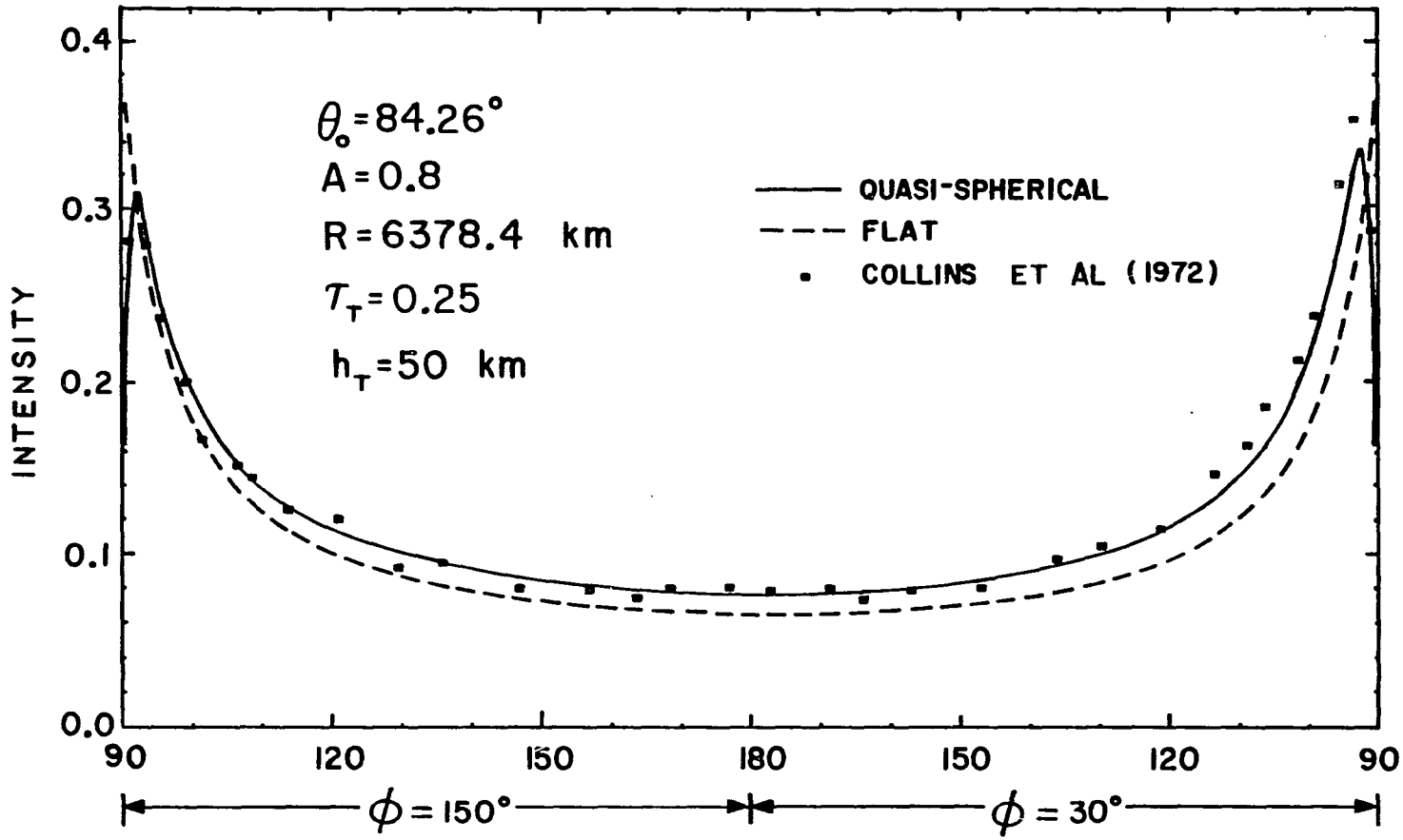

Fig. 3-14. Reflected intensity as a function of zenith angle for the azimuthal plane (30°, 150°) in a homogeneous Rayleigh atmosphere, w/A = 0.8.

Fig. 3-6 for $\theta = 85^\circ$ and A = 0 we have $I(\phi=0^\circ) = 0.143$ and $I(\phi=180^\circ) = 0.112$. Likewise, in Fig. 3-8 for the same angle but A = 0.8 we have $I(\phi=0^\circ) = 0.17$ and $I(\phi=180^\circ) = 0.138$. Consequently, the asymmetry as well as the higher values of intensities in the spherical atmosphere are attributed to the spherical geometry. Moreover, the figures show a darkening effect (or limb darkening) toward the horizon in both flat and spherical atmospheres, however, this effect is less pronounced in the spherical case. By comparing the transmitted intensities in the flat Rayleigh atmosphere with and without polarization as illustrated in Fig. 3-8, it is noticed that the intensities with polarization are larger than those without polarization as the zenith angle approaches 90° while the opposite situation occurs as θ approaches 0°. This leads us to believe that a similar behavior occurs in the spherical atmosphere. As illustrated in Figs. 3-6 through 3-9, the comparison between the transmitted intensities as computed by the Quasi-Spherical and the backward Monte Carlo methods are quite good for θ less than 70°, while for θ larger than 70° the obtained intensities by the Monte Carlo method are increasingly higher than those obtained by the Quasi-Spherical method. For example, for $\theta = 85^\circ$ the percent difference is about 10% in $\phi = 0^\circ$ and 30°, but it is much smaller in $\phi = 150^\circ$ and 180°. These differences are due partially to neglecting polarization in the calculations by the Quasi-Spherical method. Also, the approximations in evaluating single and multiple scattering contribute to these differences in addition to the inherent statistical fluctuation in the Monte Carlo calculations. Furthermore, as is the case in most complicated computer programing,

there is always a chance of programing errors in both methods. Later on we will discuss a limiting case especially designed to check for such errors. Recently, Blattner (1981) recomputed the transmitted intensities with and without polarization in the homogeneous Rayleigh atmosphere. His results show a similar behavior to that in the flat atmosphere as far as the polarization effect is concerned and the differences between the obtained results for the spherical atmosphere by the two methods have decreased. For instance, at $\theta = 85^\circ$ and $\phi = 0^\circ$ the percent difference is reduced from 10.6% to less than 5% as shown in Figs. 3-6 and 3-10, respectively.

For the above mentioned atmosphere, the reflected intensities as a function of zenith angle in the azimuthal planes (0°, 180°) and (30°, 150°) and for A = 0 and 0.8 are given in Figs. 3-11 through 3-14. In these figures we notice a reduction in the differences between the computed intensities by the Quasi-Spherical and the backward Monte Carlo methods particularly close to the horizon (i.e., $\theta \simeq 90^\circ$). Because of the spherical geometry, the major difference between the reflected intensities in the flat and the spherical atmospheres is the peak in the intensity profile at about $\theta = 92.5^\circ$. Also, as the ground reflectivity increases from 0.0 to 0.8 the differences between the corresponding intensities in the flat and spherical atmospheres are increased as illustrated in Figs. 3-11 through 3-14. Thus, the transmitted and reflected intensities as computed by the backward Monte Carlo method agree quite well with those obtained by the Quasi-Spherical method and, in fact, a

better agreement will result if polarization is included in the latter method.

Next, a vertically inhomogeneous Rayleigh atmosphere is considered with $\tau_T = 0.1$. Basically, this is the same atmosphere that was considered by Marchuk et al (1980), but again the polarization is neglected in the Quasi-Spherical method. Here, we set $\theta_o = 53.13^\circ$, $h_T = 100$ (km) and R = 6370 (km). Transmitted and reflected intensities for flat and spherical atmospheres in the azimuthal plane (0°, 180°) are shown in Figs. 3-15 through 3-18. Figs. 3-15 and 3-16 show the transmitted intensity as a function of zenith angle when A = 0.0 and 0.25, respectively. In these figures the Monte Carlo results (see Marchuk et al, 1980; Table 4.28, p. 144) are almost identical to those obtained by the Quasi-Spherical method and the very small differences can be attributed to neglecting polarization in the latter method. Similarly, the reflected intensities for A = 0 are shown in Fig. 3-17. As expected, in this more realistic Rayleigh atmosphere the intensities in the spherical case at about $\theta = 90^\circ$ are orders of magnitude smaller than the ones in the flat case. Furthermore, the results of the Monte Carlo method agree quite well with those obtained by the Quasi-Spherical method for all the zenith angle except when θ is less than 110°. Here, we suspect the disagreement is caused by positioning the observer at 100 (km) rather than 250 (km). Since it was not clear as what is the height of the observer in Marchuk's model, we did not change the height of the observer in our calculations. Because of physical considerations, one expects the reflected intensity to peak about the line of

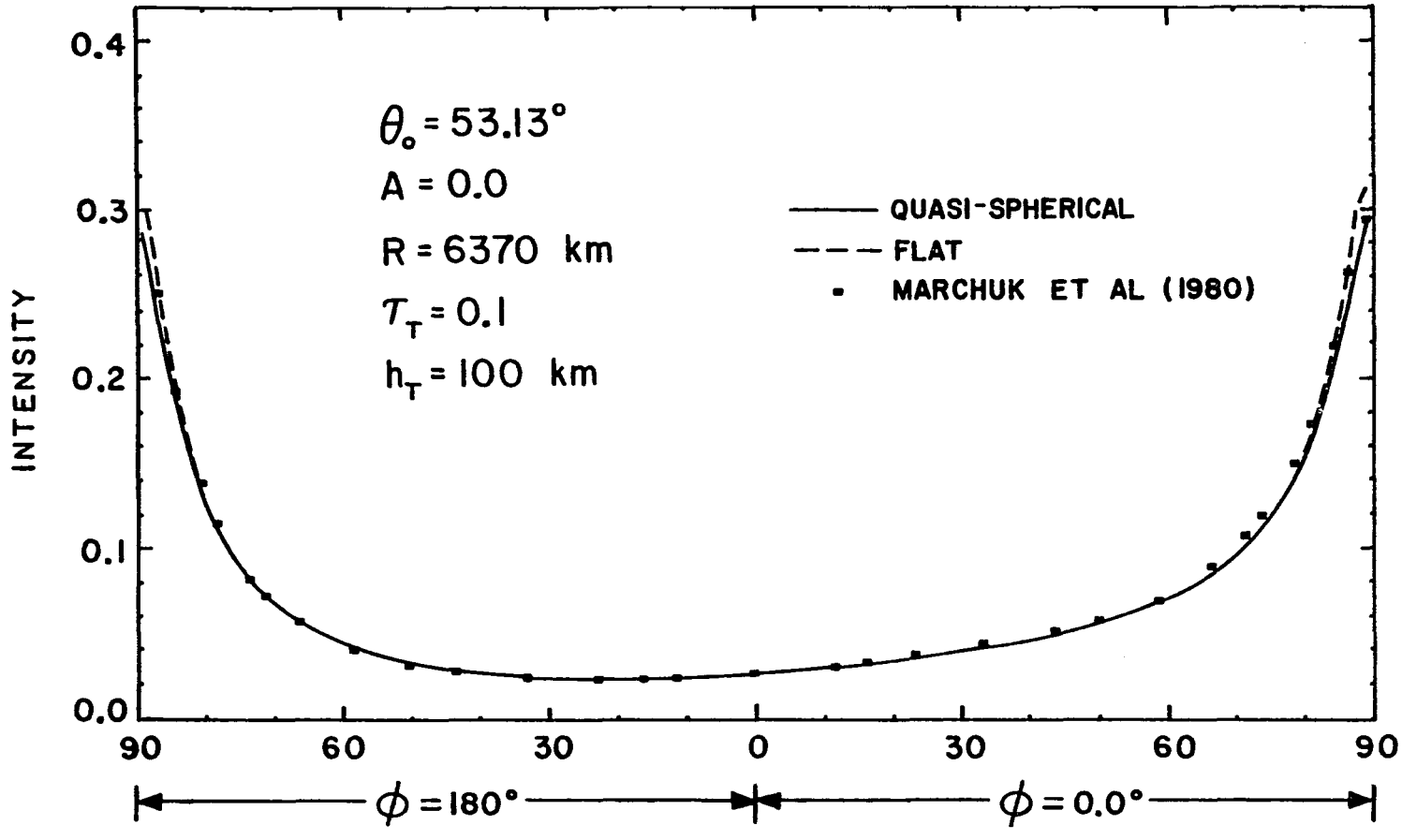

Fig. 3-15. Transmitted intensity as a function of zenith angle for the azimuthal plane (0.0°, 180°) in a non-homogeneous Rayleigh atmosphere, w/A = 0.0.

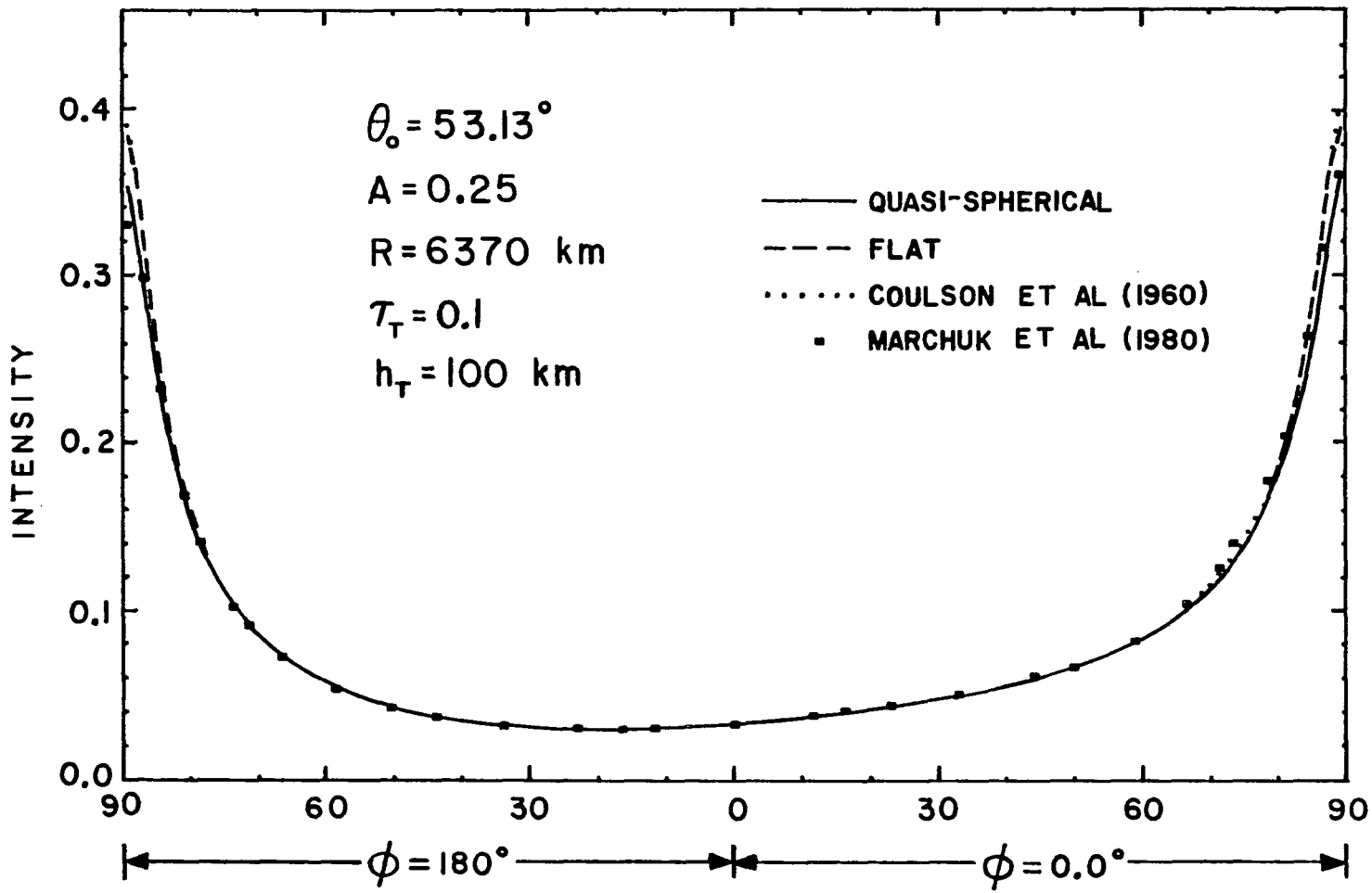

Fig. 3-16. Transmitted intensity as a function of zenith angle for the azimuthal plane (0.0°, 180°) in a non-homogeneous Rayleigh atmosphere, w/A = 0.25.

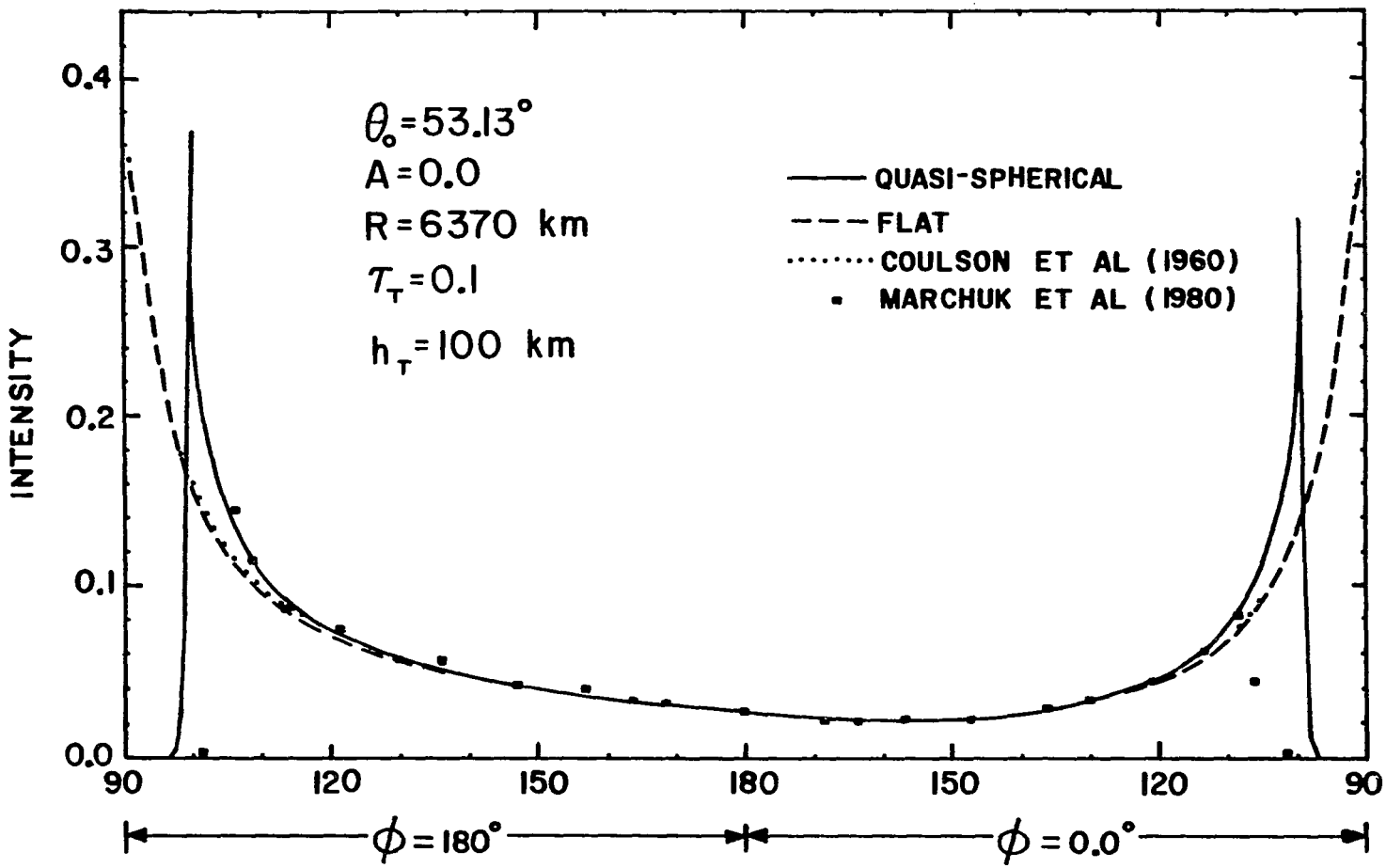

Fig. 3-17. Reflected intensity as a function of zenith angle for the azimuthal plane (0.0°, 180°) in a non-homogeneous Rayleigh atmosphere, w/A = 0.0.

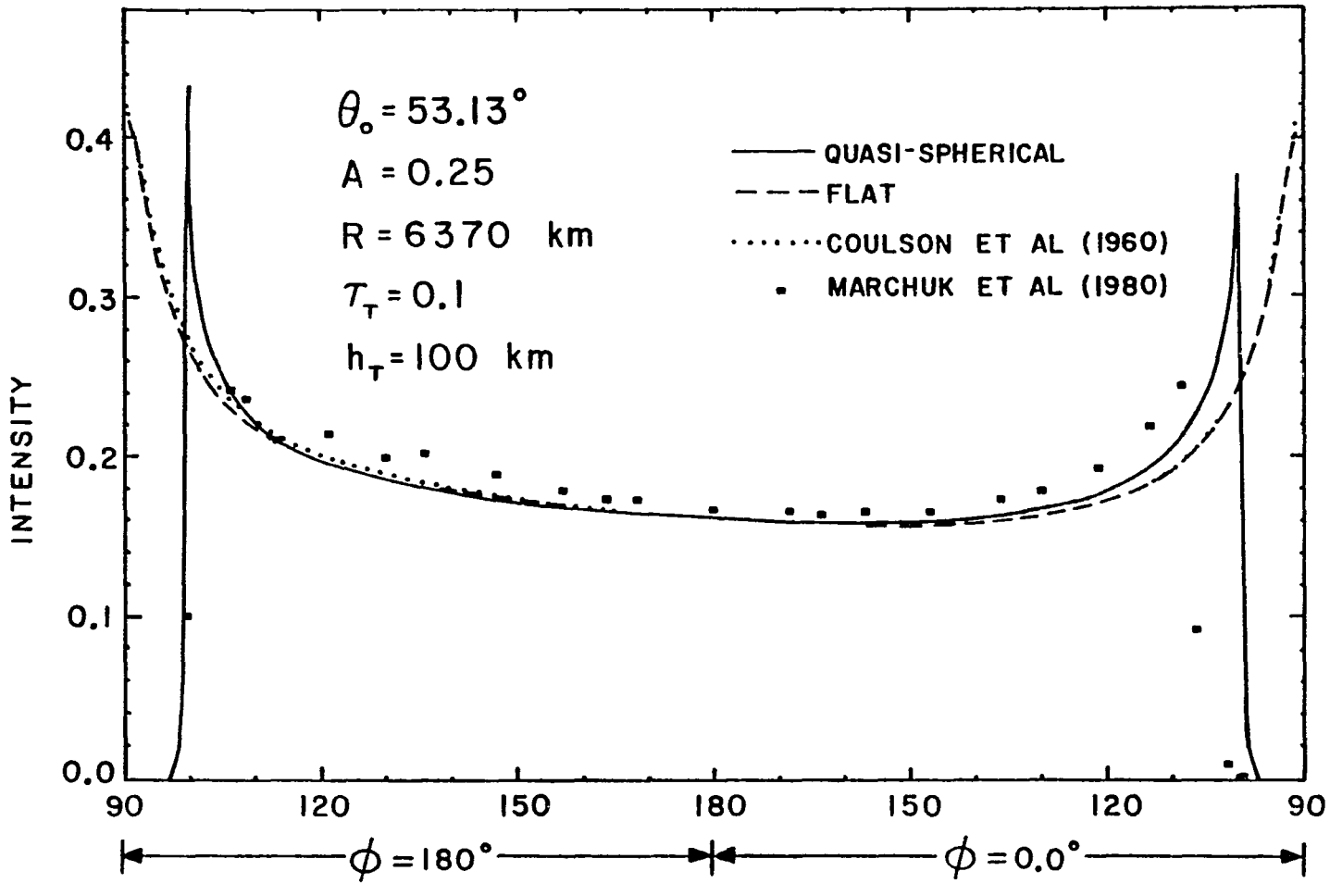

Fig. 3-18. Reflected intensity as a function of zenith angle for the azimuthal plane (0°, 180°) in a non-homogeneous Rayleigh atmosphere, w/A = 0.25.

sight tangent to the earth's surface in an optically thin atmosphere. This was confirmed by considering h_T = 50 (km) in addition to h_T = 100 (km). In the first case the reflected intensity peaked at about θ = 97°, while in the second case it peaked at about θ = 100°. Accordingly, if h_T = 250 (km) one expects the reflected intensity to peak at about θ = 106° which will bring our results much closer to Marchuk's between the zenith angles 90° and 110°. Meanwhile, when the ground reflectivity is increased to 0.25 (see Fig. 3-18) the differences between the reflected intensities as computed by the two methods have increased in contrast with the good agreement that was observed in the case of zero ground albedo. Since in our comparison with Collins et al (1972), the change in the ground albedo did not affect the resulting good agreement in the reflected intensities, we suspect that Marchuk is not considering properly the effect of the reflected radiation from the earth's surface.

Checking the results obtained by the Quasi-Spherical method against those obtained by the Monte Carlo methods indicates that this new method of computation is accurate. Also, the intensity profiles are smooth as illustrated in Figs. 3-6 through 3-18, since this method does not suffer from the inherent statistical fluctuations of the Monte Carlo methods which was evident in the results of Collins et al (1972) and Marchuk et al (1980). Above all the computing time of this method is quite fast when compared with that of the Monte Carlo methods. For example, in the case of a homogeneous Rayleigh atmosphere the computing time which includes compiling and execution times for the emerging

radiation in the spherical atmosphere is less than 90 seconds on CDC Cyber 175. Unfortunately, the computing time was not reported for the Monte Carlo calculations.

As the radius of the spherical atmosphere approaches infinity, the geometry of the atmosphere becomes essentially plane-parallel. So by increasing the radius of the earth by one hundred times, but still employing the quasi-spherical method, the resulting intensities should, in principle, be identical to those obtained in the plane-parallel or flat atmosphere. This situation provides a way to check the procedure of the Quasi-Spherical method and helps to check for computer programing errors. Now, consider a vertically inhomogeneous conservative atmosphere. Also, let the angle of the incident sun be equal to 85°, since for this low angle the differences between the results for spherical and flat atmospheres are much larger than those for a high angle of the sun. Moreover, assume $h_T = 50$ (km), $R = 100R_o$, $R_o = 6370$ (km), $F_o = 1.0$, $A = 0.1$ and $\tau_T = .195$. Here, the atmosphere consists of aerosols plus molecules. The total Rayleigh optical depth is $\tau_R = 0.145$, while the total aerosol or Mie optical depth is $\tau_m = 0.05$. The comparison between the transmitted intensities in both flat and spherical atmospheres at the zenith angles 5°, 15°,..., 75°, 85°, and for the azimuthal angles 0° and 180° are given in Table 3-1. By comparing these intensities it is obvious that their values are very close and, certainly, the maximum percent difference is less than 0.3%. Similarly, in Table 3-2 the reflected intensities are compared in both flat and spherical atmospheres at the zenith angles 95°, 105°,..., 165°, 175°. Again the intensities in both atmospheres are almost identical except

Table 3-1. Comparison of transmitted intensities in plane-parallel and spherical atmospheres for τ_T = .195. (Special Case for $\underline{R = 100R_o}$).

θ	$\phi = 0°$			$\phi = 180°$		
	I (spherical)	I (flat)	ΔI%	I (spherical)	I (flat)	ΔI%
5°	.0056646	.0056528	.209	.0054541	.0054428	.209
15°	.0063387	.0063256	.208	.0056523	.0056405	.209
25°	.0075860	.0075702	.208	.0063418	.0063286	.208
35°	.0096097	.0095895	.210	.0075612	.0075456	.206
45°	.0128659	.0128385	.213	.0094789	.0094597	.203
55°	.0184452	.0184051	.218	.0124391	.0124144	.199
65°	.0294199	.0293539	.225	.0172257	.0171926	.192
75°	.0602395	.0600983	.235	.0257159	.0256704	.177
85°	.1452139	.1448291	.266	.0374014	.0373674	.091

$$\Delta I\% = \frac{I\ (\text{spherical}) - I\ (\text{flat})}{I\ (\text{spherical})} * 100$$

Table 3-2. Comparison of reflected intensities in plane-parallel and spherical atmospheres for $\tau_T = .195$. (Special Case for $R = 100R_o$).

	$\phi = 0°$			$\phi = 180°$		
θ	I (spherical)	I (flat)	$\Delta I\%$	I (spherical)	I (flat)	$\Delta I\%$
95°	.1305647	.1294264	.879	.0681166	.0680084	.159
105°	.0481665	.0479484	.455	.0336242	.0335885	.106
115°	.0267085	.0266174	.342	.0215861	.0215583	.129
125°	.0175482	.0174967	.294	.0156173	.0155944	.147
135°	.0127344	.0127004	.268	.0121117	.0120921	.161
145°	.0099223	.0098975	.251	.0098447	.0098276	.174
155°	.0082297	.0082102	.238	.0083405	.0083251	.185
165°	.0072757	.0072591	.228	.0073896	.0073751	.196
175°	.0068693	.0068543	.218	.0068974	.0068832	.207

$$\Delta I\% = \frac{I \text{ (spherical)} - I \text{ (flat)}}{I \text{ (spherical)}} * 100$$

close to the horizon where the sphericity effect is important. The maximum percent difference in Table 3-2 occurs at $\theta = 95^\circ$ and $\phi = 0^\circ$ and is on the order of 0.88%.

Thus far, the Quasi-Spherical method has been developed to study the problem of scattering in a spherical atmosphere. This method is applicable to a planetary atmosphere when the height of the atmosphere is much smaller than the radius of the planet. The emerging radiation in homogeneous and nonhomogeneous Rayleigh atmospheres as calculated by the Quasi-Spherical and the Monte Carlo methods compare quite well, particularly if polization is neglected in the Monte Carlo calculations. Also, the emerging radiation in the conservative spherical atmosphere of $\tau_T = 0.195$ converges to that of the flat atmosphere when the radius of the earth approaches infinity.

CHAPTER IV

APPLICATIONS AND DISCUSSION

Many branches of science including radio communications, meteorology, astronomy, nuclear physics, geophysics, aviation and others require reliable information on the composition and behavior of the earth's atmosphere. Frequently, such information may be obtained through an accurate interpretation of the measured skylight. For a long time ground and balloon based measurements have been used. More recently, however, satellite and rocket based measurements have also been used. For the past three decades most analyses of measurements have been based on the application of the radiative transfer equation for a plane-parallel atmosphere. Sometimes this leads to a wrong interpretation of the physical nature of the atmosphere. These errors result primarily from the neglect of the sphericity of the atmosphere. It will be shown in this chapter that as long as the solar zenith angle is smaller than 75° the neglect of the sphericity of the atmosphere introduces no detectable errors in a ground based measurement. However, in the case of satellite based measurements the flat atmosphere gives erroneous results for zenith viewing angles close to the horizon at all solar zenith angles. Furthermore, a spherical atmosphere must be considered in analyzing measured skylight during twilight. Rozenberg (1966) has developed techniques for obtaining the distribution of

aerosols and other particles as a function of height during twilight, particularly in the upper parts of the atmosphere. The accuracy of the inferred information is highly dependent on the application of the radiative transfer equation to a spherical atmosphere. In addition, the analyses by various workers of several existing measurements of skylight during twilight are dependent upon using a realistic and economical method of solution to the problem of light scattering in the spherical atmosphere, and as a result, quantitative analyses have yet to be performed.

The Quasi-Spherical method will be used in this chapter to characterize the scattered light in a conservative and vertically inhomogeneous atmosphere containing aerosols and molecules. Again, polarzation and absorption will be neglected in all calculations. For both spherical and plane-parallel atmospheres the emerging 0.5 μm radiation will be presented for several zenith angles of incident sunlight. Flux conservation in the spherical atmosphere will also be examined. Finally, the changes in the transmitted and reflected intensities resulting from the inclusion of a stratospheric aerosol layer and two tropospheric aerosol pollution models will be discussed.

Further modification of the Quasi-Spherical method to include ray bending and refraction, which are very important when the angle of incident sunlight is close to grazing, can be used to analyze, for example, Coulson's (1980 and 1981) recent series of measurements of skylight at the zenith during twilight on the island of Hawaii. This task is not undertaken at this time and will be left for future work.

Scattering in Spherical and Plane-Parallel Atmospheres

The application of the radiative transfer equation to both plane-parallel and spherical conservative atmospheres is considered in the absence of absorption for the case of 0.5 μm radiation. The aerosols are composed of non-absorbing spherical particles. The index of refraction of these particles is assumed to be 1.54. The electromagnetic radiation scattering parameters for a spherical particle are computed from the Mie scattering formulae. Mie scattering theory is well known, and it has been discussed by several authors, for example, Stratton (1941) and Van de Hulst (1957). The size distribution of aerosols is chosen to be Junge type and is given by

$$\frac{dN}{dr} = Cr^{-(\nu + 1)}, \quad r_{min} \leq r \leq r_{max} \tag{4.1}$$

where N is the number of particles per unit volume of radius r and C is an arbitrary constant and the value of ν is assumed to be 2.5. The size of aerosols is assumed to vary from r_{min} = .02 μm to r_{max} = 5.02 μm with increments of .04 μm. Fig. 4-1 illustrates the normalized distribution of aerosols and molecules per unit volume as a function of height which are obtained from Elterman's (1968) report (See Table 4.11, p. 32). On a clear day in Tucson, Arizona, a typical value of the total optical depth of aerosols τ_m is taken to be 0.05 at 0.5 μm wavelength, and the total optical depth of molecules, τ_R, is 0.145. Thus, the total normal optical depth, τ_T, is defined as

$$\tau_T = \tau_m + \tau_R \quad . \tag{4.2}$$

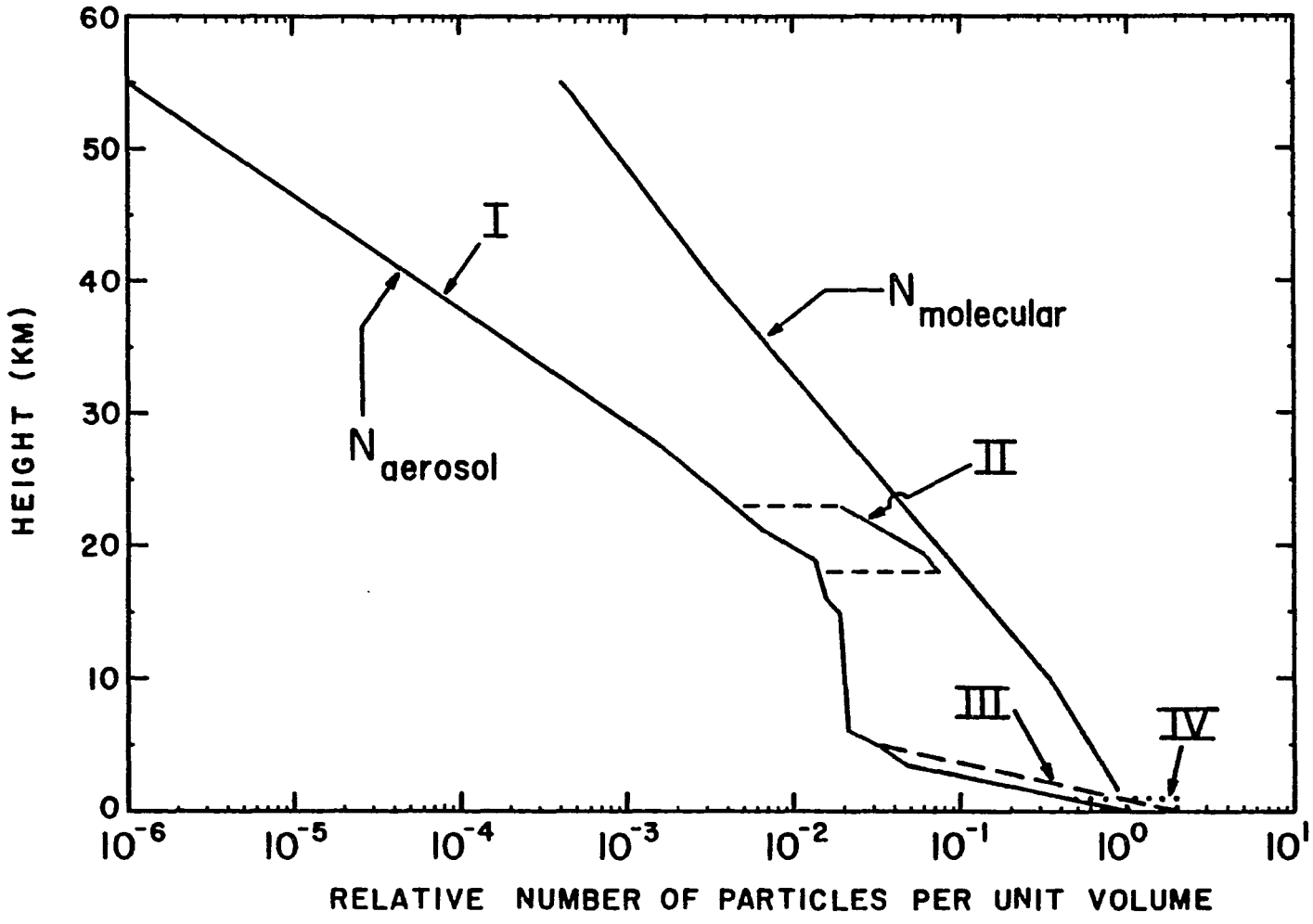

Fig. 4-1. Normalized number of molecules and aerosols as a function of height (after Elterman, 1968).

The method of obtaining the height distribution as a function of optical depth will be discussed in appendix A.

The computations of Rayleigh and Mie scattering phase functions in terms of the scattering angle are performed for the angles 0° through 180° at one degree increments. Then, the resulting value of the phase function for the scattering angle that corresponds to the midpoint of the zenith and azimuth angular interval of the incident and scattered beams is used as an average value for the whole interval. However, in the case of Mie scattering in the forward and backward directions an average value over all the angular interval is used instead of that at the midpoint. Also, normalization of the scattering phase functions are insured by applying an appropriate normalization in computing multiple scattering. Furthermore, the scattering phase function within each layer in the single and multiple scattering terms is composed of a weighted sum of the Rayleigh scattering phase function, P_R, and the Mie scattering phase function, P_m, which is equivalent to

$$P = \frac{\Delta\tau_R P_R + \Delta\tau_m P_m}{\Delta\tau_m + \Delta\tau_R} \tag{4.3}$$

where $\Delta\tau_R$ and $\Delta\tau_m$ are the Rayleigh and Mie optical depths, respectively, for the layer. For details of this procedure see Herman and Browning (1965).

The emerging radiation at the top and bottom of both spherical and plane-parallel atmospheres is computed at the previously mentioned zenith and azimuthal angles (see Chapter III). The height of both atmospheres is assumed to be 50 km. In addition, each atmosphere is

divided into ten layers of equal optical depths. Also, the following parameters are assumed: $F_o = 1.0$, $A = 0.1$ and $R = 6370.0$ km. The Quasi-Spherical method as outlined in the previous chapter is used in obtaining results in the spherical atmosphere, while a semi-analytic Gauss-Seidel iterative method that uses a linear fit for the intensity as a function of optical depth is used in the plane-parallel atmosphere (for details see Herman et al, 1980). For an observer located at the top of the spherical atmosphere the lines of sight with zenith angles between 90° and 97.155° do not touch the ground. Since the geometrical thickness of the top layer is relatively large, the atmosphere above the tangent height ($h_{tan} = 24.33$ km) of the $\theta = 95°$ line of sight is divided into 9 layers of equal heights to improve the resolution of the intensity profile as a function of height and scanning angle.

Convergence in the iteration procedure was obtained in 5 passes up and down the atmosphere, and the total computing time for both plane-parallel and spherical atmospheres on The University of Arizona CDC Cyber 175 was less than two and one-half minutes.

Downward traveling beams at the viewing zenith angles 65°, 75° and 85° for both atmospheres as a function of optical depth in the plane of incident sun of angle 85° are shown in Fig. 4-2. It is noticed that near the top of the atmosphere the intensities at each zenith angle in the flat model are larger than those in the spherical one. However, as the optical depth increases the results of the two models gradually approach one another eventually crossing, and subsequently the resulting intensities of the spherical atmosphere become increasingly larger than

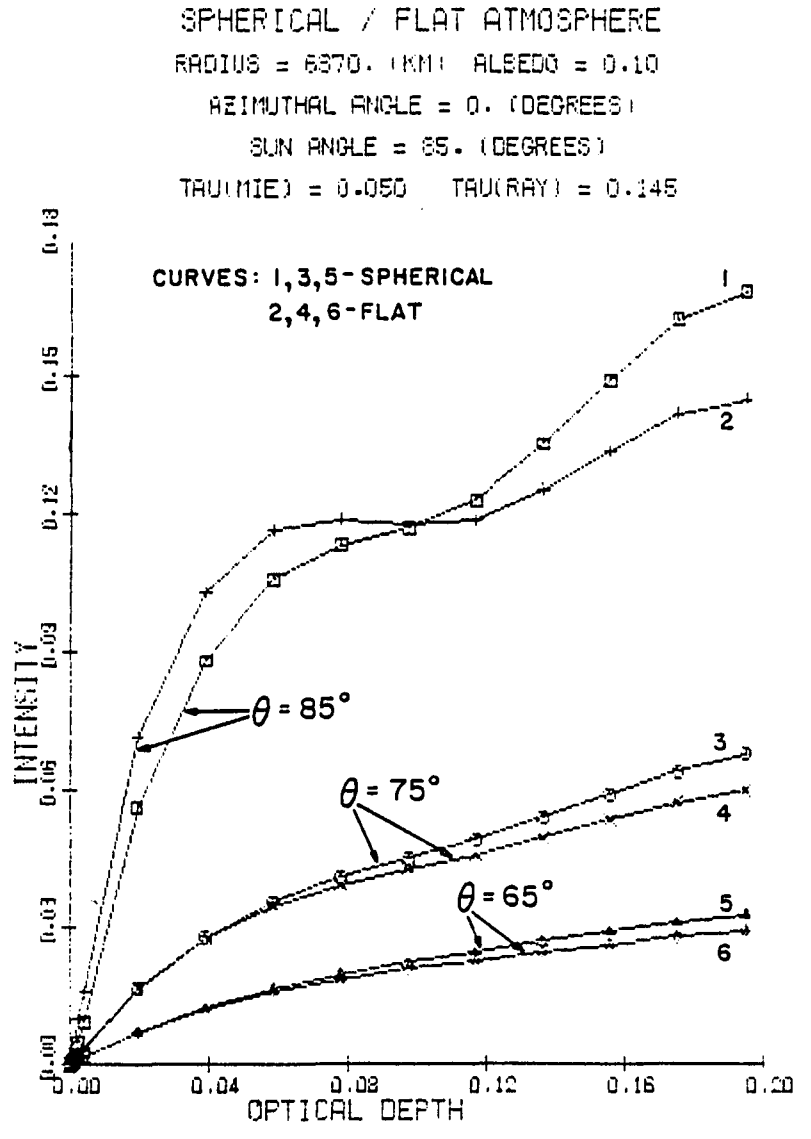

Fig. 4-2. Intensities as a function of optical depth for downward traveling beams in flat and spherical atmospheres at θ = 85°, 75° and 65°.

those of the flat atmosphere. Furthermore, the differences between the results of the two models increase as the viewing zenith angle increases. For example, on the ground (i.e., $\tau_T = .195$) at $\theta = 65^\circ$, 75° and 85° the percent differences are on the order of 10%, 13% and 16%, respectively. It is interesting to note that the height of the point at which both models give identical values decreases for increasing zenith angle. Near the ground the attenuation in the spherical atmosphere is smaller than that in the flat one which explains the resulting higher values of intensity in the spherical model. However, the larger values of intensity in the flat atmosphere near the top can be contributed to adding more multiple scattering to the total intensity with very little attenuation when compared with that in the spherical atmosphere. Similar to Fig. 4-2 a comparison of upward traveling beams in both flat and spherical atmospheres at $\theta = 95^\circ$, 105° and 115° is shown in Fig. 4-3. The major difference appears in comparing the intensity profiles at $\theta = 95^\circ$ which corresponds to a line of sight that goes through the atmosphere without touching the ground. At the top of the atmosphere the intensity of the spherical model is much smaller than that of the flat atmosphere, for instance, I(flat) = .129 and I(spherical) = .053 (see insert in Fig. 4-3). Here, the flat model gives erroneous results for the real atmosphere. Conversely, the spherical model gives results that are in agreement with physical intuition. The intensity increases from a minimum value at the top of the atmosphere to a maximum value of 0.1966 at $\tau = 6.67 \times 10^{-4}$ or h = 35.74 km, then decreases monotonically until reaching the line of sight that touches

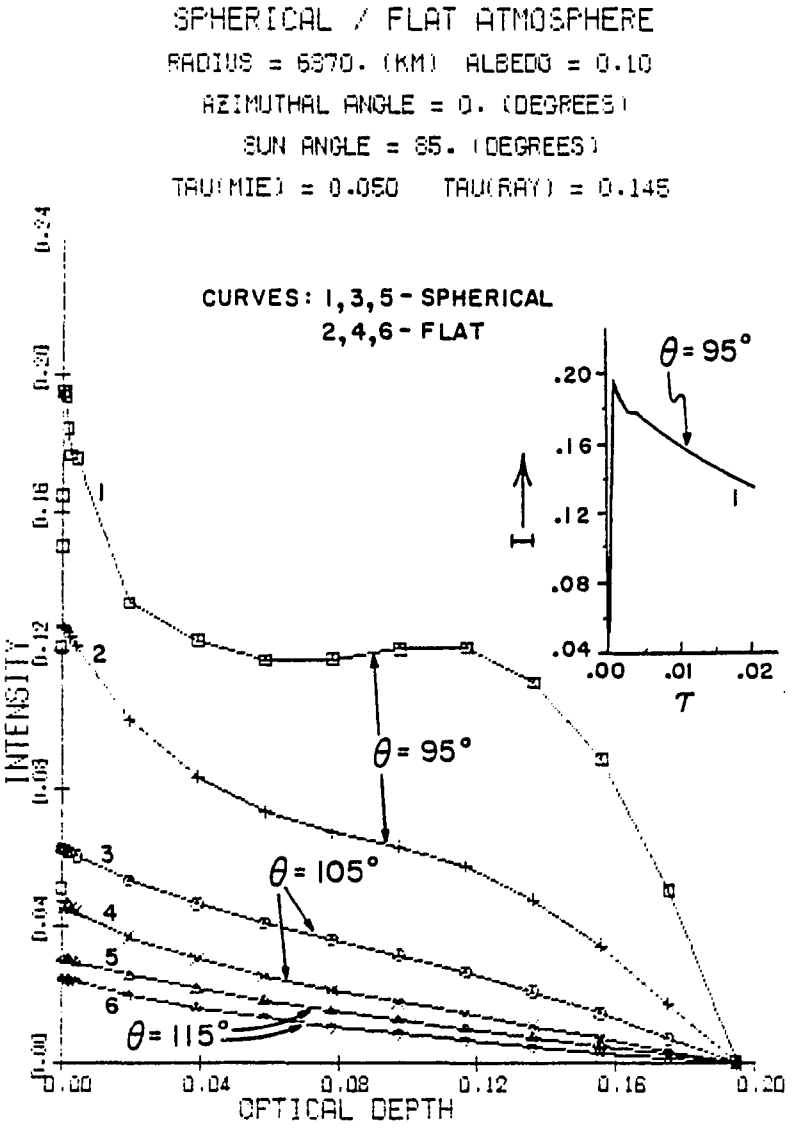

Fig. 4-3. Intensities as a function of optical depth for upward traveling beams in flat and spherical atmospheres at θ = 95°, 105° and 115°.

the ground where a discontinuity in the intensity profile could occur depending on the ground reflectivity and the total optical depth. Moreover, the upward traveling beams for all the zenith angles in the spherical atmosphere, with the exception of $\theta = 95^{\circ}$ near the top of the atmosphere, lie higher than those in the flat atmosphere and the corresponding relative differences increase as the zenith angle approaches the horizon. This behavior occurs in large part because the attenuation in the flat atmosphere is larger than that in the spherical atmosphere. Hence, the sphericity effects as a function of optical depth are more evident for upward traveling beams, particularly near the horizon. Similar observations about the intensity in both atmospheres as a function of optical depth can be made for the other azimuthal angles. However, for solar angles less than 85° these differences become smaller.

Since the application of the radiative transfer equation to a plane-parallel atmosphere is relatively simpler and more economical than that in a spherical atmosphere, it is desirable to determine when the application of the plane-parallel model is valid, particularly in finding the emerging radiation from the top and bottom of the previously mentioned atmosphere for all solar zenith angles. For example, it is desirable to determine the error in ground based measurements of skylight that results from considering a plane-parallel geometry for the atmosphere instead of a spherical one. Our results indicate that the two models give almost identical transmitted intensities for a high solar zenith angle in all azimuthal planes. However, as the solar

zenith angle approaches the horizon the difference between the results of the two models become increasingly larger. This behavior is illustrated in Figs. 4-4 through 4-6 which show the transmitted intensities as a function of zenith angle in the azimuthal plane (0°, 180°), due to incident sunlight at θ_o = 5°, 75° and 85°, respectively. The peak in the intensity profile in each figure is due to the aureole or forward scattering of aerosols in both models. As shown in Figs. 4-4 and 4-5 the resulting transmitted intensities in both models are almost identical. However, differences on the order of 10 to 30% occur when θ_o = 85° in the azimuthal plane (0°, 180°) as depicted in Fig. 4-6. Similar observations can be made about these intensities in the other azimuthal planes, for example, Fig. 4-7 shows the transmitted intensities in the azimuthal plane (30°, 150°). Further illustration of the nature of these differences can be shown when a fixed viewing zenith angle is considered for varying solar zenith angle. As an illustration, the transmitted intensities in both models in the azimuthal plane (30°, 150°) away from the aureole at the solar zenith angles 5° through 85° are shown in Fig. 4-8 for the viewing zenith angle θ = 88°, 80°, 75° and 45°. It is clear that noticable differences in the transmitted intensities occur for θ = 80° and 88°. Here the flat model shows higher values than the spherical one for θ_o<75° and the opposite behavior occurs for θ_o>75°. For example, at θ_o = 5° and ϕ = 30° and 150° the intensity in the flat model is about 1.5% larger than that in the spherical one at θ = 80° and 88°, while at θ_o = 85° and ϕ = 30° the intensity in the spherical model is larger than that in the flat one

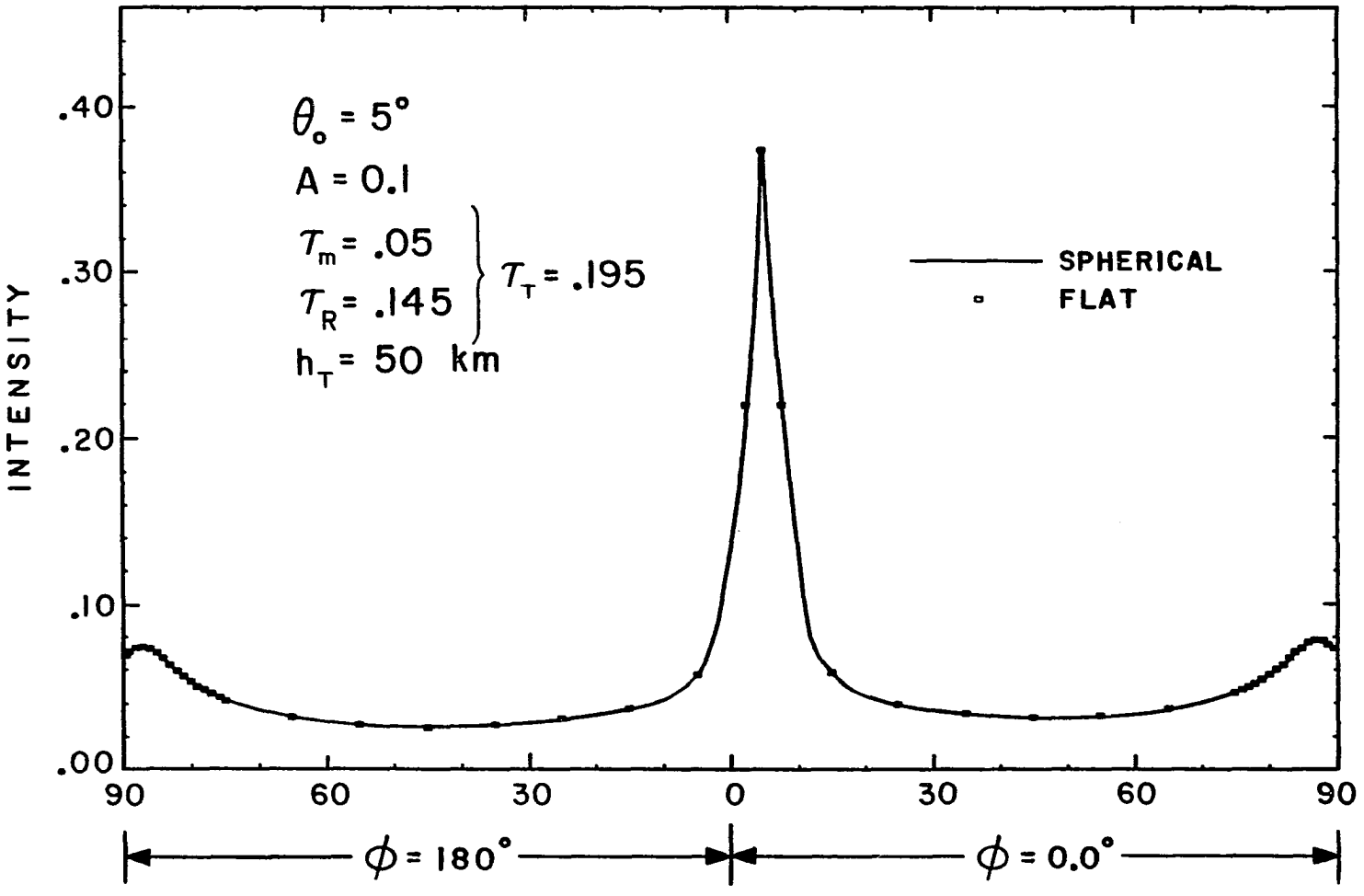

Fig. 4-4. Transmitted intensity as a function of zenith angle for the azimuthal plane (0°, 180°) in a conservative atmosphere. The solar zenith angle θ_o = 5° and τ_T = .195.

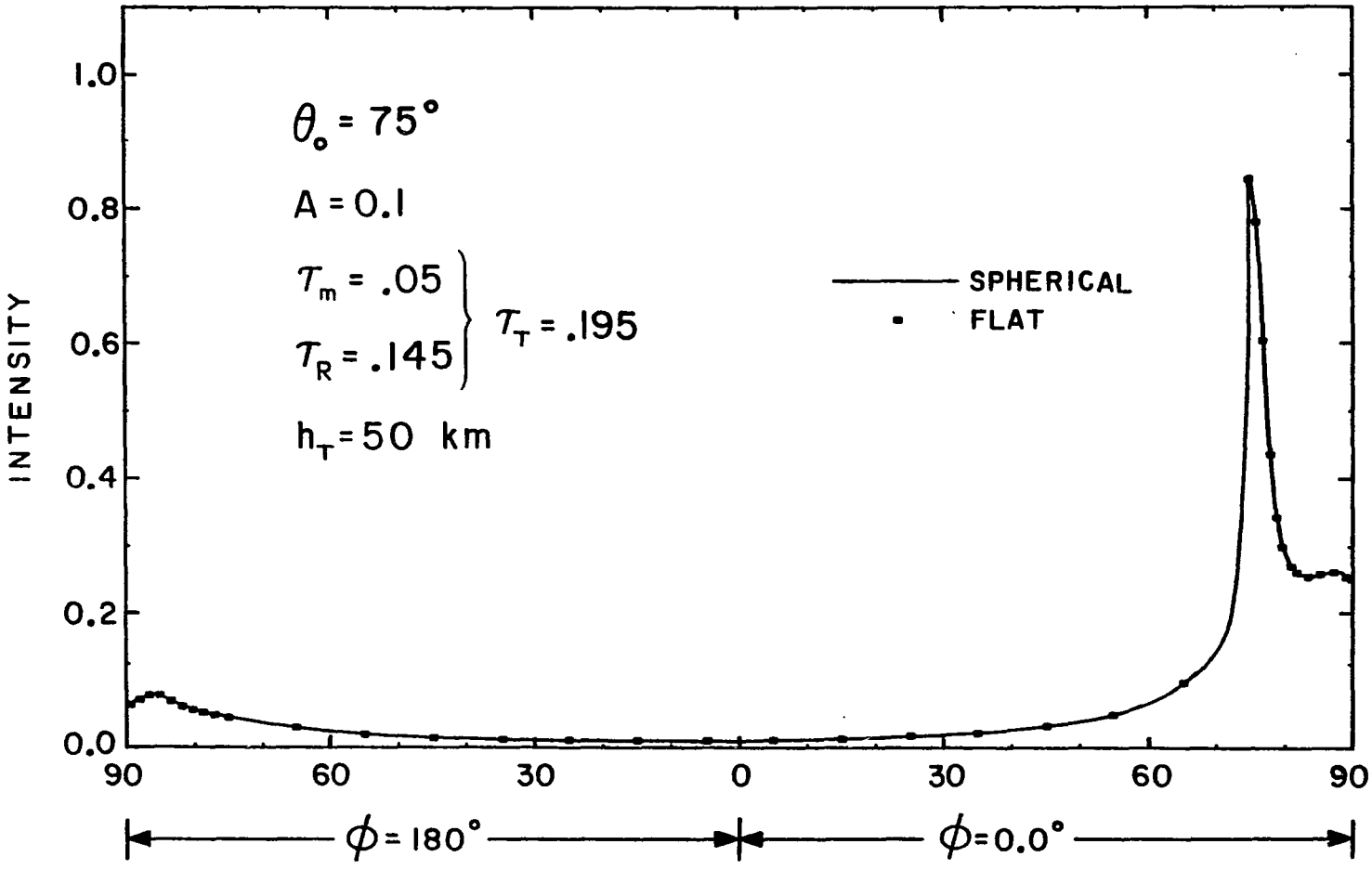

Fig. 4-5. Transmitted intensity as a function of zenith angle for the azimuthal plane (0°, 180°) in a conservative atmosphere. The solar zenith angle $\theta_o = 75°$ and $\tau_T = .195$.

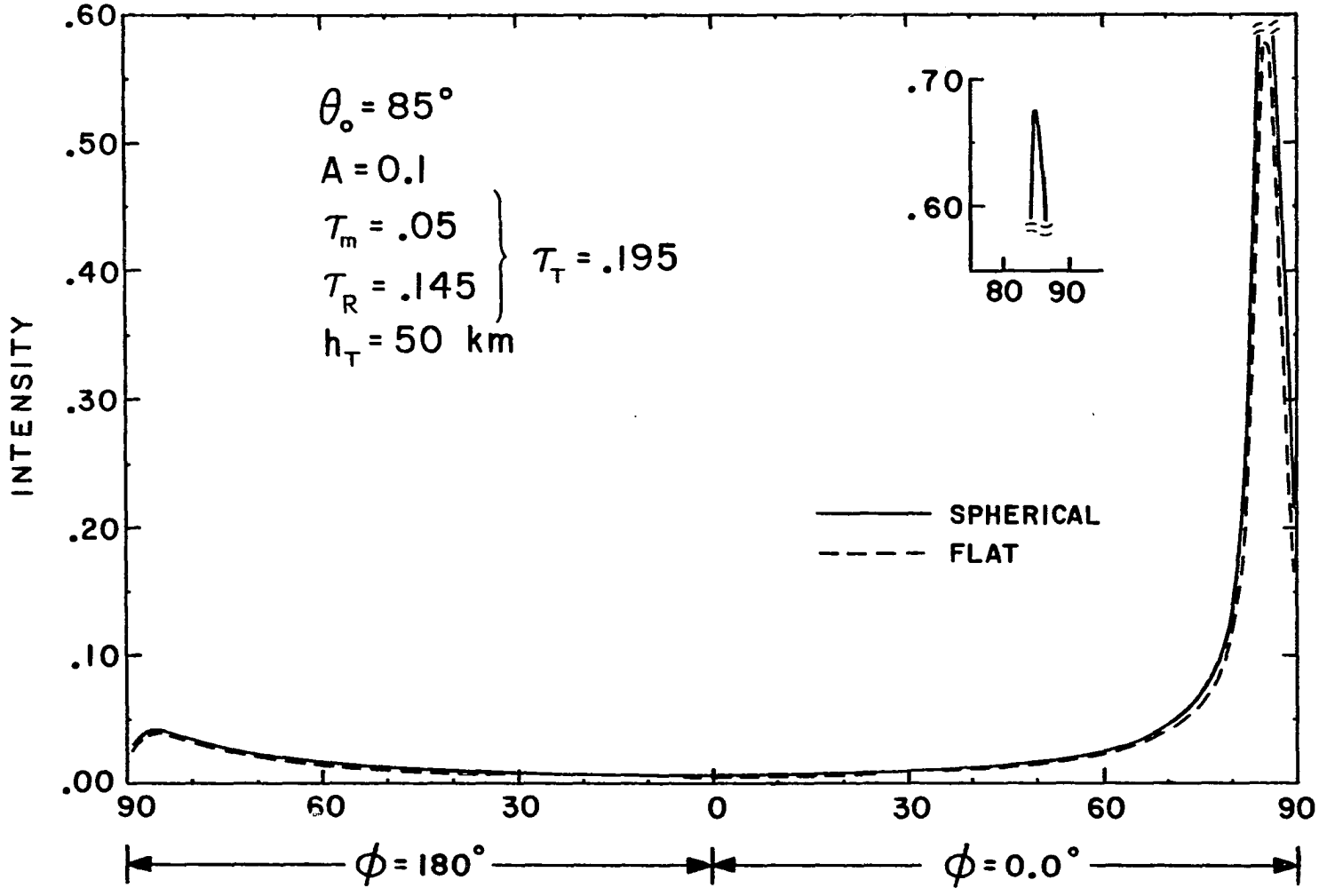

Fig. 4-6. Tansmitted intensity as a function of zenith angle for the azimuthal plane (0°, 180°) in a conservative atmosphere. The solar zenith angle $\theta_o = 85°$ and $\tau_T = .195$.

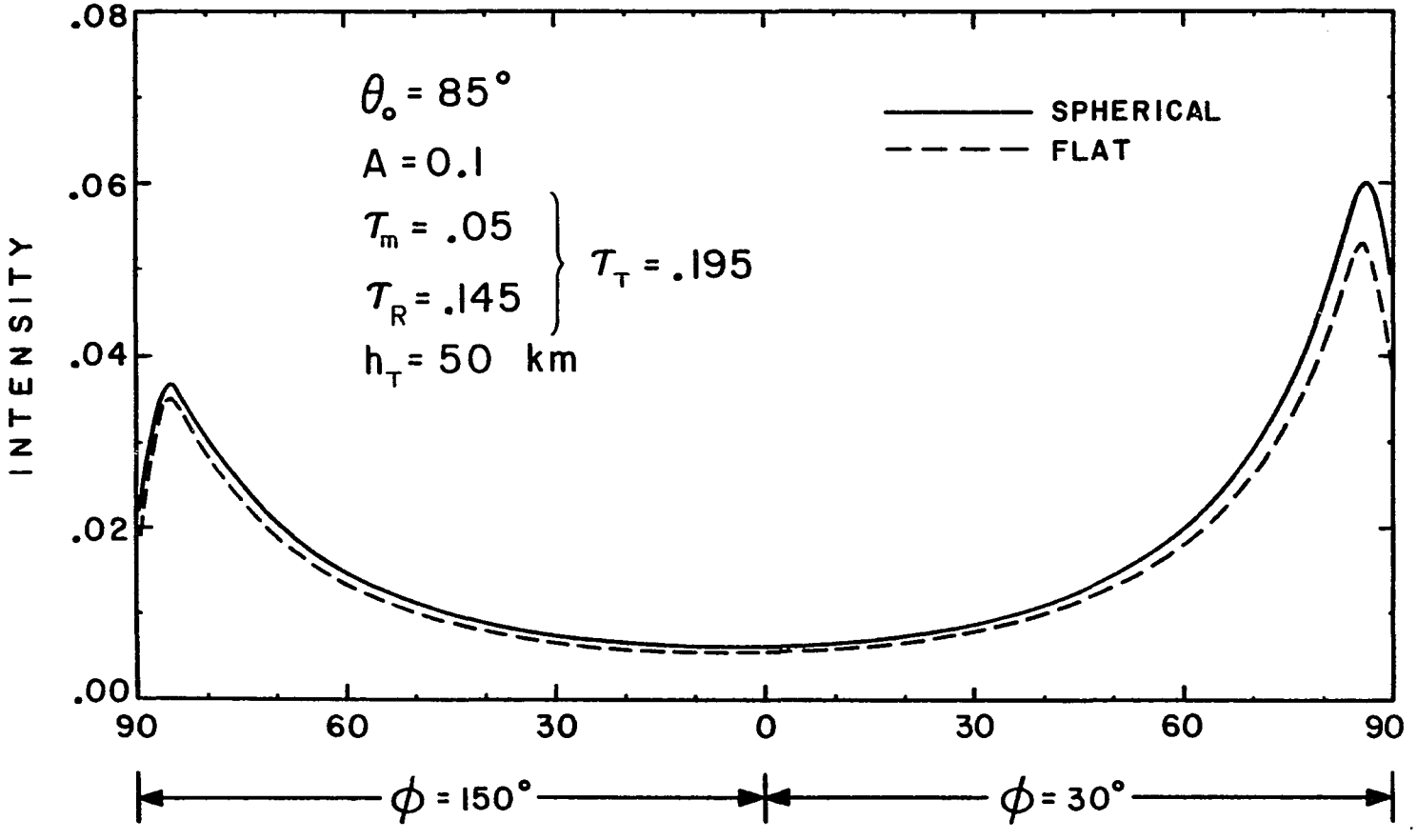

Fig. 4-7. Transmitted intensity as a function of zenith angle for the azimuthal plane (30°, 150°) in a conservative atmosphere. The solar zenith angle $\theta_o = 85°$ and $\tau_T = .195$.

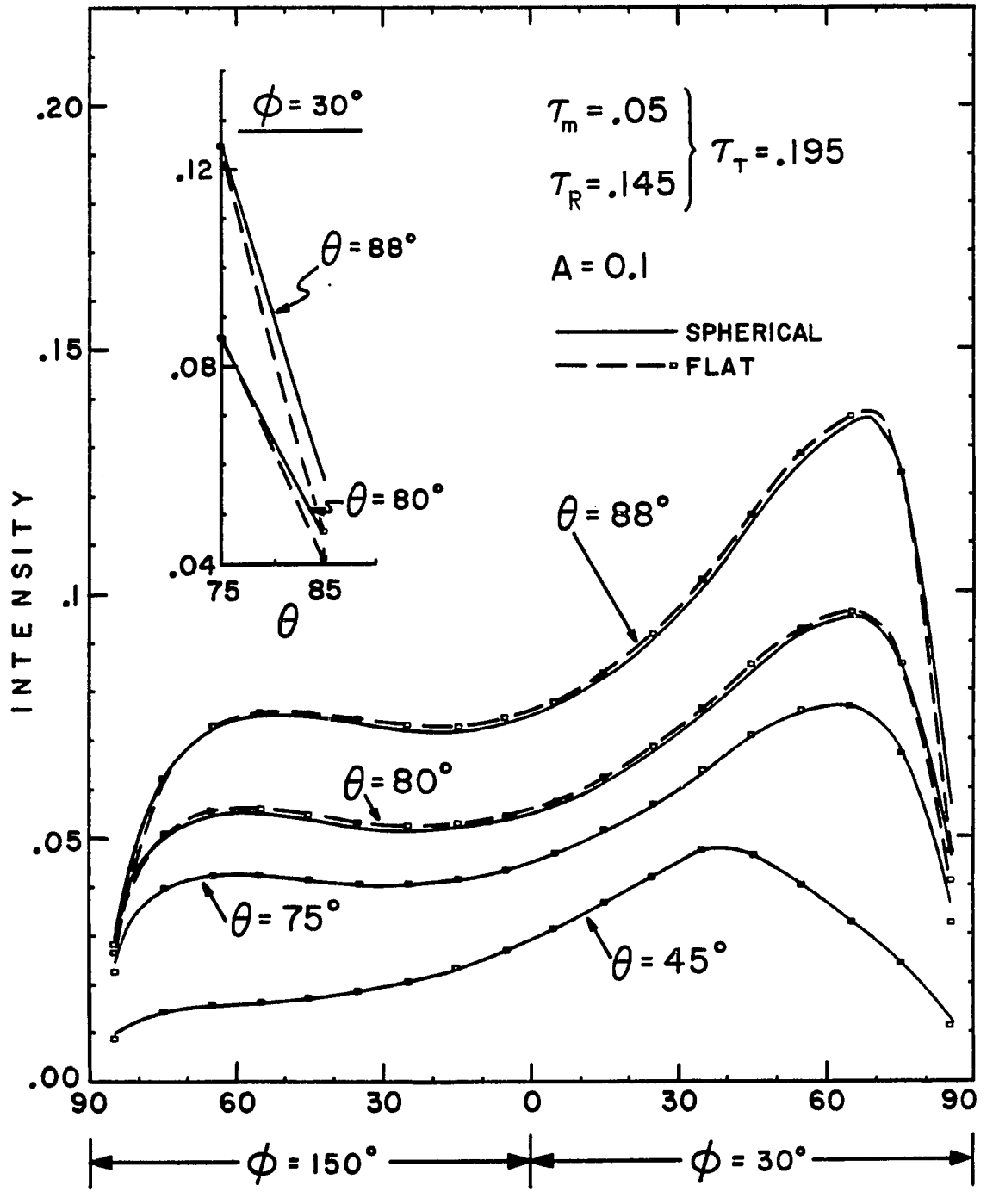

Fig. 4-8. Transmitted intensities as a function of solar zenith angle for the azimuthal plane (30°, 150°) in a conservative atmosphere. The zenith viewing angle θ = 88°, 80°, 75° and 45° and τ_T = .195.

on the order of 11.8% and 20.8% at $\theta = 80^\circ$ and 88°, respectively, (see insert in Fig. 4-8). But for $\phi = 150^\circ$ the percent differences are smaller than that in $\phi = 30^\circ$. At $\theta = 88^\circ$ the percent difference is on the order of 10.9%, while at $\theta = 80^\circ$ it is 6.5%. Therefore, neglecting the sphericity of the earth's atmosphere in a ground based radiometric measurement does not introduce measurable error until the solar zenith angle becomes larger than 80°.

Most scanning radiometric measurements on a satellite or spacecraft are confined to scan angles that do not include lines of sight penetrating through the atmosphere without touching the ground. The SAGE experiment is one exception to this type of measurement (see Chu and McCormick, 1979). For example, to improve the accuracy of the inverted data from the SAGE experiment, multiple scattering in the spherical atmosphere must be taken into consideration. For other satellite experiments, if one wishes to increase the range of the scan angle so they include lines of sight that do not touch the ground, the scattering in a spherical atmosphere must be examined.

To determine the received radiation in a simulated satellite experiment located at the top of spherical and plane-parallel atmospheres, the scattering atmosphere which was mentioned earlier is considered. The reflected intensity in both atmospheres as a function of zenith (or scan) angle in the azimuthal plane (0°, 180°) at the solar zenith angles $\theta_o = 5^\circ$, 75° and 85° are shown in Figs. 4-9 through 4-11, respectively. Fig. 4-12 is the same as Fig. 4-11 except $\phi = 30^\circ$ and 150°. At the top of the spherical atmosphere looking along the

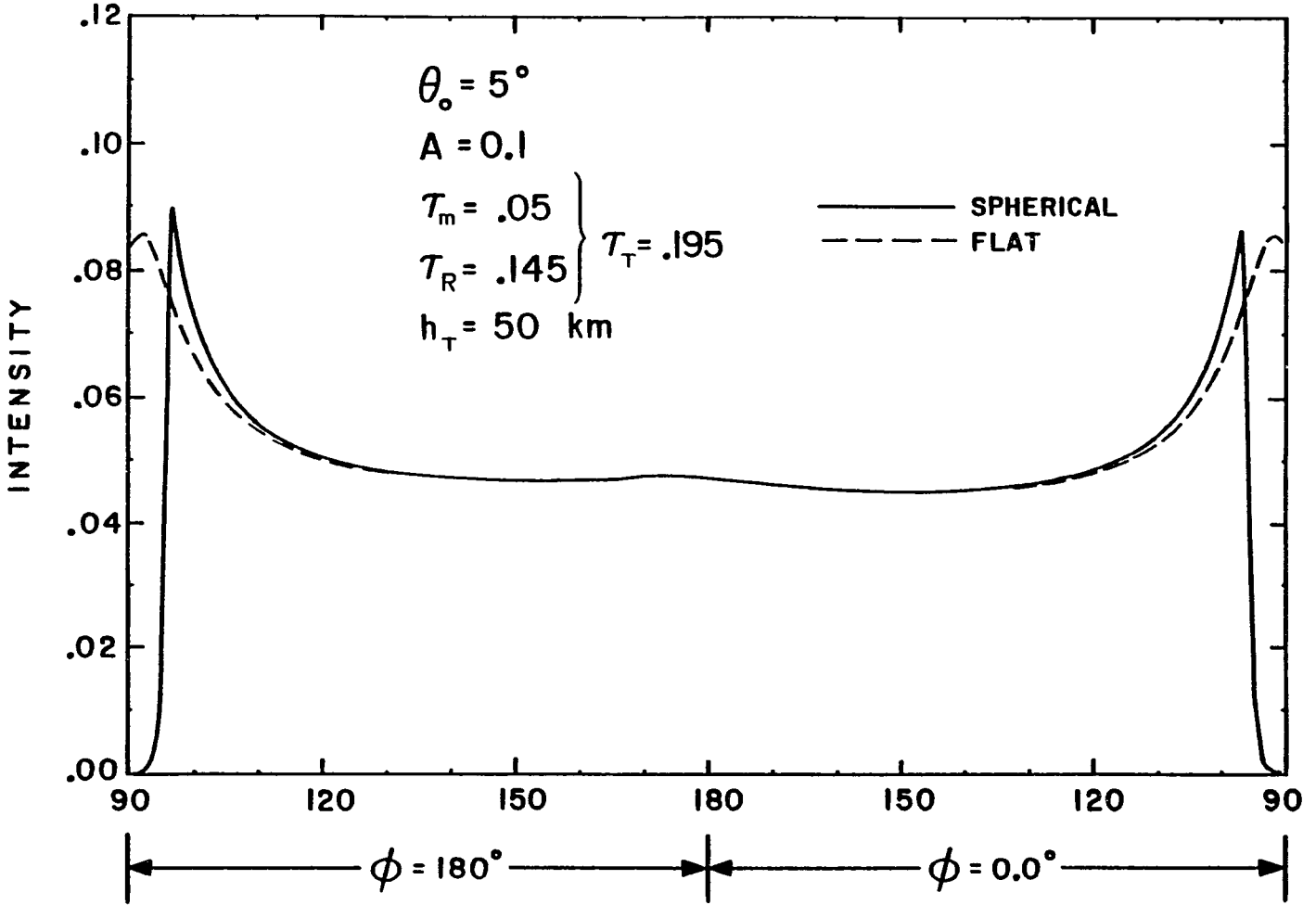

Fig. 4-9. Reflected intensity as a function of zenith angle for the azimuthal plane (0°, 180°) in a conservative atmosphere. The solar zenith angle $\theta_o = 5°$ and $\tau_T = .195$.

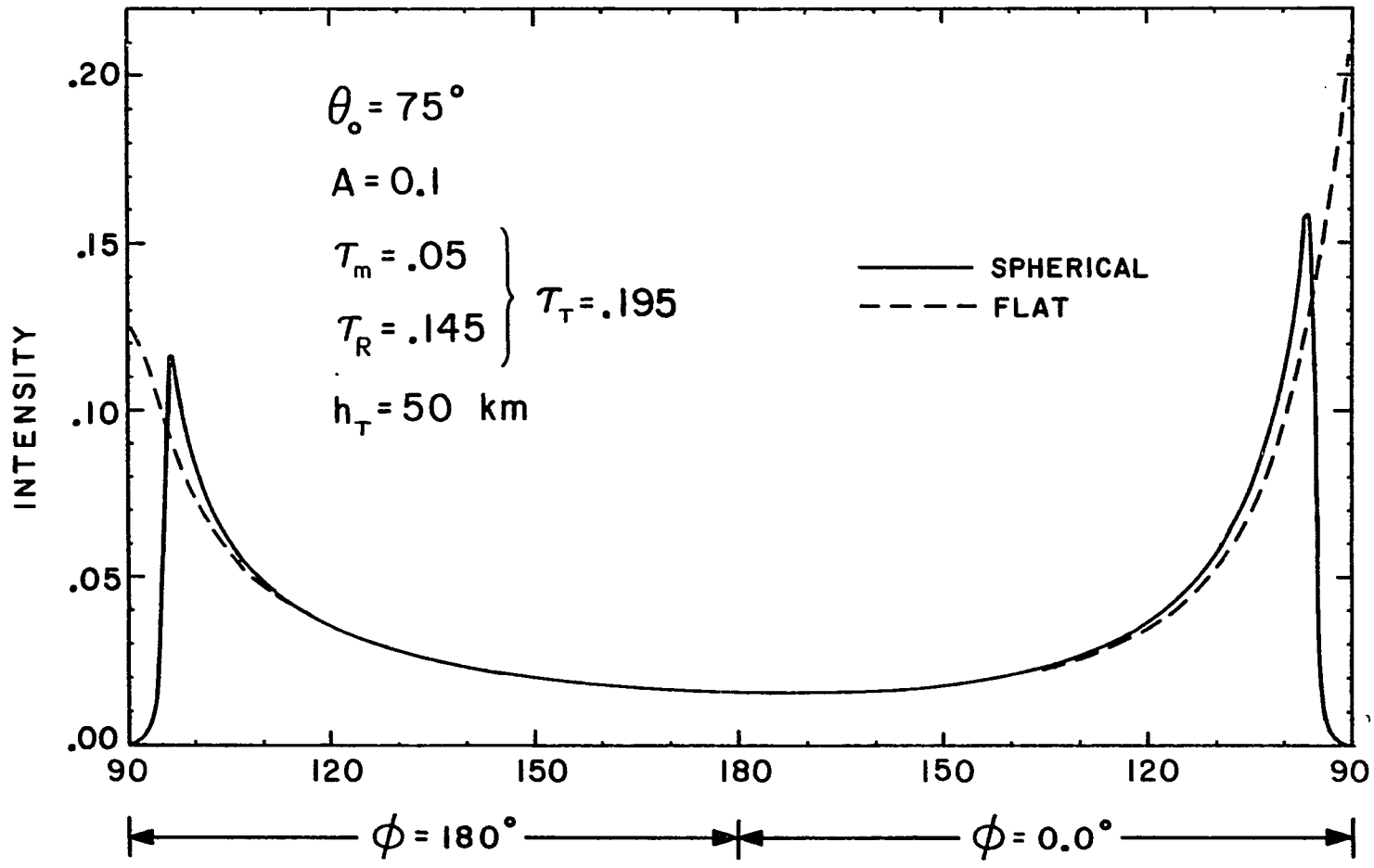

Fig. 4-10. Reflected intensity as a function of zenith angle for the azimuthal plane (0°, 180°) in a conservative atmosphere. The solar zenith angle $\theta_o = 75°$ and $\tau_T = .195$.

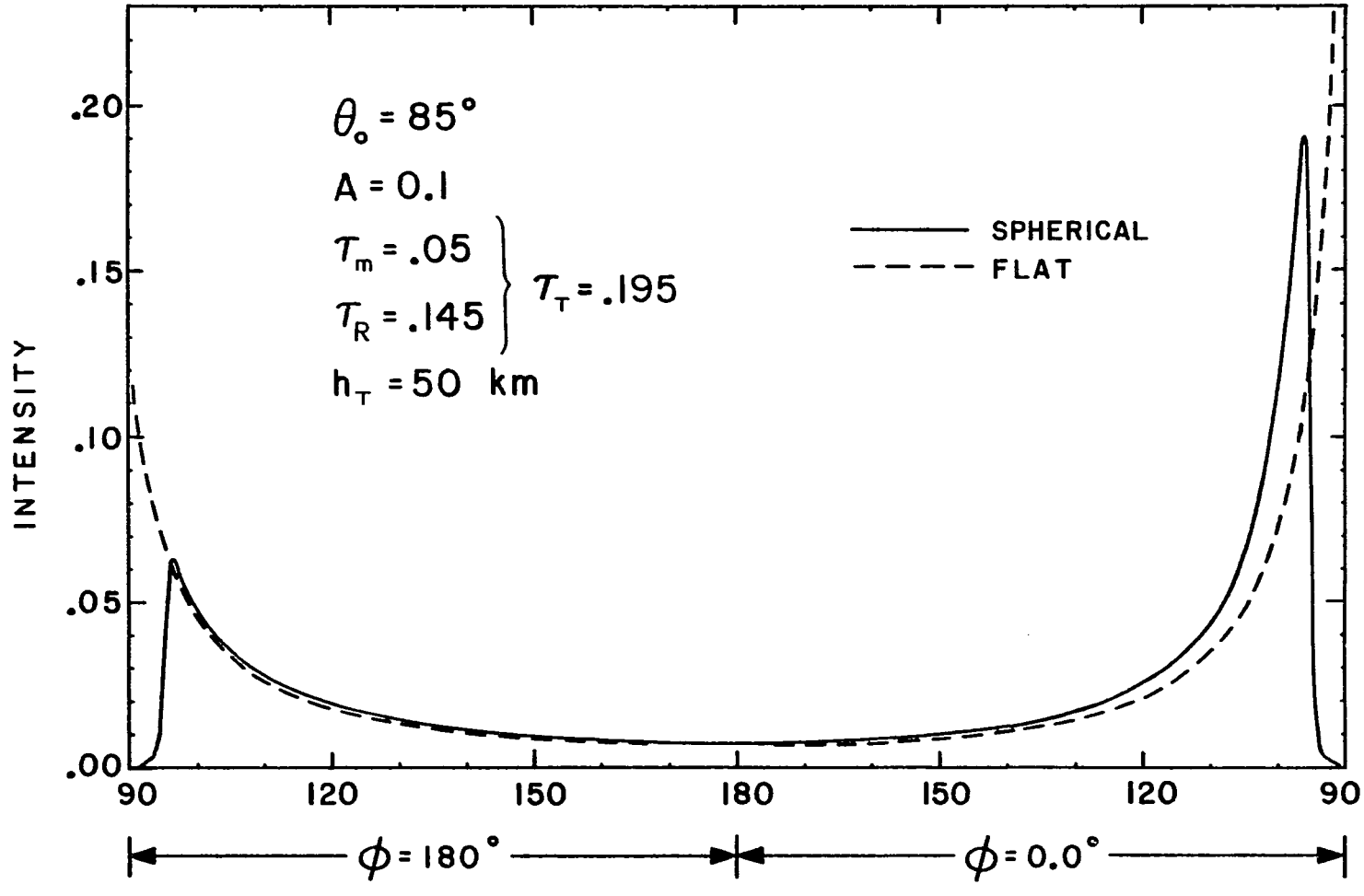

Fig. 4-11. Reflected intensity as a function of zenith angle for the azimuthal plane (0°, 180°) in a conservative atmosphere. The solar zenith angle $\theta_o = 85°$ and $\tau_T = .195$.

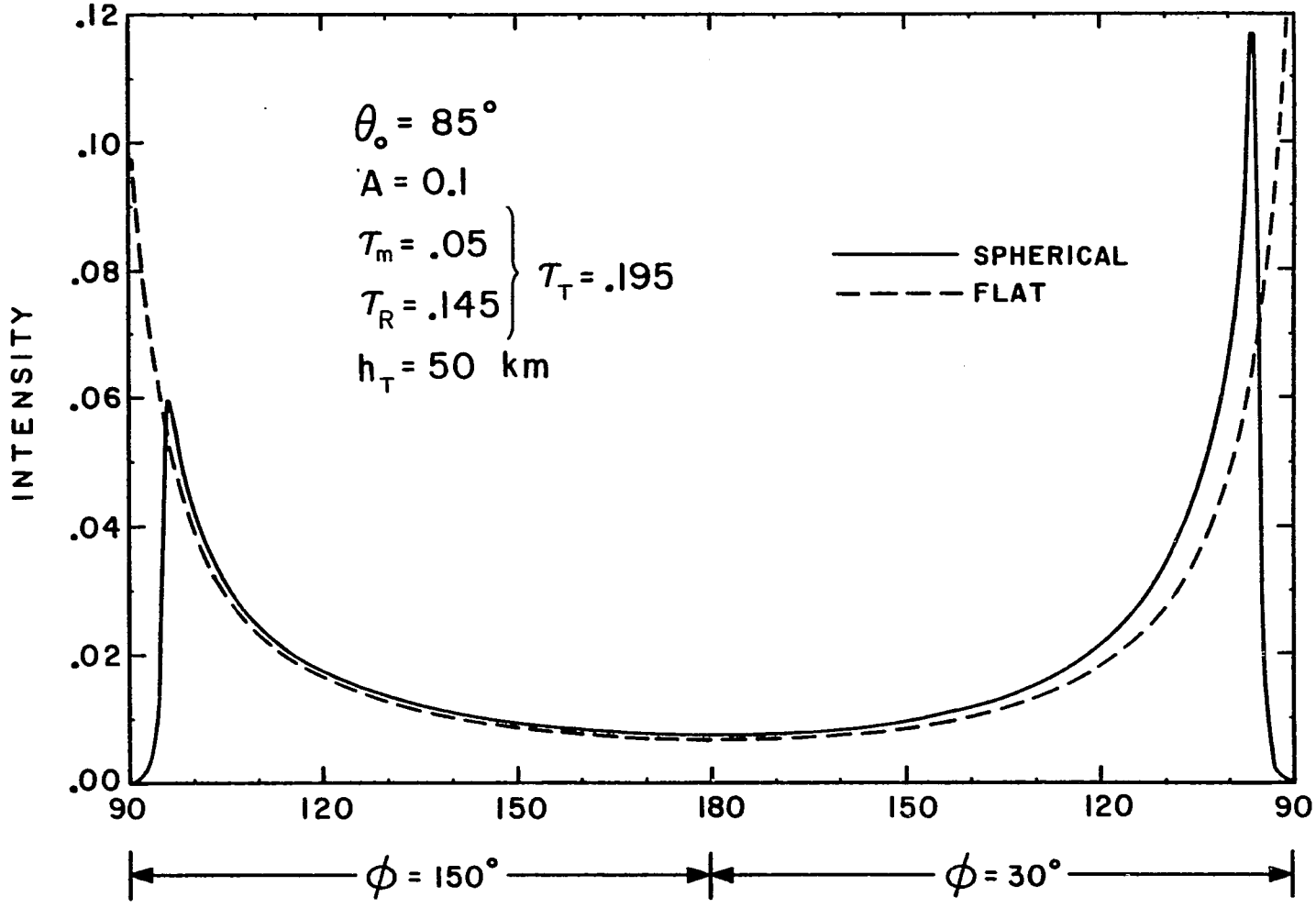

Fig. 4-12. Reflected intensity as a function of zenith angle for the azimuthal plane (30°, 150°) in a conservative atmosphere. The solar angle $\theta_o = 85°$ and $\tau_T = .195$.

horizon (i.e., $\theta = 90^\circ$), for all practical purposes, there are no particles to scatter light. Consequently, one expects no scattering of light or reflected intensity in that direction. In fact, as shown in Fig. 4-9 through 4-12 all the reflected intensities very close to the horizon for all azimuthal angles in the spherical atmosphere are almost zero, conversely the intensities in the flat atmosphere are orders of magnitude larger than those intensities in the spherical atmosphere which indicates a gross error in this situation in using the flat model for the earth's atmosphere. As the scan angle moves away from the horizon towards the normal line in the plane of incident sun $\tau_\ell(\theta)$ increases to a maximum value which occurs at the scan angle that corresponds to the line of sight tangent to the earth's surface. Afterwards, τ_ℓ decreases to a minimum value at $\theta = 180^\circ$. Similar changes in τ_ℓ occur in all the other azimuthal planes. It is apparent that in an optically thin atmosphere the intensity profile as a function of scan angle follows the changes in τ_ℓ, as illustrated in Fig. 4-9 through 4-12. At the tangent scan angle (i.e., $\theta = 97.155^\circ$) a discontinuity in the intensity profile may result from the abrupt change in τ_ℓ and from the contribution of the reflected radiation at the ground. Although the discontinuity is not apparent in the presented results, it would be more noticable when the ground albedo becomes large and/or the total normal optical depth becomes relatively small. Because of the sphericity of the atmosphere, shadowing effects on the incident sunlight occur between $\phi = 90^\circ$ and 180° when θ_o is slightly less than 90°, and are expected to become more evident as the sun descends below the

horizon. When $\theta_o = 5^\circ$, (refer to Fig. 4-9) the magnitude of the peak intensities in the spherical atmosphere are almost identical in $\phi = 0^\circ$ and 180°. This means that the intensity profile is almost symmetrical about $\theta = 180^\circ$. In fact, this observation can be made about the other azimuthal planes, and about the solar zenith angles that are less than 55°. However, as θ_o approaches the horizon the sphericity and shadowing effects become more pronounced as illustrated in Fig. 4-10 and 4-11. Here, as θ_o increases from 75° to 85° the ratios of the peak intensities at $\phi = 0^\circ$ and 180° increase from 1.36 to 2.91, respectively. Similarly, in Fig. 4-12 the ratio of the peak intensities at $\phi = 30^\circ$ and 150° is 1.975 which has increased from 1.2 at $\theta_o = 75^\circ$. In other words, the asymmetry in the intensity profile about $\theta = 180^\circ$ increases as the angle of the incident sun approaches the horizon. A comparison between the profiles of the intensity for varying scan angles, away from the horizon, at the top of both flat and spherical atmosphere reveals larger values for the intensities in the spherical atmospheres. Again, these differences become larger as the solar zenith angle approaches the horizon, because of less attenuation in the spherical atmosphere. Similar behavior was also noticed during the earlier analyses of the transmitted intensities. For example, for $\theta_o = 5^\circ$ and $\phi = 0^\circ$ the percent difference is about .08%, but when $\theta_o = 85^\circ$ it becomes much larger and it is on the order of 11%.

Flux Conservation in a Spherical Atmosphere

In a non-absorbing atmosphere the divergence of the flux density vector, $\vec{F}$, must everywhere vanish. Hence, by applying the divergence theorem we obtain

$$\int_V \nabla\cdot\vec{F}\, dv = \int_S \vec{F}\cdot\hat{n} ds = 0 \tag{4.4}$$

where $\hat{n}$ is an outward pointing unit vector on the closed surface S, and V is the total volume inside S. From Eq. (4-4) we can see that the sum of all the normal components of the flux density through any closed surface inside a non-absorbing atmosphere must vanish. Because of the symmetry in the geometry of a plane-parallel atmosphere, it is clear that the emerging normal flux densities through the top and bottom surfaces of a rectangular volume inside the atmosphere are of equal magnitudes but pointing in opposite directions. The same holds true for the other sides of the rectangle. Conversely, in a spherical atmosphere there is no symmetry as far as the rectangular surface is concerned. Consequently, the normal flux densities through the opposite sides of the rectangle are not equal, but the total flux must be conserved. Therefore, the normal flux density through the top and bottom of a spherical atmosphere may result in gain or loss depending on the angle of the incident solar radiation, the gain/loss being compensated for by an equal loss/gain through the sides.

To examine the problem of flux conservation in a spherical atmosphere, let us consider the conservative and vertically

inhomogeneous atmosphere that was described in the previous section of this chapter. The normal components of the flux density through the top and bottom of the atmosphere along the local normal are computed for $\theta_o = 5°, 15°, \ldots, 85°$. The diffuse downward flux density, F_d, on the ground is computed by numerically integrating Eq (3.23). Also, the diffuse upward flux density, F_u, at the top of the atmosphere is numerically evaluated, and it is defined as

$$F_u = \int_0^{2\pi} \int_{\pi/2}^{\pi} I(\tau_\ell=0,\theta,\phi)\, \cos\theta \sin\theta d\theta d\phi \tag{4.5}$$

where $I(\tau_\ell = 0,\theta,\phi)$ is the upward traveling intensity at h_T. Furthermore, the unscattered flux density, F_{us}, is obtained from Eq (3.24), while the normal component of the incident solar flux density, F_n, at h_T is given by

$$F_n = F_o \cos\theta_o \quad . \tag{4.6}$$

The resulting normal flux densities on the top and bottom of the atmosphere for the various solar zenith angles appear in Table 4.1. In addition, the percent loss or gain in the flux density, $\Delta F\%$, that appears in the last column in Table 4-1 is obtained as follows

$$\Delta F\% = \frac{F_n - \left(1-A\right)\cdot\left(F_d + F_{us}\right) - F_u}{F_n - F_{us}} \cdot 100 \quad . \tag{4.7}$$

Because of the spherical geometry and the nature of the incident

Table 4-1. Flux densities at various sun angles in a conservative spherical atmosphere with $\tau_T = .195$.

θ_o	F_n	F_u	F_d	F_{us}	$\Delta F\%$
5°	.9961947	.1501104	.1161993	.8190986	+2.44
15°	.9659258	.1472811	.1141985	.7893938	+3.06
25°	.9060308	.1419255	.1121738	.7309923	+3.16
35°	.8191520	.1341316	.1094826	.6459179	+2.98
45°	.7071068	.1240022	.1054275	.5372571	+2.76
55°	.5735764	.1116576	.0994737	.4093533	+2.42
65°	.4226183	.0968980	.0905741	.2685513	+1.63
75°	.2588190	.0780903	.0753661	.1264276	-0.67
85°	.0871557	.0461758	.0416896	.0170511	-16.95

sunlight, there is a flux loss for $\theta_o = 5^\circ$ through 65° while a flux gain for $\theta_o = 75^\circ$ and 85° (see Table 4-1).

For convenience, we proceed to determine the total flux through the upper hemisphere that faces the sun. This includes the hemispherical surfaces at the top and bottom of the atmosphere as well as the donut shaped surface perpendicular to the plane of the sun. The total flux, $\mathscr{F}$, through a hemispherical surface is given by

$$\mathscr{F} = \int_0^{2\pi}\int_0^{\pi/2} F_r\, r^2 \sin\theta d\theta d\phi \tag{4.8}$$

where F_r is the radial component of $\vec{F}$ at a spherical surface of radius r. Note that in the spherical geometry the normal component of $\vec{F}$ is equal to F_r. By making use of the azimuthal symmetry the ϕ-integration is Eq (4.8) becomes trivial. However, the integration over θ will be done numerically, since it cannot be done analytically. Here, the range of the angle θ will be divided into 9 equal intervals, and an average value for F_r will be taken at the midpoint of each interval. Accordingly, Eq (4.8) becomes

$$\mathscr{F} \simeq 2\pi r^2 \sum_{n=1}^{9} \bar{F}_r\left(\bar{\theta}_n\right)\cdot\left(\cos\theta_n - \cos\theta_{n+1}\right) \tag{4.9}$$

where $\bar{F}_r$ is the average radial flux density in the n^{th} interval, and $\bar{\theta}_n = \left(\theta_n + \theta_{n+1}\right)/2$. By neglecting the total flux through the donut shaped surface perpendicular to the plane of the incident sunlight, we

obtain the percent of the total flux loss, $\Delta\mathcal{F}\%$, in the sunlit hemisphere by the expression

$$\Delta\mathcal{F}\% = \frac{\mathcal{F}_{inc} - (1-A)\left(\mathcal{F}_d + \mathcal{F}_{us}\right) - \mathcal{F}_u}{\mathcal{F}_{inc}} \cdot 100 \qquad (4.10)$$

where $\mathcal{F}_{inc}$ and $\mathcal{F}_u$ are the total incident and upward diffused fluxes at $r = R+h_T$, respectively. $\mathcal{F}_d$ is the total diffused downward flux, while $\mathcal{F}_{us}$ is the total unscattered flux. Both $\mathcal{F}_d$ and $\mathcal{F}_{us}$ are evaluated at $r = R$. By using Eq (4.9) in conjunction with Table 4-1 we obtain the following:

$$\mathcal{F}_u = 2\pi(.1004929)(6420)^2, \quad \mathcal{F}_d = 2\pi(.0875631)(6370)^2,$$
$$\mathcal{F}_{us} = 2\pi(.3578318)(6370)^2, \quad \mathcal{F}_{inc} = 2\pi(.5019099)(6420)^2.$$

Now, substituting these values into Eq (4.10) yields

$$\Delta\mathcal{F}\% = 1.351\% \quad . \qquad (4.11)$$

Therefore, the total flux in the spherical atmosphere is conserved within 1.351%. This is primarily due to the neglect of the total flux through the donut shaped surface perpendicular to the plane of the sun, which requires the consideration of the twilight phenomenon, beyond the scope of the present work.

Scattering due to Stratospheric and Air Pollution Layers

The scattering of light in the earth's atmosphere due to the modification of the distribution of aerosols to include additional vertical inhomogeneities will be examined. Unless otherwise noted, all

the input parameters of the conservative and vertically inhomogeneous atmosphere at $\lambda = 0.5$ μm that were described in the first section of this chapter will be used in this section. Here the original normalized distribution of aerosols, $N_{aerosol}$, and molecules, $N_{molecule}$, as shown in Fig. 4-1 will be referred to as Case I.

A layer of volcanic dust in the stratosphere may be modelled by increasing the density of aerosols by five times between the heights of 18 and 23 (km). The addition of such a stratospheric layer to $N_{aerosol}$ of Case I is illustrated in Fig. 4-1, and it will be reffered to as Case II. Likewise, Case III is obtained by adding to $N_{aerosol}$ of Case I an air pollution layer that starts at the height of 5 (km) and increases exponentially until reaching the ground (i.e., $z = 0$) where the density is doubled as shown in Fig. 4-1. Similarly, Case IV described a homogeneous layer of air pollution near the ground that has twice the original aerosol density and a thickness of 1 (km). The distribution of molecules as shown in Fig. 4-1 will also be included in Cases II, III and IV. For case I $\tau_m = .05$. However, adding the above modifications results in increasing τ_m and consequently τ_T. Hence, the resulting total Mie or aerosol optical depths are 0.057, 0.268 and 0.116 for cases II, III and IV, respectively. The atmosphere in case I was divided in 10 layers of equal optical depth and additionally the top layer was divided into 9 layers of equal heights above h_{tan}. So the total number of layers for case I was chosen to be 20. Since τ_T for case II is increased only slightly, the total number of

layers is chosen to be 20 analogous to case I. However, for cases III and IV the total number of layers is taken to be 30 and 25, respectively.

The characterization of the scattered radiation for the additional three cases that were mentioned above is obtained by applying the Quasi-Spherical method to the spherical atmosphere and the semi-analytic technique which was discussed in the first section of this chapter to the plane-parallel or flat atmosphere. The transmitted intensities in both flat and spherical atmospheres for each case show analogous behavior to that of case I. Again, analyzing these intensities indicate larger differences between the results of spherical and flat atmospheres for each case as the solar zenith angle and/or the viewing zenith angle approaches the horizon. To illustrate this situation for cases II, III and IV at $\theta_o = 85^\circ$ the transmitted intensities in the azimuthal plane (0°, 180°) for varying zenith angle are shown in Figs. 4-13, 14 and 15, respectively. All these figures show higher values for the intensities in the spherical atmosphere due to smaller attenuation in the spherical geometry. Although the results of both models track each other closely (see Fig. 4-13 through 4-15) for most of the zenith angles, the two results become further apart as θ gets close to 90°. For example, at $\theta_o = 85^\circ$, $\phi = 0^\circ$ and $\theta = 5^\circ$ the percent differences for cases II, III and IV are 11.4%, 12.5% and 11.8%, respectively. Likewise, when $\theta = 88^\circ$ the corresponding percent differences for the same cases are 25.6%, 44.8% and 27.4%. Note that for intermediate total optical depth, $\tau_T = 0.261$, the intensity in the aureole in both geometries has the highest value as depicted in Fig. 4-15. Furthermore, the intensity in the

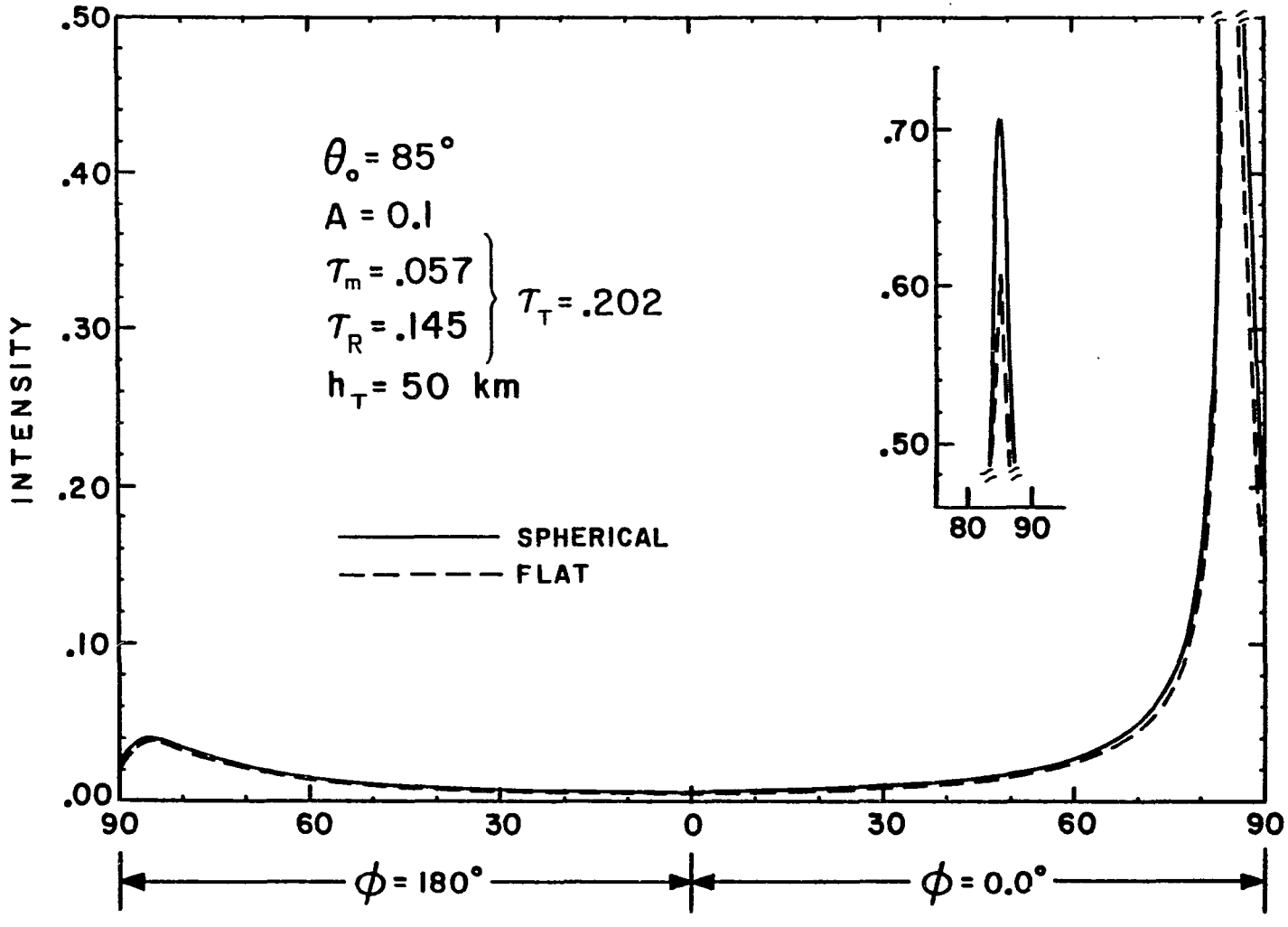

Fig. 4-13. Transmitted intensity as a function of zenith angle for the azimuthal plane (0°, 180°) in a conservative atmosphere that includes a stratospheric dust layer. The solar zenith angle $\theta_o = 85^\circ$ and $\tau_T = .202$.

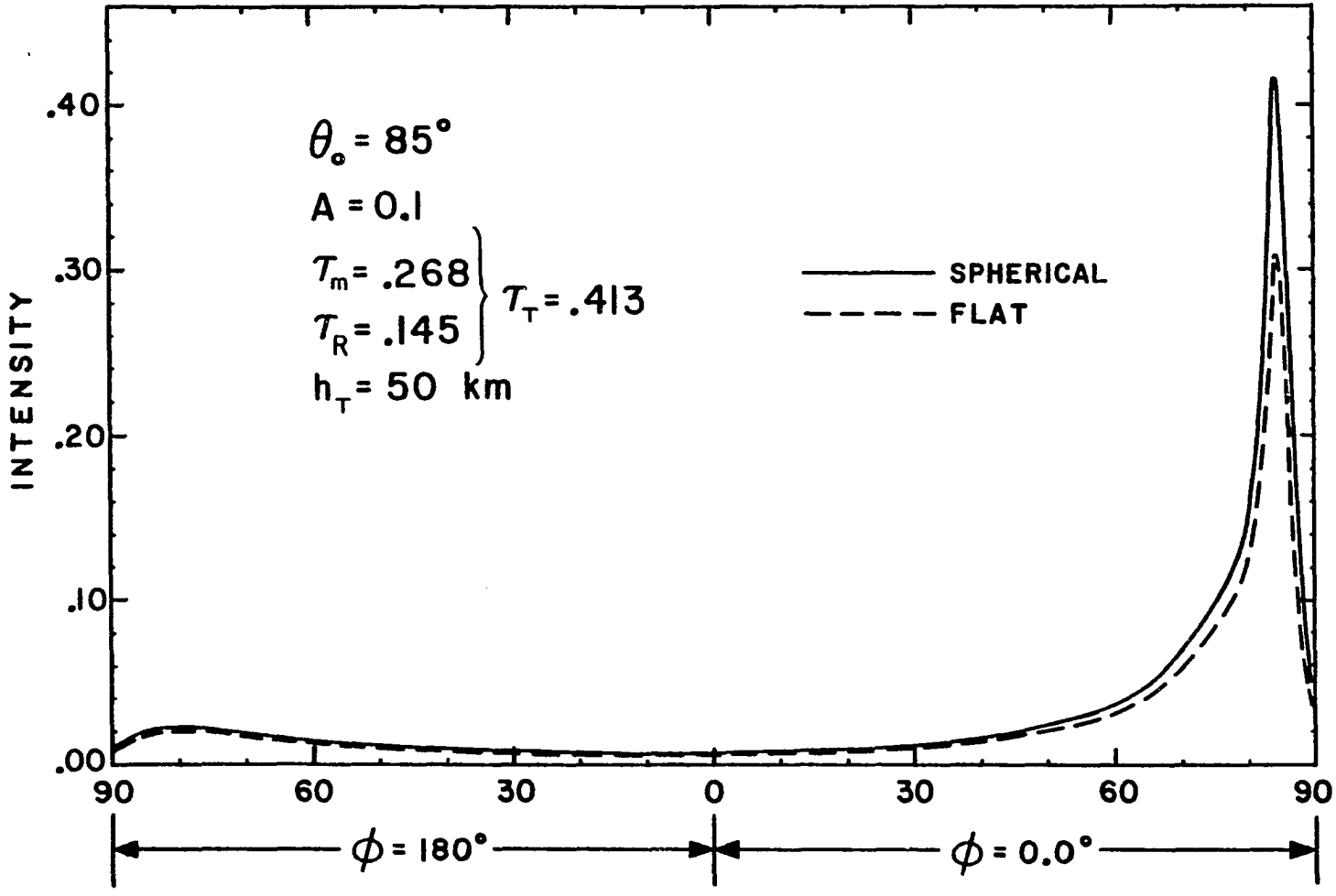

Fig. 4-14. Transmitted intensity as a function of zenith angle for the azimuthal plane (0°, 180°) in a conservative atmosphere that includes an exponential air pollution layer in the troposphere. The solar zenith angle θ_o = 85° and τ_T = .413.

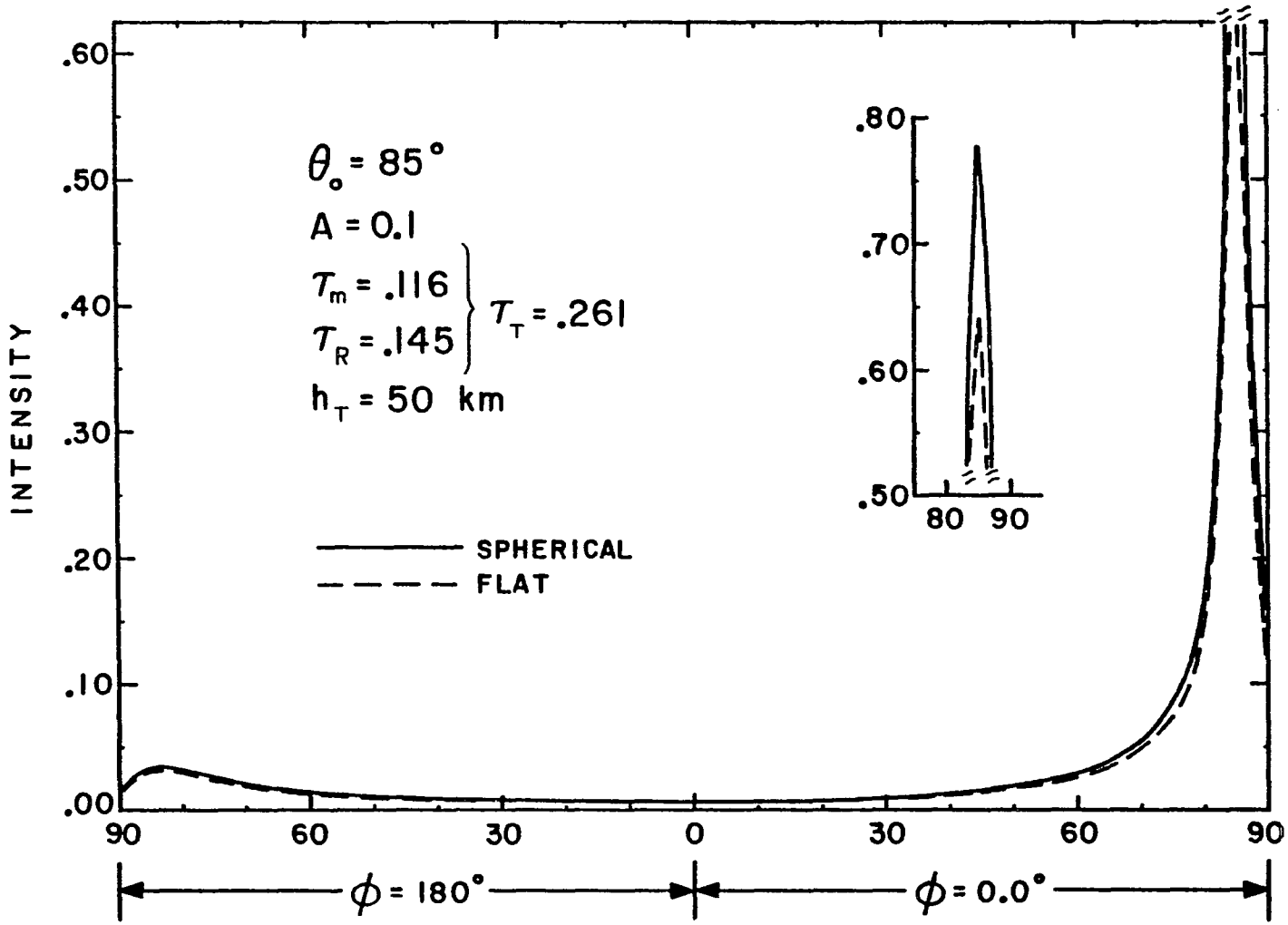

Fig. 4-15. Transmitted intensity as a function of zenith angle for the azimuthal plane (0°, 180°) in a conservative atmosphere that includes a homogeneous air pollution layer in the troposphere. The solar zenith angle $\theta_o = 85°$ and $\tau_T = .261$.

aureole has the lowest value, as shown in Fig. 4-14, for the largest τ_T due to the dominance of the attenuation over scattering at large τ_T. To examine the effects of including stratospheric and tropospheric aerosol layers on a ground based measurement of skylight, we show in Fig. 4-16 the resulting transmitted intensities in the spherical atmosphere for cases I through IV as a function of zenith angle at $\theta_o = 85^\circ$ and $\phi = 30^\circ$. Here the intensity profile in the spherical atmosphere is similar to that in the flat atmosphere, but the corresponding values of the intensities are higher. Therefore, in a ground based measurement the spherical geometry does not assist in determining the presence of additional vertical inhomogeneities in the distribution of aerosols.

Next, consider a scanning radiometer on a satellite or spacecraft that is located at $h_T = 50$ (km) for cases II, III and IV. The received radiation for case I has been discussed earlier for varying sun angles. Analogous to case I, the comparison between the reflected intensities in the flat and spherical atmospheres reveals large differences for θ close to 90°. However, as the solar zenith angle approaches the horizon the reflected intensities for the scan angles that correspond to lines of sight not touching the ground in the spherical atmosphere show noticable changes because of the introduced homogeneities. But these intensities in the flat model fail to detect any vertical inhomogeneity. Fig. 4-17 shows at $\theta_o = 85^\circ$ the reflected intensities in both flat and spherical atmospheres for case II for varying zenith angle in the azimuthal plane (0°, 180°). Similarly, Fig. 4-18 and 19 show the reflected intensities for cases III and IV,

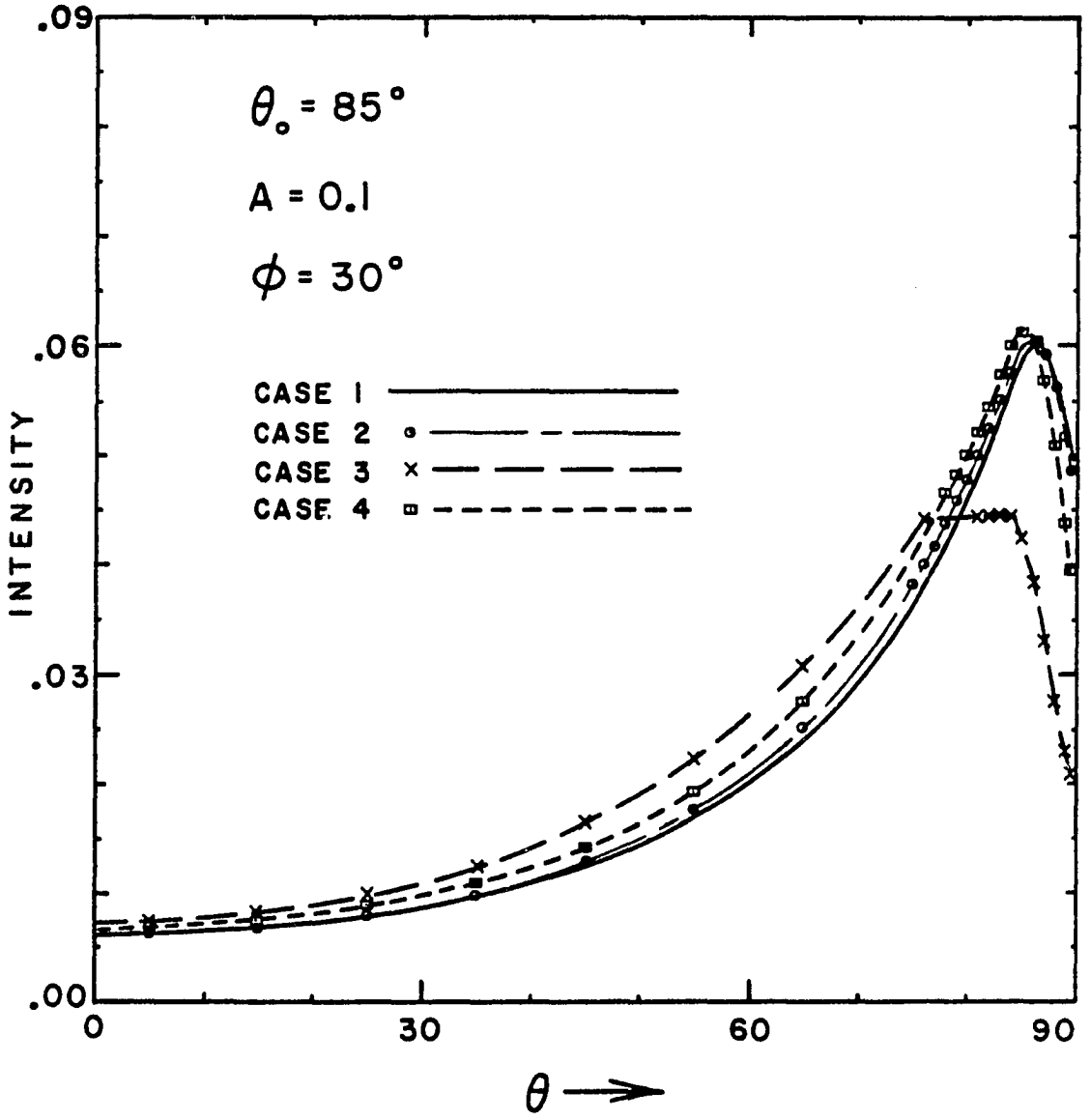

Fig. 4-16. Transmitted intensity as a function of zenith angle in a spherical atmosphere that includes four cases of vertical inhomogeneities. The solar zenith angle $\theta_o = 85^\circ$ and $\phi = 30^\circ$.

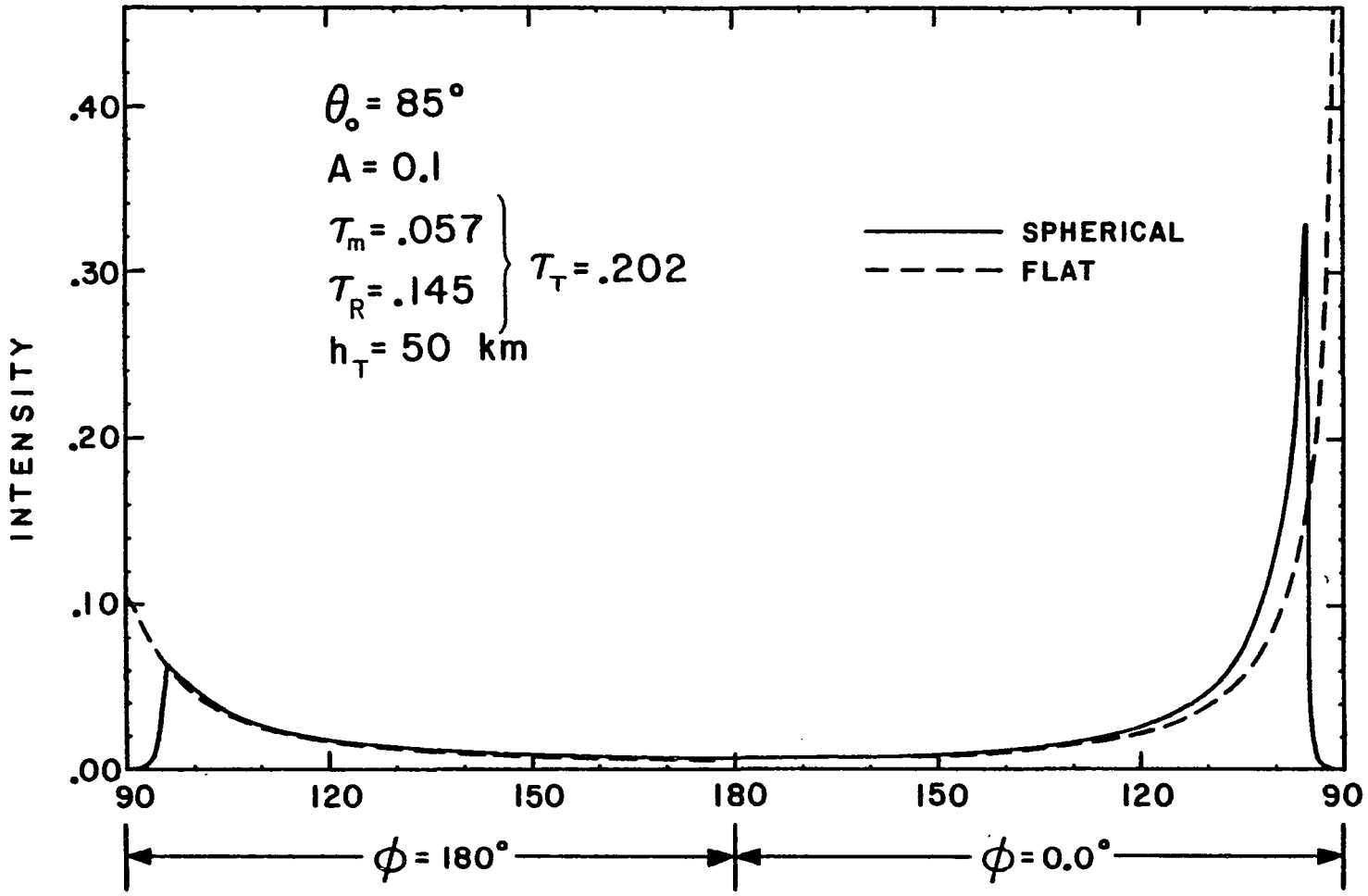

Fig. 4-17. Reflected intensity as function of zenith angle for the azimuthal plane (0°, 180°) in a conservative atmosphere that includes a stratospheric dust layer. The solar zenith angle θ_o = 85° and τ_T = .202.

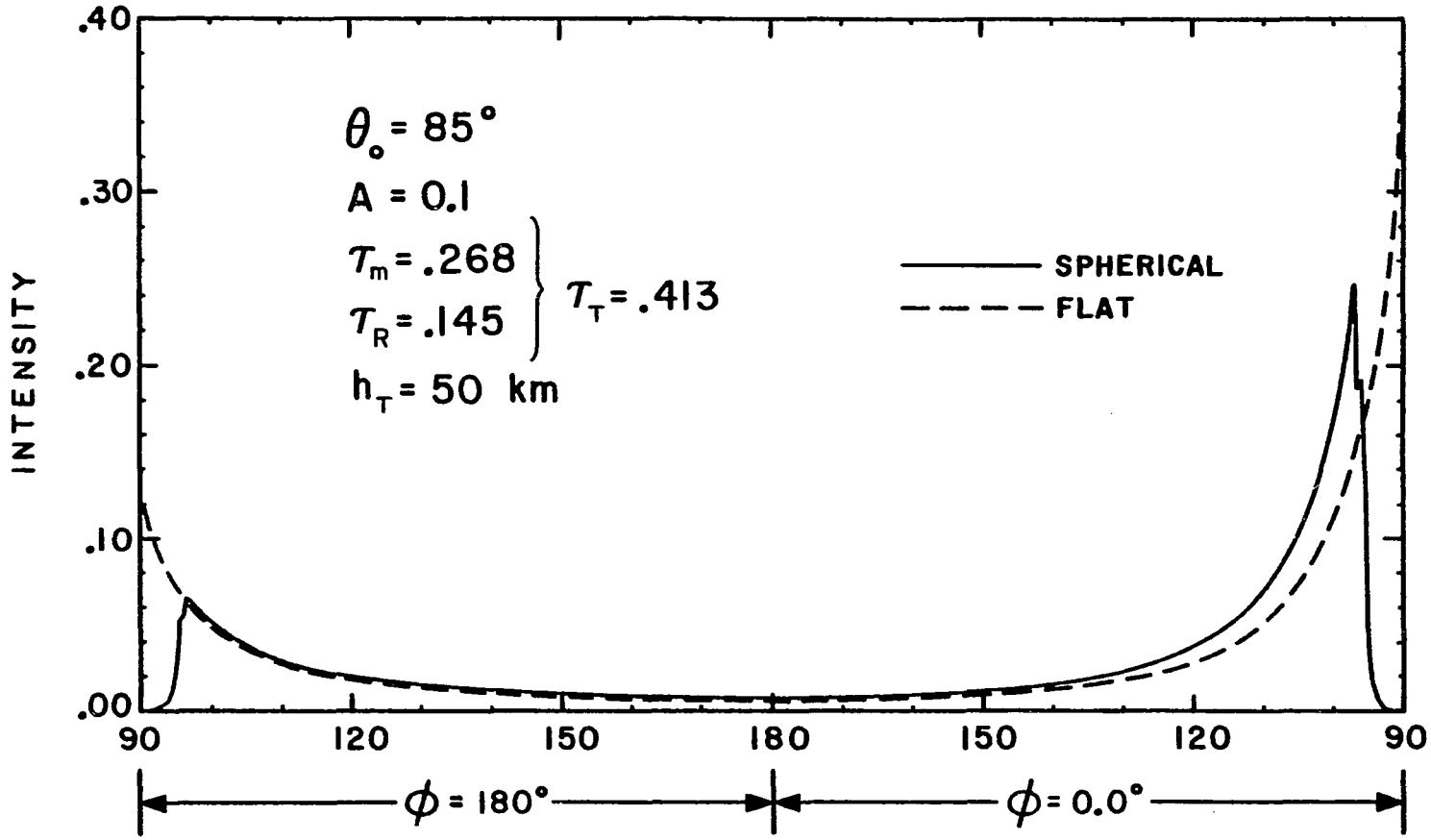

Fig. 4-18. Reflected intensity as a function of zenith angle for the azimuthal plane (0°, 180°) in a conservative atmosphere that includes an exponential air pollution layer in the troposphere. The solar zenith angle $\theta_o = 85^\circ$ and $\tau_T = .413$.

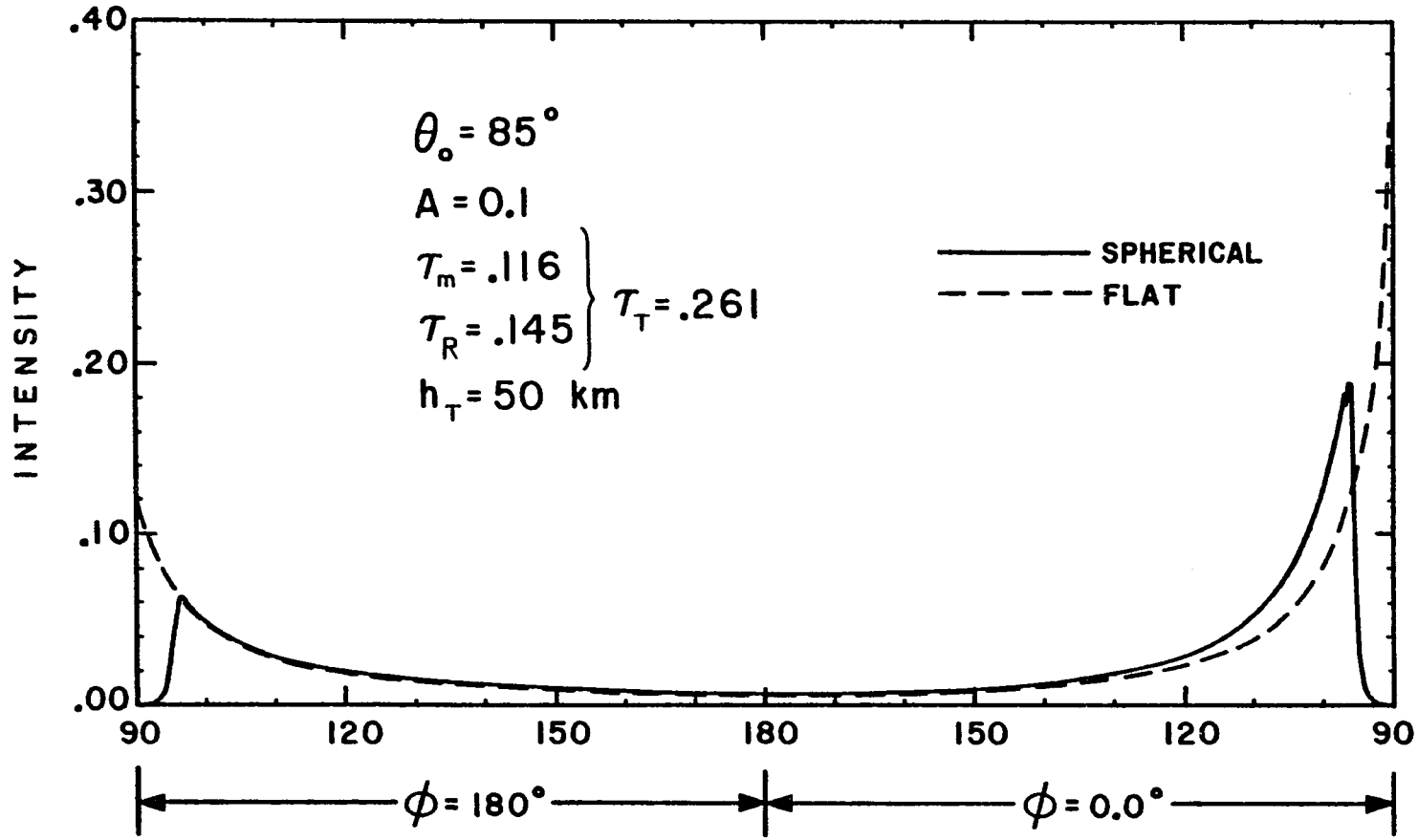

Fig. 4-19. Reflected intensity as a function of zenith angle for the azimuthal plane (0°, 180°) in a conservative atmosphere that includes a homogeneous air pollution layer in the troposphere. The solar zenith angle $\theta_o = 85°$ and $\tau_T = .261$.

respectively. It is interesting to note that for case II the peak value of the reflected intensity for $\phi = 0^\circ$ is about twice that of case I (see Fig. 4-11 and 17). Also, case III and IV show two peaks in the intensity profile for $\phi = 0^\circ$, as illustrated in Fig. 4-18 and 19. The jump in the intensity profile after the first peak occurs just as the observer sees the top of the tropospheric aerosol layers. To enhance our understanding of the various changes that result from the inclusion of stratospheric and air pollution layers we compare the reflected intensities in the spherical atmosphere for cases I through IV at $\theta_o = 85^\circ$, $\phi = 0^\circ$ and $90^\circ < \theta \leqslant 135^\circ$ as illustrated in Fig. 4-20. Here the reflected intensities for all these cases are indistinguishable for the scan angles between 90° and 95°. However, the interesting changes in the intensity profile occur between $\theta = 95^\circ$ and 97.155°. Furthermore, for larger scan angles the reflected intensities are affected primarily by the total optical depth. As shown in Fig. 4-20 for $\theta > 100^\circ$ the reflected intensities of case III have the largest values followed by case IV, II and I. The intensity profile of case I and II have a maximum value at $\theta = 96^\circ$ and 95.5° with I = .19 and .326, respectively. Just before the scan angle sees the stratospheric layer a large increase in the received radiation is noticed. Also, comparing the results of cases I and III indicates almost identical values up to $\theta = 97^\circ$. Afterwards, the intensity of case III shoots up until reaching a maximum value of 0.25 at $\theta = 97.155^\circ$. This sudden jump coincides with the penetration of the lines of sight into the pollution layer between the height of 5 (km) and the

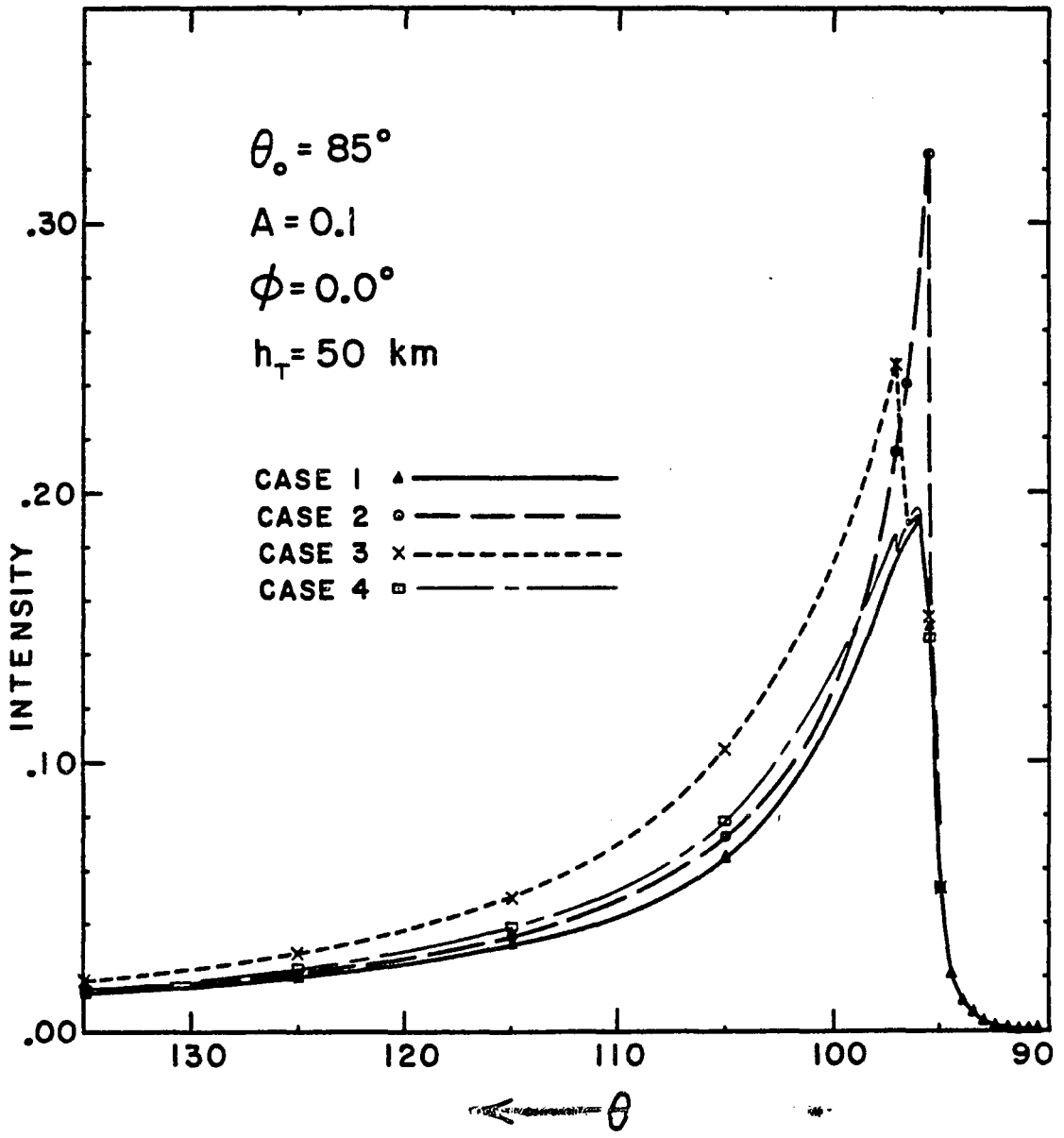

Fig. 4-20. Reflected intensity as a function of zenith angle in a spherical atmosphere that includes four cases of vertical inhomogeneities. The solar zenith angle $\theta_o = 85^\circ$ and $\phi = 0.0^\circ$.

ground. Similarly, comparing the results of cases I and IV shows a discontinuity in the intensity profile of case IV at $\theta = 97.155^{\circ}$. Again, this corresponds to receiving scattering from the 1.0 (km) layer of pollution on the ground. Such situations can also happen at the same scan angle if the ground has a very high reflectivity. Consequently, as the sun approaches the horizon a satellite or spacecraft based measurement of skylight results in distinct changes in the presence of additional vertical inhomogeneities, such as volcanic dust or air pollution layers.

Flying aircraft or balloons at different altitudes may be used to detect vertical inhomogeneities in the earth's atmosphere. This can be accomplished by monitoring the upward traveling beams at a fixed zenith angle near the horizon in the plane of incident solar radiation. The resulting upward traveling beams in the spherical model at $\theta = 95^{\circ}$ when $\theta_o = 85^{\circ}$ and $\phi = 0^{\circ}$ as a function of height for the previously mentioned four cases are shown in Fig. 4-21. The sphericity of the atmosphere and the changes of the optical depth determines the shape of the upward traveling beams at various heights. In our problem $h_{tan} = 24.33$ (km) is the height at which the line of sight of $\theta = 95^{\circ}$ touches the earth's surface. Above h_{tan} none of the lines of sight reach the ground, while below it all the lines of sight intersect the ground. In fact, as shown in Fig. 4-21 the shape of the intensity curve of cases I and II shows a discontinuity at that height. In addition, the intensity varies linearly close to the top and bottom of the atmosphere. The intensities of case II are larger than those of

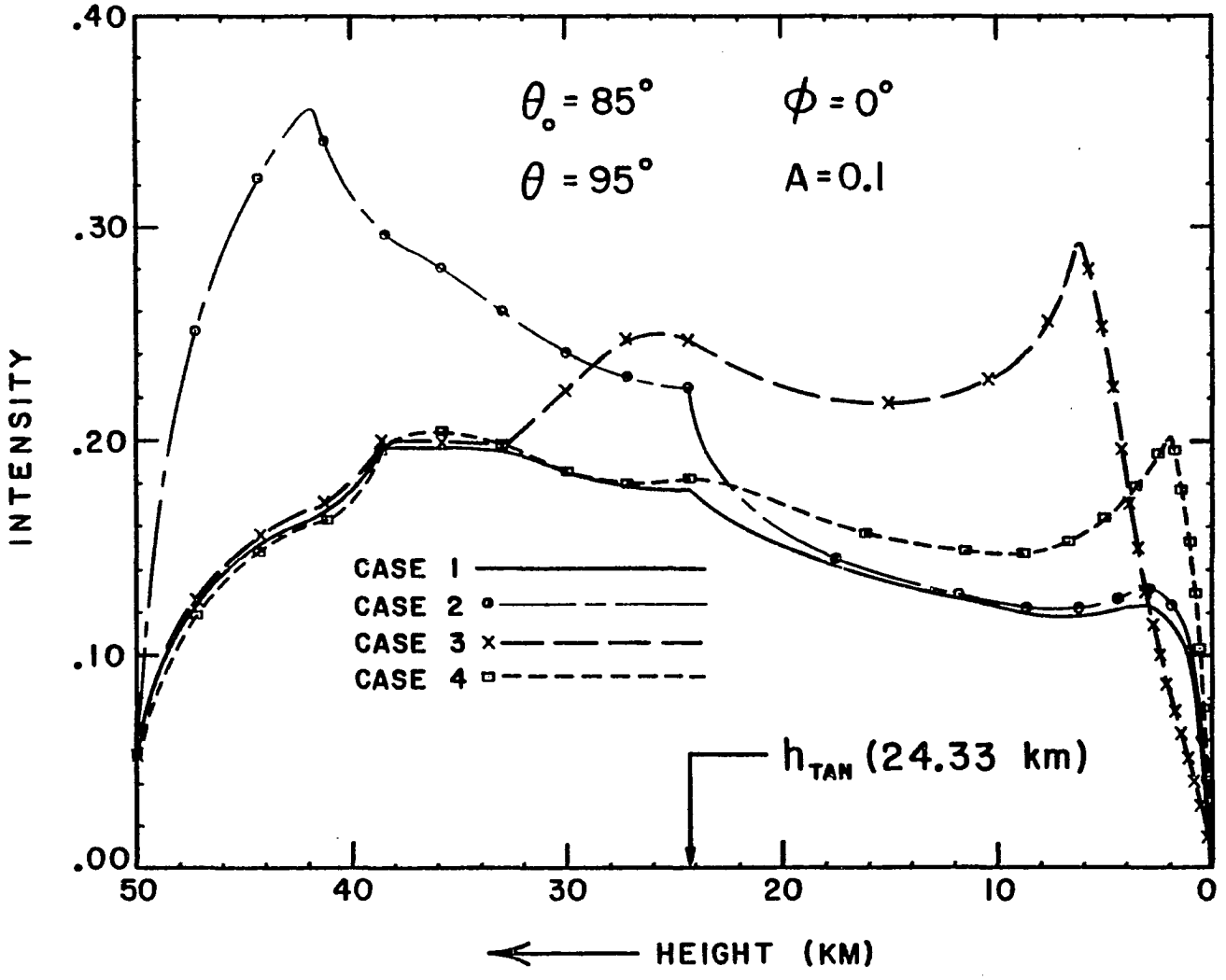

Fig. 4-21. Upward traveling beams as a function of height at $\theta = 95^\circ$ in a spherical atmosphere that includes four cases of vertical inhomogeneities. The solar zenith angle $\theta_o = 85^\circ$ and $\phi = 0^\circ$.

case I at all heights, because of more scattering in the upward direction. Furthermore, the peak in the intensity curve at $z \simeq 42$ (km) for case II is due to the upward scattering from the stratospheric layer. Between the heights 50 and 33 (km) the intensities of case III are about the same as those in case I. Then, as the scattering from the pollution layer below $z = 5$ (km) starts reaching the observer at $z \simeq 32$ (km) the intensity increases from .2 to 0.25 as shown in Fig. 4-21. Also, as the height of the observer approaches the top of the pollution layer (i.e., $z = 5$ km) the intensity curve shows a second peak at $z \simeq 6$ km then decreases almost linearly until reaching the ground. The intensity curve of case IV indicates similar behavior to that of case III, whereby the intensities of case IV are smaller and the peak occurs at $z \simeq 2$ (km). Since the scattering from the 1.0 (km) homogeneous pollution layer does not reach the observer until $z \simeq 25$ (km), the intensities of cases I and IV are practically the same between $z = 50$ and 27 (km).

The scattering of 0.5 μm radiation in a conservative and vertically inhomogeneous atmosphere has been discussed. Results of comparing the emerging radiation from plane-parallel and spherical models have been presented for four different aerosols' distributions. In all cases a measurable difference, 10 to 40%, in a ground based measurement due to the neglect of the sphericity of the atmosphere occurs when the incident solar radiation and/or the angle of observation reaches 80° to 90°. Also, in a satellite radiometric measurement, the plane-parallel model gives wrong results and, in fact, two to three orders of magnitude

differences between the two models in intensity values at $\theta \simeq 90^{\circ}$ are obtained. Furthermore, the introduction of stratospheric dust and air pollution layers into the distribution of aerosols can be detected by a scanning radiometer on a satellite and by a flying aircraft or balloon at different altitudes. In addition, it was shown that the total flux in a spherical atmosphere is conserved within 1.351% by the present Quasi-Spherical method.

CHAPTER V

SUMMARY AND CONCLUSIONS

The analysis of the radiation field in a scattering atmosphere has been presented. Since the integro-differential equation of radiative transfer in spherical geometry has no known analytic solution, a new method which is called the Quasi-Spherical method was introduced to obtain a numerical solution to the problem of scattering in a spherical atmosphere. So far, the Monte Carlo (or random walk) method is the only method that has been used in obtaining a solution to this problem. The Monte Carlo method is very slow and suffers from statistical fluctuations, while the Quasi-Spherical method is fast and has no statistical fluctuation. Nonetheless, the new method is limited to a planet with a radius much larger than the height of its atmosphere. Although polarization and absorption can be easily incorporated into the Quasi-Spherical method, we have neglected to include them in all the considered situations in this dissertation.

The emerging radiation in homogeneous and inhomogeneous molecular (Rayleigh) atmospheres have been considered. For a homogeneous molecular atmosphere with $\tau_R = .25$, $\theta_o = 84.26^\circ$ and A = 0.0 and 0.8 the reflected and transmitted intensities as computed by the Quasi-Spherical and backward Monte Carlo (see collins et al, 1972) methods

are almost identical except close to the horizon where differences on the order of 11% have resulted partially due to the inclusion of polarization by the latter method. However, if polarization is neglected in the backward Monte Carlo (see Blattner, 1981) calculations the results show a better agreement, particularly close to the horizon where the differences are reduced to 5%. Similarly, the comparison between the resulting transmitted and reflected intensities by the Quasi-Spherical and Monte Carlo (see Marchuk et al, 1980) methods in a vertically inhomogeneous molecular atmosphere with $\tau_R = 0.1$ and $\theta_o = 53.13^\circ$ shows also indistinguishable results. As a limiting case, the emerging radiation in a conservative spherical atmosphere with $\tau_T = .195$ as calculated by the new method converges to that of the plane-parallel atmosphere as the radius of the planet is increased by one hundred times.

Information on the composition of the earth's atmosphere by remote sensing methods is usually based on analyzing the measured skylight. For the past three decades such analysis has employed a plane-parallel model rather than a spherical one for the earth's atmosphere, because of its simplicity. The resulting scattered radiation by the two models reveals measurable differences for the transmitted and reflected intensities when the solar zenith angle and/or the angle of observation is within 10° of the horizon. The 0.5 μm scattered radiation in both plane-parallel and spherical atmospheres with $\tau_T = .195$ that includes aerosols and molecules has been discussed. In ground based radiometric measurements of skylight the obtained results in the spherical atmosphere are 10 to 30% higher than those in the

plane-parallel atmosphere when $\theta_o = 85^\circ$, but the negligible differences occur for $\theta_o \leqslant 75^\circ$. Furthermore, a scanning radiometric measurement of skylight by a satellite at the top of both atmospheres of 50 (km) height shows 200 to 300% differences between the two results at $\theta \simeq 90^\circ$ for all solar zenith angles, with appreciable differences between the two atmospheres existing for all observation angles between $\theta = 90^\circ$ and 97°. In addition, the obtained results in the spherical atmosphere show that additional layers of aerosols in the stratosphere and troposphere can be detected, for example, either by satellite or aircraft radiometric measurements while flat atmospheres do not permit such a detection. Therefore, the application of the Quasi-Spherical method to the earth's atmosphere provides a tool to analyze radiometric measurements from satellite or spacecraft experiments. Finally, it was shown by the present method that the total flux in the spherical atmosphere is conserved within 1.35%.

In this dissertation, we intended to introduce the Quasi-Spherical method to be used in the study of the scattering problems in planetary atmospheres. Therefore, we have not considered tne effects of polarization and absorption in these atmospheres. Also, multiple scattering can be determined more accurately, particularly for $\tau_T > 1.0$, by using the singly scattered intensities along the local normal instead of shifting them as done in the present work. In addition, further modifications of the Quasi-Spherical method, such as ray bending and refraction are needed to study the problem of twilight.

APPENDIX A

DETERMINATION OF OPTICAL DEPTH

The definition of the normal optical depth, τ, was given in Eq (2.5). Usually, τ consists of two components due to scattering (i.e., Rayleigh and Mie) and one component due to absorption. Another way of expressing any component of τ at the height z is given by

$$\tau_\lambda(z) = C\int_z^\infty \int_0^\infty Q(n,\lambda,r)\psi(r)N(z)drdz \tag{A.1}$$

where C is a constant and Q is the spectral scattering or absorption cross section of a spherical particle of radius r and index of refraction n. ψ is the size distribution function and N is the number of particles as a function of height, z.

Usually, in a direct problem the height distribution of particles is assumed to be known. Here, we will assume a normalized density of molecules and aerosols after the work of Elterman (1968) as was shown in Fig. 4-1. Furthermore, we will assume that the total molecular and aerosols optical depths at the ground (i.e., z = 0) are known. Consequently, Eq (A.1) reduces to

$$\tau_\lambda(z) = C_1(\lambda)\int_z^\infty N(z)dz = \int_z^\infty \beta(z,\lambda)dz \tag{A.2}$$

where C_1 is a constant which is equal to the product of C by the result of the integration over r, while β is the volume attenuation coefficient. Using the normalized distribution and the known attenuation coefficient at the ground $\beta(0, \lambda)$, we can determine the new attenuation coefficient as follows

$$\beta(z, \lambda) = \beta(0, \lambda) \frac{N(z)}{N(0)} \quad . \qquad (A.3)$$

Then the integration in Eq (A.2) is performed by applying the trapezoidal rule which yields

$$\tau_\lambda(z) = \frac{1}{2} \sum_{i=1,2,\ldots} \left(\beta_i+\beta_{i+1}\right)\left(z_{i+1}-z_i\right) \quad . \qquad (A.4)$$

Since Elterman's data are given at discrete values of height, for intermediate heights or optical depths the interpolation is performed by assuming a linear logarithmic variation for τ as a function of z, that is

$$z = a\ell n\tau+b \qquad (A.5)$$

where a and b are constants that depend on the data points at the two ends of the interval in question.

REFERENCES

Blattner, W. G. and M. B. Wells, 1973, Monte Carlo Studies of Sky Radiation. AFCRL Report No. TR-73-0613, Air Force Cambridge Research Laboratories, Bedford, Mass.

Blattner, W. G., G. H. Horak, D. G. Collins and M. B. Wells, 1974, Monte Carlo Studies of the Sky Radiation at Twilight. Appl. Opt., Vol. 13, pp. 534-547.

Blattner, W. G., 1981, Personal communications. Radiation Research Assoc., Fort Worth, Tex.

Chandrasekhar, S., 1960, Radiative Transfer. Dover Publications, Inc., New York.

Chapman, R. D., 1966, Radiative Transfer in Extended Stellar Atmospheres. Astrophys. J., Vol. 143, No. 1, pp. 61-74.

Collins, D. G., W. G. Blattner, M. B. Wells and H. G. Horak, 1972, Backward Monte Carlo Calculation of Polarization Characteristics of Radiation Emerging from Spherical-Shell Atmospheres. Appl. Opt., Vol. 11, No. 11, pp. 2684-2696.

Coulson, K. L., J. V. Dave and Z. Sekera, 1960, Tables Related to Radiation Emerging from a Planetary Atmosphere with Rayleigh Scattering. University of California Press, Berkeley, Calif.

Coulson, K. L., 1980, Characteristic of Skylight at the Zenith During Twilight as Indicators of Atmospheric Turbidity, 1; Degree of Polarization. Appl. Opt., Vol. 19, No. 20, pp. 3469-3480.

Coulson, K. L., 1981, Characteristic of Skylight at the Zenith During Twilight as Indicators of Atmospheric Turbidity, 2; Intensity and Color Ratio. Appl. Opt., Vol. 20, No. 20, pp. 1516-1524.

Chu, W. P. and M. P. McCormick, 1979, Inversion of Stratospheric Aerosol and Gaseous Constituents from Spacecraft Solar Extinction Data in the 0.38-1.0 μm Wavelength Region. Appl. Opt., Vol. 18, No. 9, pp. 1404-1413.

Dave, J. V. and J. Gazdag, 1970, A Modified Fourier Transform Method for Multiple Scattering Calculations in a Plane-Parallel Atmosphere. Appl. Opt., Vol. 9, pp. 1457-1466.

Elterman, L., 1968, UV, Visible and IR Attenuation for Altitudes to 50 km. AFCRL Report No. 68-0153, Air Force Cambridge Research Laboratories, Bedford, Mass.

Herman, B. M., 1963, A Numerical Solution to the Equation of Radiative Transfer for Particles in the Mie Region. Ph.D. Dissertation, Dept. of Meteorology, University of Arizona, Tucson, Ariz.

Herman, B. M. and S. R. Browning, 1965, A Numerical Solution to the Equation of Radiative Transfer. J. Atmos. Sci., Vol. 22, pp. 559-566.

Herman, B. M. and S. R. Browning, 1975, The Effect of Aerosols on the Earth-Atmosphere Albedo. J. Atmos. Sci., Vol. 32, pp. 1430-1445.

Herman, B. M., W. Asous and S. R. Browning, 1980, A Semi-Analytic Technique to Integrate the Radiative Transfer Equation Over Optical Depth. J. Atmos. Sci., Vol. 37, pp. 1828-1838.

Hummer, D. G. and G. B. Tybicki, 1971, Radiative Transfer in Spherically Symmetric Systems. The Conservative Gray Case. Mon. Not. R. Astr. Soc., Vol. 152, pp. 1-19.

Ishimaru, A., 1978, Wave Propagation and Scattering in Random Media. Vol. 1, Academic Press, Inc., New York.

Lenoble, J. and Z. Sekera, 1961, Equation of Radiative Transfer in a Planetary Spherical Atmosphere. Proc. of the National Academy of Sciences, 47. pt. 1, pp. 372-378.

Lenoble, J., 1977, Comparison of Computation Technique in Scattering Problems. Radiation in the Atmosphere. Science Press, Princeton, N. J.

Leong, T. K. and K. K. Sen, 1972, A probabilistic Model for Time-Dependent Transfer Problems in Spherical Shell Media. Mon. Not. R. Astr. Soc., 160, pp. 21-36.

Marchuk, G. K., G. A. Mikhnilov, M. A. Nazaraliev, R. A. Darbinjan, B. A. Kargin and B. S. Elepov, 1980, The Monte Carlo Methods in Atmospheric Optics. Springer-Verlag, Berlin Heidelberg, Ch. 4.

Minn, I. N. and V. V. Sobolev, 1963, The Theory of Radiation Scattering in Planetary Atmospheres. Soviet Astronomy, Vol. 7, pp. 379-383.

Rozenberg, G. V., 1966, Twilight. Plenum Press, New York

Schmid-Burgk, J., 1975, Radiative Transfer Through Spherically-Symmetric Atmospheres. Astron. & Astrophys., Vol. 40, pp. 249-255.

Simonneau, E., 1976, Radiative Transfer in Atmospheres with Spherical Symmetry. J. Quant. Spectrosc. Radiat. Transfer, Vol. 16, pp. 741-753.

Sobolev, V. V., 1963, A Treatise on Radiative Transfer. Van-Nostrand Co., N. J.

Sobolev, V. V., 1975, Light Scattering in Planetary Atmospheres. Pergamon Press Ltd., New York, Ch. 11.

Stratton, J. A., 1941, Electromagnetic Theory. McGraw-Hill Book Company, New York.

Unno, W. and M. Kondo, 1976, The Eddington Approximation Generalized for Radiative Transfer in Spherically Symmetric Systems. I. Basic Method. Publ. Astron. Soc. Japan, Vol. 28, pp. 347-354.

Van de Hulst, H. C., 1957, Light Scattering by Small Particles. John Wiley & Sons, Inc., New York.

Van de Hulst, H. C., Multiple Scattering. Academic Press, Inc., New York, Vol. 1, Ch. 3.

Whitney, W. G., R. E. Var and C. R. Gray, 1973, Research into Radiative Transfer Modeling and Applications. AFCRL Report No. TR-73-0420, Air Force Cambridge Research Laboratories, Bedford, Mass.

Wilson, S. J. and K. K. Sen, 1980, Light Scattering by an Optically Thin Inhomogeneous Spherically-Symmetric Planetary Atmosphere. Astrophys. & Space Science, Vol. 69, pp. 107-113.

Wilson, S. J. and K. K. Sen, 1980, Light Scattering by an Optically Thin Inhomogeneous Spherically-Symmetric Planetary Atmosphere; Brightness at the Zenith Near Terminator. Astrophys. & Space Science, Vol. 71, pp. 405-410.